Pathogenic Peptides to Enhance Treatment of Glioblastoma: Evaluation of RVG-29 from Rabies Virus and Chlorotoxin from Scorpion Venom

by

Rebecca Cook

A Dissertation Presented in Partial Fulfillment
of the Requirements for the Degree
Doctor of Philosophy

Approved May 2019 by the
Graduate Supervisory Committee:

Rachael Sirianni, Co-Chair
Joseph Blattman, Co-Chair
Tsafrir Mor
Karen Anderson

ARIZONA STATE UNIVERSITY

August 2019

ABSTRACT

Glioblastoma (GBM) is a highly invasive and deadly late stage tumor that develops from abnormal astrocytes in the brain. With few improvements in treatment over many decades, median patient survival is only 15 months and the 5-year survival rate hovers at 6%. Numerous challenges are encountered in the development of treatments for GBM. The blood-brain barrier (BBB) serves as a primary obstacle due to its innate ability to prevent unwanted molecules, such as most chemotherapeutics, from entering the brain tissue and reaching malignant cells. The GBM cells themselves serve as a second obstacle, having a high level of genetic and phenotypic heterogeneity. This characteristic improves the probability of a population of cells to have resistance to treatment, which ensures the survival of the tumor. Here, the development and testing of two different modes of therapy for treating GBM is described. These therapeutics were enhanced by pathogenic peptides known to improve entry into brain tissue or to bind GBM cells to overcome the BBB and/or tumor cell heterogeneity. The first therapeutic utilizes a small peptide, RVG-29, derived from the rabies virus glycoprotein to improve brain-specific delivery of nanoparticles encapsulated with a small molecule payload. RVG-29-targeted nanoparticles were observed to reach the brain of healthy mice in higher concentrations 2 hours following intravenous injection compared to control particles. However, targeted camptothecin-loaded nanoparticles were not capable of producing significant treatment benefits compared to non-targeted particles in an orthotopic mouse model of GBM. Peptide degradation following injection was shown to be a likely cause for reduced treatment benefit. The second therapeutic utilizes chlorotoxin, a non-toxic 36-amino acid peptide found in the venom of the deathstalker scorpion, expressed as a fusion to antibody fragments to enhance T cell recognition and killing of GBM. This candidate biologic, known as anti-CD3/chlorotoxin (ACDClx) is expressed as an insoluble protein in *Nicotiana benthamiana* and *Escherichia coli* and must be purified in denaturing and reducing conditions prior to being refolded. ACDClx was shown to selectively activate T cells only in the presence of GBM cells, providing evidence that further preclinical development of ACDClx as a GBM immunotherapy is warranted.

DEDICATION

To Matthew Navarro, whose battle with glioblastoma was the inspiration for this work.

To Yoni, who is battling a brain tumor as I type this.

To all of the cancer patients worldwide who donate samples, enter clinical trials, and sacrifice their precious time to further our understanding of this dreaded disease.

To my grandmother, who I lost eight days after starting my PhD, and my grandfather, both of whom always had faith in me and whose love of family was an inspiration.

To my dad, who was my inspiration for learning about the universe and who never stopped asking when I would start my PhD, until I finally did.

To my mom, who has always been there to provide advice and encouragement, who pointed out how fascinated I was by forensics (thus saving me from majoring in sociology), and who always gave me the independence to tinker, make a mess, and figure things out myself - a trait absolutely required for this project.

To my talented niece and nephew, who sacrificed many sleepovers and movie nights to my nights in the lab.

To Mr. Roger Anderson, who taught me the discipline required to achieve my goals.

To Anthony and Amanda for their priceless friendship.

To my amazing husband Jeff, whose love and unyielding support carried me through the toughest of times, who celebrated with me in the best of times, dealt with my ridiculous lab schedule, listened to all of my practice talks, took me on adventures, provided a loving home, and let me dig all the holes I wanted in the backyard. *We do what we must because we can.*

ACKNOWLEDGMENTS

I'd first like to thank the best professional mentor I've ever had – Dr. Rachael Sirianni. You took a chance on me in helping to start your first lab, and I've learned so much since then. Scientifically, your drive for rigorous experimental design and data analysis have always inspired me to always do things to the best of my ability. Personally and professionally, you are a person who listens with understanding, gives honest and excellent advice whenever asked, and serves as an advocate whenever the need arises. For the opportunity to learn, publish, travel, and discuss, I am forever grateful. Above all, I'm grateful for the opportunity you gave me to pursue my interest in pathogen interactions with the CNS, which became the inspiration for my PhD studies.

To Dr. Joseph Blattman – I've known you for a much shorter time but will never forget my first introduction to the complex dynamics of the immune system. Your teaching style turned a difficult topic into a fascinating one, and I've been inspired to learn more every day and teach others whenever the opportunity arises. Thank you for allowing me to build a bridge between immunology and brain tumors and for giving me the freedom to pursue independent research.

To Dr. Tsafrir Mor – even though you weren't my official advisor, you provided the space, equipment, and advice I needed during most of my studies with ACDClx. When everything felt like it was failing, you were the one who knew I would eventually succeed and encouraged me to keep pushing on. I could always count on you for a mini high-five celebration of the small victories, whether it be the first signal on a western blot that showed I *finally* purified or solubilized my protein, or the news of an awesome job offer. Thank you for the many hours-long brainstorming sessions intertwined with random mini discussions of movies and theater. Lastly, thank you for always inspiring us to give it our best.

To those who helped me get started on producing ACDClx, you launched it all. To Dr. Lydia Meador - I'm forever grateful for the initial introduction to protein expression, for the help with cloning the first version of ACDClx into plants, and for the continued friendship. To Book and Cherry (Thanchanok Boonsompong and Apisara Ausawasamrit) for putting in many hours during their short stay with us to help get ACDClx and chlorotoxin into plants. To the four students I have

personally mentored on the ACDClx project – Braeden Schaefer, Andrew Niemann, Sierra Bichler, and Holden Wilt. It's been an awesome experience watching you learn, experiment, and improve. I was always grateful for your help and enjoyed mentoring you while you explored your own scientific curiosities. I'm excited to see you all succeed in your future.

I would especially like to acknowledge Dr. Andy Diamos, who helped with the initial cloning and then taught me how to clone everything myself. I want to thank Aigerim Kamzina for her amazing friendship and for the countless coffee and lunchbreaks, and Joe Hunter and Michelle DiPalma for always lending an ear to my lab trials and tribulations. Finally, I want to thank Dr. Karen Anderson for her helpful advice and mentorship on my experiments and career throughout my PhD, and Dr. Hugh Mason for all of the helpful feedback along the way.

In the Blattman lab, I've had the pleasure of working with, teaching, and learning from all of you. Thank you to Kavita for always making time for helping me with little things in and out of the lab and especially for always answering my late-night calls about the flow cytometer. To Nicole Appel, Eveyln Luna, Joshua Carmen, Louie Schoettle, Ammar Tanveer, and Peaches Ulrich for the advice, the conversation, and all the help you've given me during my time there.

I especially want to thank all the members of the Sirianni lab. To Dr. John Heffernan, who became my first full-time lab mate and continues to be a great source of advice and encouragement. To Dr. Alesia Prakapenka and Danielle DiPerna for the laughter and for being my coffee partners in crime at BNI. To Dr. Kyle Householder and Eugene Chung for the jokes and for the interesting conversations. To the rest of the Arizona lab members, past and present, thank you for teaching, for listening, and for the laughs.

Lastly, I want to thank my funding sources without which none of this would be possible. The ASU GPSA provided research and travel grants that allowed me to fund important aspects of my project and present them to others in my field. The Barrow Neurological Foundation and ASU Graduate College provided research and stipend funding. I'd also like to thank Dr. Nader Sanai, the Rick Oehme Foundation, and the Biological Design Graduate Program for the financial support. Finally, I am forever grateful for the generous support I've received from Jack and Vianne Kucera as an ARCS scholar, who have inspired me to pass on their generosity.

TABLE OF CONTENTS

LIST OF TABLES

Table Page

LIST OF FIGURES

Figure Page

LIST OF ABBREVIATIONS

ACDClx	Anti-CD3/Chlorotoxin fusion protein
APC	Antigen presenting cell
BBB	Blood-brain barrier
BiTE	Bispecific T cell engager
CAI	Codon adaptation index
CAR	Chimeric antigen receptor
CHO	Chinese hamster ovary
CNS	Central nervous system
CSF	Cerebrospinal fluid
DAMPs	Damage-associated molecular patterns
DPI	Days post infiltration
DTT	Dithiothreitol
EGFR	Epidermal growth factor receptor
EGFRvIII	EGFR variant III
ER	Endoplasmic reticulum
FBS	Fetal bovine serum
Fv	Antibody variable fragment
GBM	Glioblastoma
GOI	Gene of interest
IDH	Isocitrate dehydrogenase
ITAMs	Intracellular tyrosine activation motifs
LPS	Lipopolysaccharides
MRI	Magnetic resonance imaging
MHC I	Major histocompatibility complex class I
MGMT	O-6-methylguanine-DNA methyltransferase
PLGA	Poly(lactic, co-glycolic) acid

RVG	Rabies virus glycoprotein
SB	Sample buffer
scFv	Single chain variable fragment
SP	Signal peptide
TAMs	Rumor-associated macrophages
TCR	T cell receptor
TEV	Tobacco etch virus
TMZ	Temozolomide
Treg	Regulatory CD4+ T cell
TTF	Tumor-treating field device
VEGF	Vascular endothelial growth factor
WHO	World Health Organization

CHAPTER 1

INTRODUCTION

1.1. Glioblastoma

Glioblastoma (GBM) is an aggressive, diffuse, and genetically heterogeneous brain tumor composed of one or more types of glial cells, known to be the supportive cells of the brain. GBM represents 15% of primary brain tumors and is considered incurable. Median survival for patients who receive standard of care treatment has remained steady at 15 months, with a 5-year survival rate of 5.6% [1]. Although metastases outside the brain are extremely uncommon in GBM, infiltration of malignant cells into healthy brain tissue remains a significant challenge to effective treatment. Cells that have invaded into healthy brain are typically resistant to or difficult to access with systemic chemotherapy, and multiple tumor resection surgeries are not always possible. Most patients are left with no effective treatment options after a second or third relapse. Ultimately, the cause of death in GBM patients is attributed to brain herniation resulting in impaired blood flow or shutdown of processes required for breathing, complications from seizures, and/or tumor hemorrhage; indirect complications, such as infections from tumor-related symptoms, are also reported [2].

New, more personalized treatment strategies have begun to arise for GBM patients following the recent improvement in GBM classification guidelines by the World Health Organization (WHO) in 2016 [3,4]. These new guidelines integrate molecular characteristics with the traditional histological characterization previously used for diagnosis. Thus, the term *glioblastoma* can now be subdivided by isocitrate dehydrogenase (IDH) mutation status (wildtype, mutant, or “not otherwise specified” when mutation status is unknown), which can be further subdivided within the IDH-wildtype group into epithelioid GBM, giant cell GBM, and gliosarcoma if specific additional molecular markers are present. All subtypes can include additional classifiers, such as *GBM with primitive neuronal component, small cell glioblastoma/astrocytoma,* and *granular cell glioblastoma/astrocytoma*, depending on characterized patterns observed histologically. IDH mutation status is a useful prognostic indicator for clinicians, where IDH-wildtype patients represent 90% of GBM, a higher average age at onset, and a significantly

decreased median survival time (15 months for IDH-wildtype vs 31 months for IDH-mutant) [4–7]. IDH mutation status and O-6-methylguanine-DNA methyltransferase (MGMT) methylation status, which may predict treatment sensitivity, is now a reporting requirement for cancer registries [1]. With these new guidelines, clinical testing of mutation status is likely to become more common and may uncover additional trends in treatment efficacy.

Regardless of mutation status, GBM remains a notoriously difficult tumor to treat. Standard of care is aggressive and incorporates surgical resection, radiotherapy, and chemotherapy. In 2005, the chemotherapeutic temozolomide (TMZ) was approved for treating GBM in combination with radiotherapy after demonstrating an increase in median survival from 12.1 to 14.6 months compared to radiotherapy alone [8]. Concomitant treatment with TMZ in turn results in a small fraction of patients experiencing grade 3 and 4 adverse events related to immune suppression and thrombocytopenia, increasing the risk of infection and hemorrhage. Though modest, this increase in survival benefit was the greatest contribution to GBM patient survival in decades, highlighting the struggles with treating GBM in the clinic compared to most other cancers.

Four primary factors are obstacles to effective treatment of GBM: (1) tumor location, where complete tumor resection would damage brain tissue necessary for function and survival, (2) the blood-brain barrier (BBB), which serves to prevent >98% of chemotherapeutics from entering healthy brain tissue where invasive cells might reside [9], (3) genetic heterogeneity, which provides GBM cells the diversity necessary to develop treatment resistance [10], and (4) an immunosuppressive environment, which prevents the natural capacity of the patient's immune system from destroying the tumor [11]. Successful treatment of GBM thus presents the daunting task of overcoming all four issues. Current and experimental therapies that are designed to overcome some or all of these issues are described below.

1.2. Therapeutic strategies for treating GBM

1.2.1. Standard of Care and Second Line Therapies

The treatment plan chosen for a GBM patient depends on multiple factors that consider tumor location, patient condition, and the patient's wishes. Current standard of care involves resection followed by radiation with concomitant TMZ, termed the Stupp Protocol. However, in many cases, one or more components of the Stupp Protocol are not undertaken. Regardless of treatment plan, most patients relapse and may undergo additional surgical resection or are treated with one or more of the FDA-approved second line therapies, including the vascular endothelial growth factor (VEGF) inhibitor bevacizumab (Avastin®), alkylating agents carmustine and lomustine, or a tumor-treating field device (TTF) (Optune®). Whether second-line treatment with bevacizumb provides benefit is under dispute, however, some survival benefit is gained when a Gliadel® wafer is placed in the tumor resection cavity. Gliadel® wafers are composed of a slow-release polymer, polyanhydride poly[bis(p-carboxyphenoxy)propane:sebacic acid] impregnated with carmustine [12]. These wafers provide localized, controlled release of the chemotherapeutic to any remaining cells on the border of the resection. Use of Gliadel® provides a survival advantage of approximately 6 weeks, with efficacy limited by poor drug diffusion into tissue and major concerns regarding side effects such as local edema and infection. More recently, the TTF device Optune® has made surprising headway towards improving patient survival. TTF devices are wearable devices that function by generating local low intensity electric fields in regions of malignant cells, preventing cell division [13]. In clinical trials, Optune® has been reported to increase median survival from 16 to 20 months, bringing the 5-year survival rates from 5% to 13% when added to the Stupp regimen. Importantly, use of Optune® provides improvements in quality of life for patients [14,15].

1.2.2. Immunotherapies

The lack of curative treatments available for GBM in combination with scientific advancement in the fields of nanotechnology, immunology, and virotherapy have ushered in a wave of promising experimental treatments. Clinical trials aimed at activating or re-activating the immune system for malignant cell destruction are underway, with trials reporting positive results with some important caveats. Notably, peptide vaccines, adoptive cell therapy with chimeric

antigen receptor (CAR) T cells, and immune checkpoint trials report minor improvements in survival but with strong evidence of treatment resistance. The ReACT (phase II) and ACT-IV (phase III) trials tested efficacy of an epidermal growth factor receptor variant III (EGFRvIII) peptide vaccine for recurrent and newly diagnosed EGFRvIII+ GBM, respectively [16,17]. This vaccine was designed to elicit an immune response against a mutated EGFR epitope expressed at high levels (>75% of cells) in 30% of GBM patients [18]. Although the ReACT study showed improvements in progression-free survival and median survival in 72 patients [16], the ACT-IV trial ultimately failed. Important differences between these two studies include disease status (newly diagnosed vs recurrent) within the patient population, and the drug it was paired with for concomitant treatment (bevacizumab for ReACT and TMZ for ACT-IV). These conflicting results suggest that anti-angiogenic therapy with bevacizumab may be more beneficial or have a lesser detrimental effect on the immune system compared to TMZ, which is known to be immunosuppressive at the doses used in the study. In both studies, post-treatment biopsies revealed loss of EGFRvIII expression, indicating immune escape as a likely cause for treatment failure. Similar observations were made after treating patients with an EGFRvIII-specific CAR T cell therapy [19]. Together, these studies suggest that an immune response is occurring in the tumor environment following treatment but is met with a stronger opposing force as tumor cells not expressing the targeted antigen expand rapidly in response to the death of EGFRvIII-positive cells, indicating an intense need for targeting the entire tumor cell population. However, evidence of an anti-tumor immune response within these patients is encouraging for development of future immunotherapies.

Other immunotherapies have been tested without significant clinical success, most notably immune checkpoint inhibitors for PD-1, [20–22]. The failure of checkpoint inhibitors despite widespread success in hematological malignancies and melanoma, combined with the characterization of GBM immunotherapy responders vs non-responders [23], point to a strong effect of an exhausted and immunosuppressive environment characteristic of GBM, discussed in more detail later. Further complicating the evaluation of immune checkpoint inhibition and other immunotherapies is the method used to monitor tumor progression, as treatment-associated

inflammation has a similar appearance on magnetic resonance imaging (MRI) as a tumor mass (known as psuedoprogression), which often results in treatment cessation [24]. Thus, new methods for monitoring immune-based treatment efficacy are also under evaluation.

1.2.3. Virotherapies

Further along the lines of immune-based therapies is virotherapy, a novel approach for targeted destruction of cancer cells for which the first results from clinical trials in GBM patients began surfacing in December 2017. Four virotherapies have thus far completed varying phases of clinical trials for treating recurrent GBM, and early results are encouraging. PVSRIPO, a polio/rhinovirus chimera, targets CD155 and is primarily composed of attenuated poliovirus with its internal ribosome site switched with that of human rhinovirus, making it incapable of infecting neuronal tissue [25]. Phase II clinical trial results reported in mid-2018 are promising, with >25% of patients surviving more than 24 months post-recurrence and 2/35 patients still alive nearly 6 years after recurrence [26]. A phase I trial was recently completed with DNX-2401, an engineered oncolytic adenovirus whose replication is restricted to mutant Retinoblastoma-positive malignant cells [27]. In this small scale trial, 20% (5/25) of patients who received the treatment survived three years post-recurrence/treatment (median time since initial diagnosis at time of treatment: 14.9 months). A late 2017 report described results of a Phase I/IIa trial for an oncolytic parvovirus, H-1PV [28]. Patient survival was unclear due to a small sample size and staggered start times for treatment, but initial results appear promising, with the longest-running group reporting 2 out of 3 patients surviving more than two years post-recurrence. Lastly, Toca 511, a replication competent, non-lytic gamma retrovirus-based vector selective for dividing cells and combined with 5-fluorocytosine pro-drug treatment, was observed to provide a durable response during a dose-escalation trial in 6/53 patients [29,30]. A subgroup of these patients who met criteria for entering a phase III trial had the highest proportion of durable response (5/23 patients). Strikingly, all responding patients had a complete response, defined as an absence of detectable disease (range of survival post-treatment until last follow-up prior to publication: 33.9-52.2 months). This vector enables expression of cytosine deaminase that converts 5-fluorocytosine to

5-fluorouracil (5-FU), an antineoplastic that works to block thymidine synthesis. Future reports from these and other virotherapy trials are eagerly anticipated.

1.2.4. Upcoming therapies

A myriad of therapeutic strategies designed to enhance drug delivery are also in the works for GBM, though none have reported results from clinical trials as of yet. Of note is focused ultrasound, which functions by temporarily opening the blood-brain barrier to allow for greater chemotherapeutic access [31,32]. Various forms of nanotechnology, including polymer nanoparticles for controlled release of therapeutics [33–36], iron oxide nanoparticles for thermo therapy and enhancing radiation therapy [37–39], and carbon nanotubes for drug delivery [40–42], are also being investigated.

A significant effort is being made to improve delivery of non-BBB penetrable chemotherapeutics via slow-release formulations using polymeric nanoparticles. Among the most pursued polymers is poly(lactic, co-glycolic) acid (PLGA), a biodegradable polymer that has been in use in the clinic for over 30 years [43] for indications such as slow-release drug depots and dissolvable sutures. PLGA nanoparticle formulations aimed at increasing delivery of therapeutics, including small molecule drugs, nucleic acids, and proteins to the brain often focus on the use of targeting moieties attached to the surface of the particle to improve entry into the brain parenchyma [44]. Typically, the goal of these formulations is to improve the therapeutic dose that reaches the brain following intravenous delivery while reducing delivery to peripheral organs. Improved delivery of targeted formulations to the brain then allows for the slow release of the encapsulated drug to reduce frequency and/or total dose required for dosing regiments [33,34]. Other methods of delivery have also focused on injection directly into the tumor site during surgery or intrathecal injection into the cerebrospinal fluid (CSF) [35,36]. Ultimately, a truly effective therapy for GBM will need to be capable of destroying bulk tumor, invasive cells, and glioma stem cells. Thus far, no single therapy has been proven to have this trifecta of effects, though a combination of multiple therapies may be key in future treatment regimens.

1.3. An overview of the immune system and the immune landscape in GBM

Improving treatment of GBM requires an understanding of the tumor microenvironment, which becomes increasingly complex when the immune component is considered. Just as each patient's tumor is genetically distinct from another, so is the immune repertoire within it. In general, the GBM microenvironment is considered overwhelmingly immune suppressive [45]. Immune suppression is exacerbated by the addition of medications typically provided to patients following surgery, including anti-inflammatory drugs (e.g. steroids) and chemotherapeutics like TMZ.

The immune system is composed of two branches that work in concert. Upon initial exposure to a potential pathogen, the innate system provides a rapid and generalized immune response which includes activation of the adaptive system. The adaptive response is initially generated through a slower process to provide a more specific immune response that includes elicitation of immunological memory, resulting in a more rapid adaptive immune response in subsequent exposures to the same pathogen. The innate system is composed of cells that recognize conserved constituents of pathogens such as lipopolysaccharide (LPS, endotoxins found in the outer membranes of all Gram-negative bacteria), or extracellular RNA and DNA associated with viruses. Also recognized are abnormal cellular characteristics, such as an absence of major histocompatibility complex proteins on the cell surface. These cells are typically responsible for the inflammation observed immediately after an infection or a wound is inflicted. Bridging the gap between the innate and adaptive systems are professional antigen-presenting cells (APCs), such as dendritic cells and macrophages. APCs quickly respond to pathogens or cell debris by internalizing, processing, and displaying digested protein fragments on their surface for recognition by cells of the adaptive system.

The adaptive system is composed of two main cell types, B and T lymphocytes, which are responsible for producing antibodies and mediating cellular immunity, respectively. During the development of these cells, a highly diverse array of cell surface receptors are generated by the process of random somatic mutation, resulting in a single, distinct receptor for each cell. As part of the maturation process, B and T cells bearing receptors that have the capacity to recognize

host proteins are selected against, leaving a multitude of cells capable of recognizing a wide array of foreign proteins; the random generation of each cell's receptor combined with the sheer number of possible receptors significantly increases the probability of recognizing newly encountered proteins. Thus, when an APC displays ("presents") peptides from foreign proteins ("antigens") on its surface in an inflammatory context that are subsequently recognized by their cognate B or T cell receptors, an overwhelming response is coordinated to produce antigen specific antibodies and effector T cells. These effector T cells can further direct the immunological responses (CD4+ "helper" T cells) or quickly destroy affected/infected cells by initiating caspase-mediated cell death mechanisms (CD8+ "killer" T cells).

The highly orchestrated response of the innate and adaptive system is useful in the context of infection or cancer. In the case of infection, pathogens are quickly neutralized by the innate and adaptive system and remembered by the adaptive system for a quicker response during the next infection. In the case of cancer, malignant cells are quickly recognized to possess proteins that look abnormal as a result of genetic mutation or under/overexpression.

As in most systems, the ideal situation is not always reality. In both infection and cancer, it is possible for the pathogen or malignant cells to evolve, enabling immune evasion, expansion, and persistence. On the opposite side of the possible spectrum of immune responses, an uncontrolled issue can lead to a chronic inflammatory response in the context of a more difficult infection or malignant growth. In this instance, suppressive immune cells step in to prevent an ongoing response, thought to occur as a mechanism of host protection. Both non-ideal situations are well-characterized in the context of GBM, where inflammation as a result of immune-mediated or hypoxia-induced cell death results in ongoing immune cell activation, which is quickly converted to an immunosuppressed environment following the secretion of cytokines, expression of inhibitory receptors, and proliferation of suppressive immune cells (discussed in greater detail below) [45–48].

In a healthy brain, resident immune cells known as microglia monitor tissue for signs of infection and provide support to the brain parenchyma in the form of debris clearance, neuronal maintenance, and recruitment of peripheral immune cells when necessary (for a recent

comprehensive overview of neuroimmunology, see references [49] and [50]). Though previously considered immunologically-privileged, lymphatic vessels within the brain were recently discovered to exist along blood vessels and within the dural sinuses, providing a specialized transportation route for debris clearance and cells of the immune system [51]. These vessels drain into the cervical lymph nodes where antigens can be presented to lymphocytes to activate an immune response.

How the immune system is first activated in the context of GBM is currently unknown. It is speculated that growth of malignant cells within the brain results in cell death and tissue damage, which likely sets off an immune response following initial recognition of released intracellular components known as damage-associated molecular patterns (DAMPs) by microglia; others speculate that inflammation may be the initiator of GBM tumorigenesis following recognition of mutated protein [52]. These signals can then lead to recruitment of natural killer (NK) cells to the tumor and send microglia to serve as APCs within the cervical lymph node where recognition of mutated proteins by lymphocytes occurs. Immune activation results in release of chemokines to recruit additional immune cells from the periphery. At this point, it is thought that dendritic cells, monocytes (progenitors of macrophages and dendritic cells), and lymphocytes follow these chemokine gradients and enter the brain tissue. In tissue samples removed during surgical resection, studies have found that 30-40% of the tumor itself is composed of tumor-associated macrophages (TAMs), including microglia [53]. It is likely that most of these TAMs are in fact not brain-derived microglia but are instead monocytes that have entered the tumor tissue from the blood as macrophages [54]. These TAMs are thought to eventually switch from a pro-inflammatory M1 phenotype to play a more immunosuppressive role as M2 macrophages, secreting cytokines that prevent antigen presentation and immune clearance of the tumor [48].

1.4. Mechanisms of immune suppression in GBM

The immune microenvironment within GBM is known to be complex and is still not fully understood (for recent reviews, see references [11,45,55]). The overall lack of significant changes in tumor recurrence and patient survival following immunotherapy for GBM, despite dramatic

success for peripheral solid tumors, indicates that multiple points of attack may be necessary to truly control the tumor, including pan-GBM targeting within the tumor core and in healthy tissue where invasive cells reside, immune checkpoint blockade, and reinvigoration of the pro-tumor response. This becomes more obvious when examining the microenvironment and the multiple immune factors contributing to GBM growth and invasion. The sequence of events leading to immunosuppression within GBM are still under investigation, but many interconnected factors and events contribute to the overall suppressive landscape. Within a tumor, GBM cells work well in conjunction with cytokines and suppressive immune cells to prevent antigen presentation, T cell-mediated tumor killing, and proliferation of pro-inflammatory immune cell subsets that are necessary for full tumor control [45].

Orchestrating these events as a whole are cytokines secreted by both GBM cells and leukocytes that work to influence the entire tumor environment by inducing and maintaining immunosuppression. In particular, IL-10 and TGF-β in the GBM microenvironment play major roles in preventing APCs from successfully trafficking to lymph nodes to activate anti-tumor responses and are also known to inhibit CD8+ T cells by blocking T cell proliferation and reducing expression of proteins responsible for cell killing, such as perforin and granzyme [56–59]. Consequently, IL-10 and TGF-β secreted by GBM cells can result in induction and improved survival of regulatory T cells (Tregs) [60]. Both cytokines are further secreted by suppressive macrophages and Tregs which provides a feed-forward system of immunosuppression [61]. Though tightly associated with one another, IL-10 and TGF-β can be separately classified as having a stronger role in CD8+ T cell suppression and induction/maintenance of Tregs, respectively [62].

Tregs play a critical role in GBM immune suppression and many other tumor types, though their role in preventing autoimmunity in other contexts is equally critical [63–65]. To prevent attack of host cells, Tregs secrete suppressive cytokines described above, but also function to kill, inhibit proliferation of, and induce exhaustion of CD8+ T cells [66]. Treg-mediated killing is often accomplished via Fas/FasL interactions but may also occur by perforin/granzyme pathways [67–69]. Tregs can also passively inhibit T cell proliferation via overexpression of the

high-affinity IL-2 receptor, CD25, which serves as a sponge for IL-2, a well-known cytokine required for CD8+ T cell survival and proliferation [70].

As another mechanism of GBM immunosuppression, inhibition of APCs can occur in several ways. Downregulation of major histocompatibility complex (MHC) proteins on both GBM cells and professional APCs results in the ability to avoid recognition by CD8+ T cells and induce an effective antitumor response, respectively [71,72]. Downregulation of MHC I on GBM cells is considered an effective immune evasion strategy and is especially important in the context of immune checkpoint inhibition therapy, as CD8+ cells have no ability to kill target cells without recognizing cognate antigen presented on MHC I [71]. Preventing professional APCs from traveling to the lymph node and presenting tumor antigens becomes especially detrimental to the possibility of an anti-tumor response, since naïve lymphocytes with receptors specific for tumor antigens may not be activated and expanded. Lastly, recent investigations into the interactions between Tregs and APCs have revealed the possibility of antigen presentation inhibition via trogocytosis, where Tregs may act to prevent tumor killing and immune activation by “biting off” MHC-antigen complexes present on the surface of professional antigen presenting cells [73].

Killer T cells are the major players in tumor cell destruction and overall tumor obliteration and are thus a major target of immunosuppressive mechanisms. This is evidenced by recent success in immunotherapy trials for peripheral solid and liquid tumors, where blocking inhibitory T cell checkpoint proteins (immune checkpoint blockade) results in dramatic reduction in tumor mass, and in many cases, complete tumor control [74]. Achievement of cell killing within minutes combined with rapid proliferation of anti-tumor T cell clones makes CD8+ T cells a large anti-tumor force to be reckoned with. However, in the GBM microenvironment, multiple mechanisms are at work to disable or kill these cells. Tumor biopsies from GBM patients consistently reveal low numbers of CD8+ T cells or an exhausted CD8+ T cell population, characterized by expression of key immune checkpoint proteins CTLA-4 and PD-1, among many others, on the cell surface [75]. Expression of immune checkpoint proteins signals the broad downregulation of key cell killing machinery, including perforin and granzyme, and reduced inflammatory cytokine secretion, effectively blocking target cell killing and autocrine proliferation signals, respectively. As

previously discussed, immune checkpoint proteins are also expressed on the surface of GBM cells as a “don’t kill me” signal to CD8+ T cells and are also expressed on Tregs for the purpose of inducing CD8+ T cell exhaustion.

In total, the environment within the tumor is overwhelmingly suppressive and will require a highly coordinated attack to enable an anti-tumor response to occur via resident immune cells and result in tumor control without resulting in fatal toxicity to nearby neurons and peripheral tissue. Clinical trials are underway to investigate the effects of single and combinatorial use of immunotherapies in the context of GBM.

1.5. Recombinant bispecific fusion proteins for engaging T cells against cancer (BiTEs)

In 1985, Uwe Staerz, a graduate student in the laboratory of famed immunologist Michael Bevan, proposed the idea and presented the first evidence for enhancing T cell recognition and killing of target cells without the need for a specific T cell receptor. This was accomplished by artificially induced recognition through chemical crosslinking of two antibodies: one that bound the T cell via the T cell receptor (TCR) complex, and one that bound the target cell, to engage the two cells and induce T cell activation [76]. Improvements to this idea came in the form of using only the essential components for this process: antibody variable fragments (Fv) that contain the regions of the antibody’s antigen binding domains of the heavy and light chains. Fvs were able to significantly decrease the overall size of the fusion constructs from 300 kDa to 50 kDa and enabled the molecule to avoid spurious activation via antibody constant regions or divalency of the T cell binding domain. Improvements in recombinant protein expression and a more advanced understanding of the TCR complex resulted in the expression of a single chain (sc) bispecific molecule (bispecific scFv) ten years later in Peter Kufer’s lab [77]. Their new bispecific antibody-like molecule was designed to engage T cells via CD3 present in the TCR complex on one end, and EpCAM, a tumor-associated antigen, on the other end. Selective engagement of T cells and tumor cells via the bispecific molecule induced fast, potent killing of EpCAM-positive carcinoma cells, thus setting off a wave of similar bispecific fusion proteins selective for various tumor antigens [78,79].

The efficiency behind this new molecule, later renamed a “bispecific T cell engager” (BiTE), lies in the elegance of its design of selective T cell activation. The TCR complex is composed of the TCR responsible through its extracellular domains for antigen binding and host recognition, and six proteins for signal transduction: two ζ chains and four CD3 chains (δ, γ, and two ε chains) (Figure 1A). Each T cell has a unique TCR, selected during T cell development to ensure recognition of host MHC but selected against the capacity to recognize host cell proteins presented on MHC. In the periphery, when a T cell recognizes a foreign protein fragment being presented on host MHC (Figure 1B) (which may occur following viral infection or genetic mutation, for example), structural changes occur that allow intracellular tyrosine activation motifs (ITAMs) present within the signaling domain to be phosphorylated, setting off signal transduction events that result in T cell activation. Sustained activation can then result in T cell mediated killing of the engaged target cell, cytokine release, proliferation, and prolonged T cell survival. In the case of a BiTE (Figure 1C), an activating scFv recognizing CD3ε is capable of inducing these structural changes when the target-specific scFv is also bound to the target cell (Figure 1D). T cell activation in this context does not require MHC-peptide recognition via the TCR, thus BiTEs are said to induce polyclonal T cell activation – activation that occurs irrespective of T cell receptor specificity. Overcoming TCR/MHC requirements thus allows BiTEs to engage non-tumor specific T cells already present in the periphery and also allows them to target tumor cells that have downregulated their MHC receptors as a form of immune evasion or interrupted protein expression. The specificity to the target cells is nonetheless maintained through the other end of the BiTE fusion protein, which is an Fv that recognizes a protein which is ideally exclusively expressed on the surface of the target tumor cell.

Kufer’s anti-EpCAM BiTE was the first to enter clinical trials under the name “MT110” for treatment of solid tumors [80]. Meanwhile, another promising BiTE, Blincyto, was being developed for the treatment of B cell malignancies, targeting the B cell-specific antigen CD19, known to be overexpressed on the cell surface in B cell lymphomas. Though not tumor specific, CD19 is only expressed on B cells, a cell type that can be replenished by the bone marrow and is thus temporarily disposable under controlled conditions. In 2014 Blincyto became the first FDA-

approved BiTE, indicated for relapsed or refractory B cell precursor acute lymphoblastic leukemia (ALL) [81] and in 2018 was approved for minimal residual disease-positive B cell precursor ALL [82]. Future indications for Blincyto are likely to be approved as more clinical data proves efficacy or superiority over current therapies.

Though BiTEs often show similar efficacy against malignant cells as CAR T cells [83], which often are designed to recognize the same antigens, BiTEs provide benefit over CAR T cells by having the ability to be produced more economically and off the shelf, being a single-chain recombinant protein [84]. In comparison, CAR T cells require plasmapheresis of the patient, careful culture of the patient's T cells, transduction with the CAR of interest, cell survival, and finally, transfusion into the patient, which is a prohibitively expensive process for most patients. However, CAR T cells have a major benefit over BiTEs in that they have the capacity to proliferate within the patient, resulting in long-lived production of the therapeutic. BiTEs must be transfused continuously to maintain a therapeutic concentration in hematological cancers, although transfusion guidelines for solid tumors are still in development and may require less frequent transfusion. Ultimately, BiTE therapy may be more economically viable for the majority of cancer patients.

BiTEs are known to be effective for hematologic cancers that have easily targetable surface antigens and excellent exposure to circulating BiTEs. However, progress in targeting solid tumors has been slower due to issues with reaching therapeutic levels. This is a particular challenge for the treatment of large tumors that are inadequately perfused. In the case of GBM, significant heterogeneity within the malignant cell population dictates that all cells within a tumor must be targeted, otherwise clonal expansion of cells not harboring the target antigen can quickly expand to fill the space previously occupied by cells expressing the target antigen. Several BiTEs have been developed for the purpose of treating GBM, namely against EGFRvIII and IL-12Rα2, tumor-specific and tumor-associated antigens, respectively. These antigens are well-known to not be homogenously expressed within the tumor [18], however, and evidence for immune evasion in the face of an EGFRvIII vaccine [85] and an EGFRvIII CAR T cell [19] resulting in therapeutic resistance has been observed in clinical studies. Thus, for any antigen-specific therapeutic

developed for GBM, antigen expression must be evident throughout the entire tumor unless the therapeutic is meant only as an auxiliary therapy accompanying the generalized anti-tumor standard treatment.

1.6. Peptides for enhancing treatment of brain tumors

A primary challenge for improving access of therapeutics to the entire GBM cell population is the BBB (for a more comprehensive introduction to the structure and function of the BBB in relation to drug transport, see reference [86]). The BBB is a highly selective network of cells and membrane proteins that line the brain vasculature and serve to prevent potentially harmful molecules in the blood from gaining access to sensitive neuronal tissue. Discrimination is primarily based on molecular weight, hydrophobicity, and binding to efflux molecules such as P-glycoprotein. Highly charged molecules and neutral molecules of more than 500 Daltons are generally excluded and typically require transporters or rely on transcytosis [9,86,87], though some exceptions exist [88]. Therefore, although the brain is highly vascularized to supply its immense requirement for oxygen, only 1-2% of small molecules present in the blood are capable of reaching the brain in relevant concentrations [9]. Methods for improving brain access of therapeutics are thus in high demand. Common approaches for bypassing the BBB include non-selective manipulation of targeted regions or the entire BBB by chemical or biophysical manipulation (small molecules, focused ultrasound) or the use of targeting agents (antibodies, peptides) to enable transcytosis of a therapeutic. Small molecules such as mannitol and bradykinin function by non-selectively opening the BBB as a whole and can be considered dangerous to patients [89], thus molecules that can be attached to the therapeutic itself, for the purpose of targeting, are generally preferred.

Peptides are especially enticing for use as a method of therapeutic targeting due to their small size and ease of production. One area of study has focused on utilizing the natural capacity of certain peptides derived from toxins, viruses, and bacteria to enter the central nervous system (CNS) for enhancing delivery of therapeutics to brain tumors [44]. Though most of these peptides are used for more broadly enhancing delivery to the entire CNS rather than the tumor itself, some

peptides have been demonstrated to selectively bind brain tumor cells relative to healthy brain and peripheral tissue. Perhaps the most well-known peptide in this category is chlorotoxin, a 36-amino acid peptide found in the venom of the deathstalker scorpion. Originally isolated in 1993 by DeBin et al [90], chlorotoxin was first reported as having the capacity to bind astrocytoma cells in 1996 by Nicole Ullrich in Harald Sontheimer's group [91] and was then thoroughly characterized by Susan Lyons in the same lab in 2002 for its capacity to selectively bind brain tumor cells while having no affinity for healthy tissues [92].

Brain tumors composed of cells originating from the neuroectoderm during fetal development such as astrocytoma, medulloblastoma, meningoma, and others were also bound by chlorotoxin [92]. Interestingly, it was observed in glioma that the number of malignant cells chlorotoxin bound to was directly related to the severity of the tumor, with chlorotoxin binding >95% of cells of grade IV samples (GBM). The selectivity of chlorotoxin for tumors was highlighted when 17 healthy tissue types were examined, including uninvolved brain tissue, and were found to have no affinity for chlorotoxin [92]. Other tumor types of neuroectodermal origin were also tested for recognition by chlorotoxin in the same study, including small cell lung carcinoma, melanoma, and Ewing's sarcoma. The characterization of chlorotoxin binding by the Sontheimer lab greatly broadened our appreciation of the possible uses for chlorotoxin in enhancing targeting of therapeutics and imaging agents to tumors. Finding that such a highly selective peptide for GBM and other malignant neoplasms is unable to bind healthy tissue highlights its potential value for targeted therapy.

Chlorotoxin also maintains other interesting properties that make its use as a pharmaceutical agent compelling. Some preclinical evidence points to the possibility that chlorotoxin has the capacity to breach the BBB. Using a transgenic mouse model of medulloblastoma which arises spontaneously and grows without BBB disruption, Veiseh *et al* first demonstrated that the BBB remained intact via contrast-enhanced MRI and via injection of Evan's blue, a molecule that is unable to cross the BBB [93]. In these studies, they demonstrated that in the presence of an intact BBB, chlorotoxin conjugated to Cy5.5 was capable of entering brain

parenchyma and binding to the medulloblastoma cells. These data indicated that chlorotoxin could not only bypass the BBB, but that it could do so with a payload covalently attached.

Chlorotoxin has since risen as a novel ligand for enhancing visualization of malignant cells that would otherwise be invisible to a neurosurgical team. One such product created for this purpose is marketed as Tumor Paint, first developed by Dr. James Olson at the Fred Hutch Research Center in Seattle, WA and commercialized by Blaze Biosciences [94]. Tumor Paint (sometimes referred to as *tozuleristide*) incorporates a chlorotoxin-like ligand with optimized molecular structure [95]. The modified version was designed to have enhanced circulation time via peptide circularization and to have a single amino group for ensuring monoconjugation of small molecules via lysine substitution to arginine for two of the three lysine residues found naturally in the peptide. In the case of Tumor Paint, it is conjugated to the infrared dye Cy5.5 for selective visualization in the tumor resection field with a specialized fluorescent imaging system. This novel molecule has been shown to be effective in imaging GBM when injected intravenously in murine models [94,96]. Phase I-III trials in humans to evaluate safety, pharmacokinetics, ability to label tumor cells in ambiguous tissue, and ability to assist in complete tumor resection following intravenous injection are ongoing or awaiting publication of results [97–101].

Other potentially useful peptides are abundant in nature. Several “chlorotoxin-like” peptides have since emerged that have been extracted from other scorpion venoms, including BmK CT from the venom of the Chinese scorpion *Buthus martensii* (Karsch) [102] and AaCtx from *Androctonus australis* [103]. While some evidence of therapeutic use has been found, thorough characterization of their selectivity for malignant vs healthy cells has yet to surface. In bacteria, no specific peptides have been identified, though some evidence exists that several full-sized bacterial proteins achieve CNS entry, with the heavy chains of the tetanus toxin derived from *Clostridium tetani* being the most noteworthy [104]. Even more useful ligands have been derived from proteins of neurotropic viruses. Rabies is of particular interest due to its well-characterized capacity to infect the CNS [105]. Entry is mediated via transport from peripheral to central neurons via the rabies virus glycoprotein (RVG). Several key studies, including one

described in the next chapter, have evaluated the use of RVG-derived peptides to enhance delivery of various therapeutics to the CNS with mixed success [106].

1.7. Methods of recombinant protein production

To enable the testing of pathogenic ligands in their capacity to enhance treatment of CNS disease, the economical and efficient production of peptides and related proteins in research laboratories is of special importance. When producing proteins for therapeutic use, a myriad of platforms are available for expression, purification, and related processing. Choosing which platform to use can depend on the yield and purity desired, protein structure, post-translational modifications, and presence of disulfide bonds in the protein of interest. The platforms used most commonly for proteins to be used clinically rely on expression in mammalian cell suspension cultures, such as HEK293 (derived from human kidney epithelium) and CHO (derived from Chinese hamster ovarian cells) cell lines [107]. Other platforms are becoming more popular, including expression in the tobacco relative *Nicotiana benthamiana*. Each platform and their merits and pitfalls are discussed here in detail.

In the laboratory, expression of recombinant proteins is commonly performed in *Escherichia coli* for basic science studies to investigate structure, function, and to investigate preclinical efficacy. *E. coli* is especially useful here due to the ease of cloning and transfection, the wide variety of commercially available vectors, extremely rapid cell growth, fast expression (within hours), scalability, and typically high yield (mg-g/L). However, *E. coli* is incapable of eukaryotic post-translational modification, thus the production of glycosylated proteins, for example, must be performed in a different system. Because prokaryotes have no endoplasmic reticulum (ER), proteins with disulfide bonds are also difficult to produce in a functional form. Targeting to the periplasm's oxidative environment, co-expressing disulfide bond isomerases, or using specialized commercial strains that contain mutations in thioredoxin reductase and/or glutathione reductase may improve correct disulfide production for some recombinant proteins. Production of *E. coli* produced proteins can be easier, which is an advantage. However, due to the natural presence of highly inflammatory molecules such as LPS (endotoxin) within the

bacterial outer membrane, careful purification is essential. Improperly purified proteins produced in *E. coli* can potently activate the immune system which can result in anaphylaxis when present in high concentrations of substances injected intravenously. LPS is very difficult and costly to remove to clinically acceptable levels [108], thus pharmaceutical production of protein therapeutics is typically produced in other systems.

Protein expression in yeast cells shares commonality with *E coli* in that rapid cell growth and high protein yields contribute to the popularity of the system [109]. For producing proteins for preclinical testing for humans, yeast suffer from an increased variety of possible glycosylation profiles which presents an immunologic risk for use in humans. To counter this issue, genetically engineered yeast were created to produce a glycosylation profile closer to humans [110].

More recently, the use of plants to express proteins for structural, preclinical, and clinical studies has gained attention. In 2012, ELELYSO, recombinant human beta-glucocerebrosidase for the treatment of Gaucher's disease, became the first plant-derived protein pharmaceutical (biologic) to be approved for commercial use in humans by the FDA [111]. Even more recently, large scale clinical trials have been conducted in western Africa with ZMapp, an antibody cocktail used as a passive immunization for treating Ebola infection for which first in human trials received emergency FDA approval during the 2014 major outbreak [112–114]. The three antibodies that construe ZMapp are produced in *N. benthamiana*, a relative of the common tobacco plant that is useful for its fast growth and high biomass [115]. Production of correctly-folded and fully functional eukaryotic (including human) proteins is facilitated by the plant's ER for disulfide bond formation and post-translational modification. Importantly, plant-specific post-translational modification (fucosylation and xylosylation) of N-glycan core structures shared with humans can be reduced though the use of transgenic *N. benthamiana* plants [116,117]. These transgenic plants lack expression of α1,3-fucosyltransferase and β1,2-xylosyltransferase, the enzymes responsible for fucosylation and xylosylation, respectively. As a result, recombinant protein containing N-linked glycosylation sites are produced as a homogenous N-glycan species containing only the core N-glycan (N-acetylglucosamine disaccharide) rather than a mixture of

glycan modifications [116]. This, in turn, reduces the chance of engaging an unwanted immune response against proteins used in the clinic [118].

Proteins produced in plants can be purified from plant tissue for injectable use, though edible protein therapeutics are also being developed, notably for vaccination strategies. Some of the highest yields of recombinant protein expression are reported in plants following transient expression using plant virus-derived vectors, including vectors developed by Hugh Mason's lab that are based on the genomes of Geminiviruses. Using these vectors, recombinant proteins can be produced on the order of ~1 gram of protein per kilogram of leaf material due to various genetic elements borrowed from other organisms and viruses for enhancing translation and preventing gene silencing, among others [119]. Transient expression in *N. benthamiana* is typically achieved via agrobacteria-mediated delivery of the plasmid encoding the gene of interest (GOI). *Agrobacteria tumefaciens* is a known plant pathogen that can transfer genetic material from plasmid DNA through its double membrane envelope, the plant cell wall and plasma membrane, and into the plant cell nuclear envelope where it is incorporated into the genome [120]. This naturally-occurring example of cross-domain horizontal gene transfer can be exploited for introducing GOI DNA into plant cell nuclei resulting in transient gene expression or stable transformation of the plant genome [121]. For proteins that are of interest for long term study and are non-toxic to the plant itself, transgenic *N. benthamiana* can be produced that can be easily propagated by seed and do not require agrobacterial introduction. At least one facility in the United States, Kentucky Bioprocessing, is capable of large scale agrobacterial infiltration of *N. benthamiana* for protein production, where it produces therapeutic proteins, cosmetics, and nutritional supplements [122].

For proteins that are difficult to express in *E. coli* and yeast, researchers often turn to insect cell-based expression vectors. Production in insect cells is typically mediated by baculovirus-driven expression and provides the advantage of glycosylation compared to bacterial-produced protein, however, like plants, the glycosylation profiles differ significantly from human profiles. More commonly, baculovirus use in insect cells is especially useful for producing virus-like particles (VLPs) and is notable for being the system used to produce the VLP-based HPV

vaccine, Cervarix™ [123]. The baculovirus process is innately more time consuming relative to bacterial expression, requiring transfection of insect cells with a plasmid of interest to produce a baculovirus stock, followed by subsequent transfection of a new stock of insect cells for protein production [124]. As a benefit, expression in insect cells is typically more cost-effective than expression in other eukaryotic systems and requires only standard cell culture equipment, in comparison to plant-based production which can require specialized plant growth chambers or greenhouses, or mammalian cell production which requires expensive media, discussed below.

For production of proteins for clinical testing, mammalian cell lines are often preferred by pharmaceutical companies on a large scale. The Chinese hamster ovary (CHO) and human embryonic kidney 293 or 293T (HEK293/HEK293T) cell lines are widely used by researchers due to their capacity for post-translational modification and formation of disulfide bonds, lack of pathogenic and animal contaminants, purification ease, and scalability as suspension cultures [107]. Both systems suffer from the low yield relative to production in *E. coli* and from the expensive transfection and cell culture reagents required for producing useful quantities of recombinant protein. Though creating stably transfected lines reduces costs of transfection reagents, the cost of medium that allows for sufficient growth in the absence of animal products, such as fetal bovine serum, becomes cost-prohibitive; serum-free medium can be up to 10 times the price of unsupplemented medium. For pharmaceutical companies, production of therapeutic proteins must be produced in these conditions in order to minimize production-related immunological side effects. Other mammalian cell lines used for pharmaceutical grade protein production include NS0, Sp2/0, BHK, and HT-1080 [107], but are less well known in academic research labs due to a lack of published protocols and available reagents in comparison to HEK and CHO expression.

Choosing between the CHO and HEK expression systems depends on the user's end requirements; CHO cells are often used for high expression of proteins via stable transfection, while HEK cells are more widely used for transient transfection due to its permissivity to common transfection reagents. HEK cells are thus useful for studying functionality and interactions of different proteins and their variants. Other factors must be taken into consideration, however,

regarding the end use of the protein of interest. Proteins produced in CHO cells suffer from a non-human glycosylation profile, ruling CHO expression out for glycosylated proteins unless an immune response against the protein is desired [125].

An upcoming option for producing proteins without the need for significant purification is cell-free protein expression. This technology works by utilizing only the components required for protein synthesis (DNA, ribosomes, tRNA, etc.) and completing synthesis in the appropriate conditions in a test tube. While this technology is especially desirable for proteins that are difficult to purify, the current protocols, throughput, yield, and expense of these methods are currently prohibitive towards producing useful quantities of proteins even for sufficient biochemical characterization, let alone preclinical testing [126].

1.8. Overview and specific aims

Given the significant barriers for effective treatment of GBM, it is clear that highly targeted, potent therapeutics capable of reaching both core and invasive, highly heterogeneous cells are desperately needed. This document outlines two distinct methods for accomplishing this, with the overarching goal of enhancing GBM therapy using naturally-derived peptides known to improve access to the brain. In chapter 2, we test the hypothesis that a small peptide derived from the rabies virus glycoprotein (RVG29) can improve delivery of polymeric nanoparticles to the brain and reduce tumor burden and mortality in an orthotopic mouse model of GBM. In chapter 3, we introduce the concept and initial production of a new immunotherapy for GBM, anti-CD3/chlorotoxin (ACDClx), and test the hypothesis that this molecule can selectively enhance recognition of GBM cells by polyclonal T cells using the scorpion venom-derived peptide, chlorotoxin, and anti-CD3 antibody variable fragments for cell recognition. Chapter 3 also tests the hypothesis that ER-targeted ACDClx can be produced as a soluble protein in *N. benthamiana*. In chapter 4, we investigate the hypothesis that *E. coli* might be used to produce ACDClx in higher yields. This chapter also introduces a new variant, ACDClxΔ15, for treatment of GBM cells, and tests its capacity for GBM cell binding in vitro.

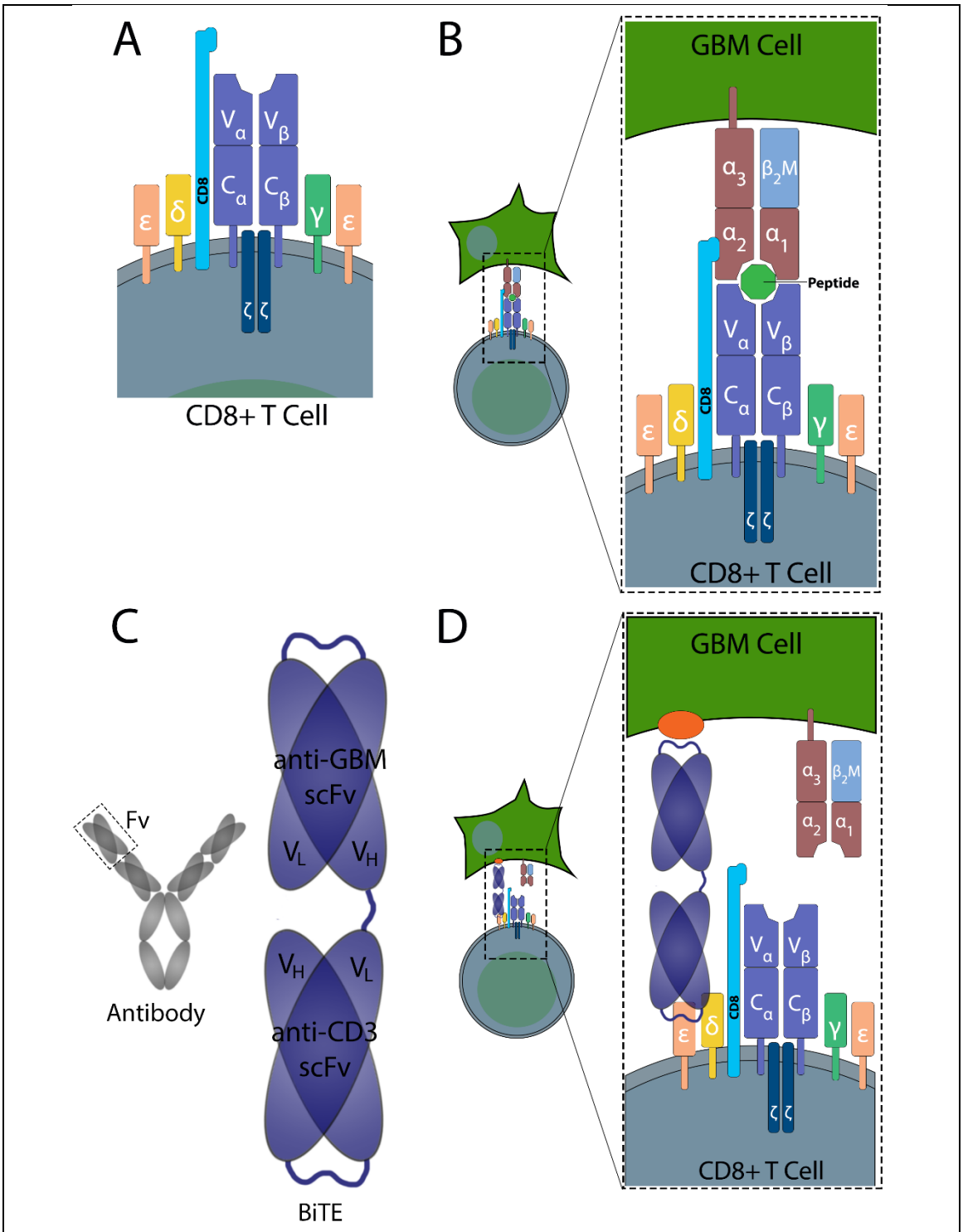

Figure 1: Schematic of TCR/MHC and BiTE interactions. (A) The T cell receptor complex of a CD8+ T cell. (B) A schematic of an interaction between a GBM cell expressing the MHC I receptor, presenting a peptide derived from a mutated GBM protein (mut) to a T cell with a mut-specific TCR.(C) A schematic of a bispecific T cell engager (BiTE). A traditional BiTE is composed two sets of variable light and variable heavy fragments (Fv) that recognize a tumor-specific protein and CD3 on a T cell. (D) Schematic of a GBM-specific BiTE engaging a GBM cell and a T cell without the need for traditional MHC/TCR interactions.

CHAPTER 2

A CRITICAL EVALUATION OF DRUG DELIVERY FROM LIGAND-MODIFIED NANOPARTICLES: CONFOUNDING SMALL MOLECULE DISTRIBUTION AND EFFICACY IN THE CENTRAL NERVOUS SYSTEM

2.1. Abstract

In this work, we sought to test how surface modification of poly(lactic-co-glycolic acid) (PLGA) nanoparticles with peptide ligand alters the brain specific delivery of encapsulated molecules. For biodistribution studies, nanoparticles modified with rabies virus glycoprotein (RVG29) were loaded with small molecule drug surrogates and administered to healthy mice by lateral tail vein injection. Mice were perfused two hours after injection and major anatomical regions of the CNS were dissected (striatum, midbrain, cerebellum, hippocampus, cortex, olfactory bulb, brainstem, and cervical, thoracic, lumbar and sacral spinal cord). For functional studies, surface modified nanoparticles were loaded with the chemotherapeutic camptothecin (CPT) and administered to mice bearing intracranial GL261-Luc2 gliomas. Outcome measures included tumor growth, as measured by bioluminescent imaging, and median survival time. We observed that small molecule delivery from PLGA nanoparticles varied by as much as 150% for different tissue regions within the CNS. These differences were directly correlated to regional differences in cerebral blood volume. Although the presence of RVG29 enhanced apparent brain delivery for multiple small molecule payloads, we observed minimal evidence for targeting to muscle or spinal cord, which are the known sites for rabies virus entry into the CNS, and enhancements in brain delivery were not prolonged due to an apparent aqueous instability of the RVG29 ligand. Furthermore, we have identified concerning differences in apparent delivery kinetics as measured by different payloads: nanoparticle encapsulated DiR was observed to accumulate in the brain, whereas encapsulated Nile red was rapidly cleared. Although systemically administered CPT loaded nanoparticles slowed the growth of orthotopic brain tumors

to prolong survival, the presence of RVG29 did not enhance therapeutic efficacy compared to control nanoparticles. These data are consistent with a model of delivery of hydrophobic small molecules to the brain that does not rely on internalization of polymer nanoparticles in target tissue. We discuss an important risk for discordance between biodistribution, as typically measured by drug surrogate, and therapeutic outcome, as determined by clinically relevant measurement of drug function in a disease model. These results pose critical considerations for the methods used to design and evaluate targeted drug delivery systems in vivo.

2.2. Introduction

Drug delivery remains a critical barrier to the treatment of central nervous system (CNS) tumors such as glioblastoma (GBM). The access of systemically administered drugs to cells residing beyond the primary tumor mass remains poor, and peripheral toxicity often limits total dose. A multitude of reports suggest that encapsulation of small molecules in nanoparticles can improve their delivery or function in the CNS [127–132], however, whether these improvements are due to actual movement of the nanoparticle across an intact blood-brain barrier (BBB) into the parenchyma remains unclear.

In the context of cancer, non-specific tumor targeting is achieved by the enhanced permeability and retention (EPR) effect, whereby nanoparticles circulating in peripheral vasculature are believed to exit leaky, angiogenic tumor vasculature to selectively accumulate in tumor core [133]. Surface modification of nanoparticles with targeting ligands has been proposed as a method for enhancing delivery of nanoparticle encapsulated payloads to specific tissue sites, including tumor or brain. Recently, a peptide derived from rabies virus glycoprotein emerged as a promising candidate for brain-targeted drug delivery. RVG29 is the 29 amino acid fragment of the rabies virus coat protein whose presence is both necessary and sufficient for the interaction of virus with cell surface receptors to promote retrograde transport of virus along motor neurons into the brain. RVG29 has been reported to govern the interaction of viral particles with at least three known receptors, including neural cell adhesion molecule (NCAM), the p75 neurotrophin receptor (P75NTR), and nicotinic acetylcholine receptors (NAChRs) [134,135]. NAChRs were suggested

to be responsible for the transvascular delivery of nucleic acids tethered to an RVG29-9R conjugate [136], although a recent report studying the uptake of RVG29-tethered dendrimers provided evidence for the involvement of gamma-aminobutyric acid B receptors ($GABA_BRs$) instead [137]. The RVG29 peptide has been demonstrated to enhance the brain-specific function of a range of systemically delivered agents, particularly nucleic acids [136,138–141] and has also been used to facilitate the CNS efficacy of nanoscale drug and gene carriers, including proteins and biologically derived or synthetic nanoparticles [142–148,137]. Notably, RVG29-mediated delivery of small molecule therapeutics remains relatively unexplored [148].

In prior work, we demonstrated that systemically administered nanoparticles composed of PLGA and loaded with the chemotherapeutic camptothecin (CPT) slowed the growth of orthotopic, murine GBM to prolong survival [33]. Improved therapy of nanoparticle encapsulated CPT was primarily mediated by EPR and increased dose due to enhanced tolerability of encapsulated drug. Here, we were interested to test how modification of PLGA nanoparticles with RVG29 would alter the delivery and efficacy of small molecule payloads in the brain.

2.3. Methods

2.3.1. Materials

RVG29-biotin peptide (sequence: N term-YTIWMPENPRPGTPCDIFTNSRGKRASNG-C2-Biotin) was synthesized by American Peptide Company (Sunnyvale, CA, USA). 50:50 Poly(DL-lactide-co-glycolide) (PLGA, ester terminated, 0.55 - 0.75 IV) was obtained from Durect Corporation (Cupertino, CA, USA). Reagents for nanoparticle preparation were purchased from Sigma-Aldrich (St. Louis, MO, USA). Cell culture reagents (DMEM, FBS, Geneticin) and DiR were purchased from Life Technologies (Carlsbad, CA, USA).

2.3.2. Nanoparticle Preparation

PLGA nanoparticles were prepared by the single emulsion method as described previously [33,149]. Avidin-palmitate conjugation was performed as described elsewhere [150]. Briefly, 25 mg of avidin was reacted with 1 mg palmitic acid-NHS overnight while stirring at 37°C

in 2% w/v sodium deoxycholate in PBS. The conjugate was purified by 48 hours of dialysis against 0.15% w/v sodium deoxycholate in PBS (MW cutoff of 14 kDa). For dye loaded nanoparticles (biodistribution studies), 200 mg of PLGA was dissolved in 2 mL dichloromethane (DCM) with either 50 µL of DiR in ethanol (25 mg/mL) or 100 µL Nile red (NR) in DCM (25 mg/mL). This solution was added drop-wise to a vortexing aqueous phase containing 1 mL 5 mg/mL avidin-palmitate, 1 mL H2O, and 2 mL 5% w/v polyvinyl alcohol (PVA) to form an emulsion. The emulsion was sonicated in three, ten-second bursts (Fisher Scientific Model 705 Sonic Dismembrator, 40% amplitude) and hardened for three hours by stirring in 84 mL 0.3% PVA. Particles were washed twice in diH2O by centrifuging for 15 minutes at 17,400 xg (Beckman L8-80M Ultracentrifuge, 50.2TI rotor). CPT nanoparticles were prepared using the same technique with the following parameters: 12 mg of CPT was added to 200 mg of PLGA in 2 mL DCM and emulsified with an aqueous phase containing 1 mL 5 mg/mL avidin-palmitate, 3 mL H2O, and 4 mL 5% PVA.

2.3.3. Nanoparticle Peptide Conjugation

For surface modification, nanoparticles were incubated with a 10x molar excess of RVG29-biotin (RVG-PLGA) or biotin (Biotin-PLGA) for one hour. Nanoparticles were washed by centrifugation to remove excess ligand. A small sample was removed for scanning electron microscopy (SEM) characterization and trehalose (25 mg per 100 mg PLGA) was added to the remaining nanoparticle solution as a cryoprotectant. The nanoparticle solution was either aliquotted for immediate use for in vivo studies or frozen, lyophilized, and stored at -80°C.

2.3.4. Nanoparticle Characterization

Nanoparticles were characterized for size and morphology with scanning electron microscopy (SEM, FEI XL30) and for hydrodynamic diameter with dynamic light scattering (DLS, NanoBrook 90Plus Zeta particle analyzer, Brookhaven Instruments, Hotsville, NY). Samples were prepared for SEM by sputter coating for 2 minutes with gold-palladium and imaged at a working distance of 5-15 mm, 2-10 kV, spot size of 1-5, and 10,000-40,000X magnification. Average

nanoparticle size for each batch was calculated from SEM images using the measure function in ImageJ (National Institutes of Health) with a minimum of 150 measurements from two or more images. Polydispersity (PD) was calculated by taking the standard deviation of these measurements, or the mean standard deviation if more than one batch was prepared. For DLS measurements, average and PD were calculated by Particle Solutions Software (Brookhaven Instruments, Hotsville, NY). Loading of DiR, NR or CPT was determined by comparing nanoparticle samples dissolved in DMSO at a concentration of 5 mg/ml to a control curve prepared from blank nanoparticles spiked with known concentrations of dye or drug in DMSO. Loading was calculated by determining the weight of encapsulated molecule per nanoparticle batch, and dividing this value by the weight of PLGA (non-encapsulated molecule, non-trehalose weight) per batch.

To obtain a profile of CPT release from nanoparticles, RVG-PLGA-CPT nanoparticles with an equivalent mass of 6.5 µg CPT were added to a total volume of 2 mL release medium (PBS + 2% Tween-80) for each time point to be measured. This concentration assured sink conditions (reported solubility of CPT in PBS + 2% Tween-80 is 79 µg/mL) [151,152]. Samples were incubated while rotating at 37°C. At each time point, corresponding samples were removed and centrifuged for ten minutes at 20,000 xg. 30 µL of supernatant was removed and mixed with 970 µL release medium. CPT fluorescence was measured at an excitation/emission of 370 nm/428 nm and compared to a standard of free CPT in release medium to determine concentration.

2.3.5. Cell Culture

GL261-Luc2 cells were a generous gift from Dr. Adrienne C. Scheck at Barrow Neurological Institute and were maintained in DMEM supplemented with 10% FBS and 100 µg/mL Geneticin in a humidified chamber at 37°C with 5% CO2. For tumor inductions, cells were washed, detached with trypsin, and centrifuged to obtain a pellet. Cells were resuspended in plain DMEM at a concentration of 3.75e7 cells/mL for injection.

2.3.6. Animal Studies

All mice were housed in a 12:12 light dark cycle with food and water provided ad libitum. Nanoparticles were administered via injection into the lateral tail vein either as freshly prepared (treatment studies) or immediately following resuspension via sonication in sterile saline (biodistribution studies). All experimental procedures were performed in compliance with Barrow Neurological Institute's Institutional Animal Care and Use Committee (IACUC) regulations.

2.3.7. Biodistribution

Nanoparticles were administered at a dose of 200-250 mg/kg to 6-8 week old female BalbC mice (Charles River Laboratories, USA). Subjects were sacrificed 2 hours post injection (n = 6 per group), and a blood sample was obtained by cardiac puncture. Mice were perfused with heparinized saline (10 U/mL) until the livers cleared. Peripheral organs were removed, as well as whole brain, which was immediately dissected into major anatomical regions (olfactory bulb, cortex, striatum, midbrain, hippocampus, cerebellum, and brain stem) with fine pointed forceps under a dissecting microscope. Surgical scissors were also used to make a cut at the lower lumbar portion of the spine and a 1 mL syringe filled with saline attached to a 22G needle was inserted into the spinal canal opening. Spinal cords were rapidly ejected following applied pressure to the syringe plunger [153]. Spinal cords were dissected into its major anatomical parts (cervical, thoracic, lumbar, and sacral) using the spinal cord intumescences as guides. All samples were frozen at -80oC until further processing. Values for cerebral blood volume in the mouse brain were obtained from published data for the mouse [154]. The cerebral blood volume value for brainstem was estimated by averaging the pons and medulla.

Peripheral organ tissue was thawed on ice and finely minced into a pulp. 10% w/v diH2O was added to each sample. Tissue was physically disrupted in a bead homogenizer for 10 minutes at the highest speed and lysed by probe sonication (40% amplitude for 10 seconds, 2x) on ice. CNS tissue was processed by the same method, except samples were not bead homogenized. CNS homogenates (40 µL) and peripheral organ homogenates (50 µL) were added to a 96-well plate with 10 µL of DMSO. Fluorescence intensity was read on a plate

spectrophotometer (Tecan Infinite 2000, 750/780 nm or 552/636 nm excitation/emission for DiR or NR, respectively). To convert AU values to concentration, control curves were constructed for each organ by spiking control tissue homogenates with known quantities of DiR-loaded nanoparticles. All samples were read in triplicate. In multiple experiments, we confirmed that there were no differences in control curve fluorescence for different CNS regions for tissue spiked either with free or nanoparticle encapsulated DiR (data not shown).

2.3.8. Treatment Study

The syngeneic GL261-Luc2 tumor model used in this study is an infiltrative model of GBM [155] that has been stably transfected with luciferase to enable noninvasive monitoring of tumor growth by bioluminescent imaging. Tumors were induced in the dorsal striatum of C57Bl/6 albino mice as previously described [33]. Briefly, mice were anesthetized using a cocktail of ketamine (100 mg/kg) and xylazine (10 mg/kg) provided by intraperitoneal (IP) injection. An incision was made down the midline of the scalp to expose the skull and a hole was drilled 2 mm lateral, 0.1 mm posterior from bregma using a Dremel (Mount Prospect, IL). A Hamilton syringe filled with 2 µL of the cell suspension (75,000 cells) was lowered to a depth of 3 mm and the tissue allowed to equilibrate for 1 minute. The syringe was then withdrawn to a depth of 2.6 mm and the cells injected over 2 minutes. After the injection, the syringe was left for 1 minute before it was removed to reduce back flow. The incision was closed using staples and triple antibiotic ointment was applied to the scalp before placing the animal in a clean cage over a heating pad to recover. All animals received a subcutaneous injection of buprenorphine SR (Reckitt Benckiser, Hull, England) (0.2 mg/kg) after surgery to control pain.

Weekly treatments were administered by lateral tail vein injection beginning on day 8 after tumor induction. Animals were randomized to four treatment groups: saline (n=6), RVG-PLGA (n=5), Biotin-PLGA-CPT (n=6), or RVG-PLGA-CPT (n=6). Drug treated mice received an average of 12 mg/kg CPT (RVG-PLGA-CPT or Biotin-PLGA-CPT) per injection. The RVG-PLGA group was dosed based on the average equivalent PLGA dose administered to Biotin-PLGA-CPT

and RVG-PLGA-CPT groups. Mice were observed daily and euthanized following greater than 20% weight loss or development of neurological symptoms.

Tumor growth was monitored throughout the study using an In Vivo Imaging System (IVIS) bioluminescent imager (Perkin Elmer, Waltham, MA), a method which has been well-validated for the GL261-Luc2 model and allows for tumor detection by day four following tumor induction [156]. Mice were anesthetized in an induction chamber under 2% isoflurane in oxygen. Once anesthetized, mice were injected subcutaneously with 150 mg luciferin/kg body weight and imaged 25 minutes later. Tumor size was measured by total flux (photons/second) as determined by the Living Image software for each region of interest (ROI) drawn around the tumor signal.

2.3.9. Statistics

Statistical analyses were conducted in GraphPad Prism 5.0 (GraphPad Software, Inc., La Jolla CA). Analysis of targeting to whole organs was conducted using a one-tailed Student's t-test. Regional analysis of biodistribution was conducted with a two-way, repeated measures (mixed model) ANOVA followed by a Student's t-test with a Bonferroni posthoc correction for multiple comparisons. Tumor growth profiles were fit by an exponential growth equation with ordinary least squares to estimate doubling time. Kaplan-Meier curves were constructed for treatment studies, using the Mantel-Cox test to probe for differences in survival. Significance is reported for an alpha level of 0.05.

2.4. Results

2.4.1. Nanoparticle characterization and biodistribution

SEM imaging confirmed that PLGA nanoparticles were spherical with smooth surface morphology (Figure 2). DiR, NR and CPT loaded nanoparticles were characterized by a similar average diameter (129-141 nm, 111-132 nm, and 134-142 nm±10 nm, respectively, Table 1). Loading, calculated as the average weight percent of encapsulated molecule in the final yield of PLGA, was 0.26% for DiR, 0.87% for NR, and 6.87% for CPT, with encapsulation efficiencies of 38.1%, 54.6%, and 80.3%, respectively. Surface charge was close to neutral. The rate of CPT

release was determined by incubating RVG-PLGA-CPT nanoparticles in PBS and centrifuging at regular time intervals to sample supernatant. A burst release was observed at early time points, with almost all remaining camptothecin released by 3 hours (Figure 3), whereas less than 5% of NR or DiR was released in 24 hours (data not shown).

To measure biodistribution of nanoparticle payload, we first analyzed the delivery of DiR from nanoparticles administered by injection into the lateral tail vein of healthy mice. DiR was detected two hours following intravenous administration in the kidneys, liver, lungs, heart, femur muscle, and uterine horns (Figure 4). The greatest amount of DiR was detected in the liver (13.9 µg/g and 13.1 µg/g for biotin-PLGA-DiR and RVG-PLGA-DiR, respectively), followed by the lungs (4.52 µg/g and 4.35 µg/g, for biotin-PLGA-DiR and RVG-PLGA-DiR respectively). No significant differences in delivery were observed for RVG29- versus biotin-modified nanoparticles in any peripheral organs or blood plasma. DiR was detected readily in the brain at a concentration of 79.5 ng/g and 101 ng/g for biotin- versus RVG29-modified formulations, respectively. RVG29-modification of nanoparticles thus produced a 27% increase in delivery to the brain at two hours, which was significant ($p=0.041$, Student's 1-tailed t-test). In whole spinal cord, DiR was detected at 51.4 ng/g for both RVG29- and biotin-modified formulations. Thus, delivery to the spinal cord was lower than delivery to the brain, and no enhancement due to RVG29 was observed. To determine whether the brain targeting effects reflected some unique feature of the DiR payload, we also evaluated the brain-specific delivery of other encapsulated small molecules, including coumarin 6 and NR. These data demonstrated that the targeting effects were consistent, if not higher, for different payloads; significantly increased delivery (40-60%) was observed in the brain two hours after injection for these agents in multiple experimental repeats (Supplementary Figure 1).

We were interested to determine whether there would be differences in the quantity of payload delivered to major anatomical regions within the brain and spinal cord (Figure 5 and Table 2). A two-way analysis of variance (ANOVA) identified significant effects of CNS region ($F(10,90=21.19$, $p<0.001$) and significant interaction between CNS region and targeting ($F(10,90)=2.39$, $p=0.0145$) on delivered payload concentration. The highest delivery was detected

in the cortex for both RVG29- and biotin-modified formulations (123 versus 89.6 ng/g, respectively), followed by the cerebellum (98.8 versus 79.9 ng/g, respectively). We hypothesized that variations in payload delivery to different regions within the brain would be due to regional differences in blood volume; consistent with this hypothesis, the relationship between cerebral blood volume [154] and DiR delivered from nanoparticles was linear for both targeted and non-targeted formulations (Figure 6), with calculated Pearson correlation coefficients of 0.979 and 0.854 for biotin- and RVG29-modified nanoparticles ($p<0.01$ for both). For the spinal cord, payload delivery tended to increase slightly in the caudal direction (48.7, 49.9, 53.2, and 55.1 ng/g in cervical, thoracic, lumbar, and sacral segments). Some evidence for apparent targeting (i.e., increased delivery for RVG29- versus biotin-modified formulations) was observed in the cervical region of the spinal cord (15% increase for RVG29- versus biotin-modified nanoparticles), although mild decreases in delivery were observed for targeted formulations in thoracic, lumbar, and sacral regions. In contrast to the spinal cord, enhancements were observed consistently across all major brain regions for RVG29 modified nanoparticles, with each region displaying a higher concentration of DiR delivered from RVG29-modified nanoparticles than DiR from biotin-modified nanoparticles. The highest targeted delivery was observed in the cortex (36.8% increase) and cerebellum (23.6% increase), followed closely by the midbrain (22.4% increase) and striatum (21.4% increase). There was no relationship between targeting ratio by brain region and cerebral blood volume, which had a Pearson correlation coefficient of 0.246 (data not shown). For the RVG29-modified group, delivery was significantly lower to the striatum than many other brain regions, including cortex, midbrain, cerebellum, and brainstem (Figure 5A, $p<0.001$, 0.01, 0.001, 0.05, respectively, Bonferroni posttest).

2.4.2. Treatment of Intracranial Tumors with Targeted Nanoparticles

The next series of experiments were designed to test whether enhanced delivery via RVG29 targeting would enhance the efficacy of the encapsulated chemotherapeutic camptothecin (CPT). Syngeneic GL261-Luc2 tumors were induced in the striatum of immune competent mice. Saline, RVG-PLGA (drug empty nanoparticles), Biotin-PLGA-CPT, or RVG-

PLGA-CPT were administered on a weekly basis to match a 12 mg/kg CPT dose by injection into the lateral tail vein beginning 8 days after tumor induction. Consistent with prior work [33], encapsulated CPT was effective at slowing tumor growth compared to saline injected controls (Figure 7A and 7C). No differences in tumor growth were detected between RVG29 and biotin nanoparticle modifications. Median survival for saline, RVG-PLGA, Biotin-PLGA-CPT, and RVG-PLGA-CPT was 16.5, 19, 27, and 23 days, respectively (Figure 7B). Survival was significantly prolonged for Biotin-PLGA-CPT and RVG-PLGA-CPT treated subjects relative to either saline or RVG-PLGA controls ($p<0.05$ for each comparison), although RVG-PLGA-CPT did not prolong survival in comparison to Biotin-PLGA-CPT. Taken as a whole, these data demonstrate that encapsulated CPT slowed tumor growth, resulting in prolonged survival, but targeting did not enhance treatment efficacy.

2.4.3. Evaluation of apparent brain targeting kinetics

The biodistribution experiments suggested a consistent enhancement in delivery of small molecules from RVG29-modified nanoparticles 2 hours after injection. However, when we examined the biodistribution of DiR or NR loaded nanoparticles 6 hours after administration (Figure 8), the presence of the targeting ligand did not affect or even tended to reduce whole brain delivery of encapsulated payloads (targeting ratio, RVG29 average divided by biotin average, of 0.98 and 0.93 for NR and DiR experiments, respectively). The apparent targeting measurements were therefore reproducible at two hours and generalizable to at least three encapsulated small molecules, but targeting was not prolonged (i.e., no enhancements in delivery were observed after six hours). To test the aqueous stability of RVG29, mice were injected with nanoparticles that had been pre-incubated in saline at 37°C for four hours (Figure 8). No apparent targeting was observed two hours after injection of these pre-incubated nanoparticles (targeting ratio, RVG29 average divided by biotin average, of 0.96). To test whether aggregation accounted for this loss of targeting, a sample of nanoparticles was maintained at 37°C for 6 hours; DLS measurement confirmed that the average hydrodynamic diameter did not increase over time (Supplementary Figure 2). Additional loss in targeting may occur in vivo via formation of

a protein corona on the outer surface of the nanoparticle [157]. This was not investigated since incubation in saline was sufficient to remove the targeting ability of RVG29-modified nanoparticles. In the process of debugging the lost targeting, we conducted kinetic experiments that measured the delivery of different payloads over multiple time points. These experiments demonstrated that NR and DiR produce opposite interpretations of apparent nanoparticle delivery. For NR-loaded nanoparticles, we observed rapid clearance of NR from the brain, whereas, for DiR-loaded nanoparticles, we observed an apparent accumulation of DiR in the brain over time (Figure 9a). When free DiR was administered by tail vein injection, the brain signal also increased over time (Figure 9b), with free DiR accounting for up to 38% and 40% of the signal at 30 minutes and 6 hours, respectively. To our knowledge, brain measurements following an injection of free DiR have not been reported in literature. Brain accumulation of DiR following administration as a bolus intravenous injection was not expected and is not typical kinetic behavior for a small molecule. These data demonstrate that an increase in DiR signal over time does not necessarily reflect accumulation of the nanocarrier itself, and instead could be accounted for by the behavior of free (non-encapsulated) DiR.

2.5. Discussion

These studies are some of the first to measure quantitative differences in small molecule delivery to different tissue sites within the CNS for intravenously administered nanoparticles. Calvo and colleagues tracked the distribution of 14C-labeled, PEGylated polycyanoacrylated nanoparticles and identified significant within-CNS regional differences in delivery that would be expected to influence drug function [158]. In our experiments, nanoparticle-mediated delivery of encapsulated DiR from nanoparticles was also not uniform. For both targeted and non-targeted formulations, brain delivery was directly correlated to regional cerebral blood volume. Delivery magnitude to different regions varied by as much as 60-80% within the brain, and by as much as 150% across the entire CNS (e.g., cortex versus thoracic spinal cord). These differences suggest that the targeting ability of a nanoparticle would need to be high to overcome differences in small molecule exposure to specific brain regions as governed by blood flow, especially in GBM, where

EPR effects in the bulk tumor may easily mask small gains made from improved drug targeting to invading cells. Delivery to the striatum, where tumors were induced, was significantly lower than other brain regions, including other common sites for brain tumors, such as cortex, cerebellum, and brainstem. Further, we observed that apparent targeting to the cortex (which represented 44% of the total brain mass) was twice as high as the brain averages with cortex removed. High cortex values drive whole brain homogenate values, thus potentially misrepresenting the delivery of brain available agents that would occur for any disease not occurring in the cortex. Although the delivery of DiR would not be expected to represent the spatial pattern of delivery for all encapsulated molecules, these studies highlight the importance of considering CNS region in the development of new small molecule delivery strategies. It will be an interesting subject of future work to determine whether engineering strategies that enhance nanoparticle or drug interaction with defined regions of brain or brain vasculature [44] would improve exposure of circulating agents to specific CNS regions.

Nanoparticles have been studied extensively for their ability to deliver encapsulated agents selectively to the injured or diseased spinal cord, such as in neurodegeneration or inflammation [159–162]. By comparison, relatively little is known about the features that govern delivery of encapsulated agents from nanoparticles to intact spinal cord. The blood spinal cord barrier (BSCB) is often thought of as a physiological extension of the BBB, possessing non-fenestrated capillary endothelium, tight junctions, and efflux pumps. However, morphological and functional characteristics of barrier endothelial cells vary by location and are distinct in the spine relative to the brain [163]. Given that the rabies virus itself possesses tropism for motor neurons, we expected to observe targeting in the spinal cord. Nanoparticles delivered payload to spinal cord, however, no apparent enhancement in delivery from RVG29 was observed in the spinal cord. GABAB receptors, a class of proteins that were recently described as a potential binding partner for RVG29 [137], are present both on neurons and on the brain capillary endothelial cells that compose the BBB. Interestingly, relative to other brain regions, GABABR is reported to be highly enriched in the cortex and present in much lower quantities in hippocampus, bulk striatum, and spinal cord [164], which mirrors the patterns of apparent delivery enhancements observed for

RVG29-modified nanoparticles. Our data support a model of “targeting” whereby RVG29 modification of PLGA nanoparticles transiently enhances their affinity for the surface of brain endothelial cells via interaction with GABABRs. The fact that the enhancement in delivery observed for RVG29-modified nanoparticles is not maintained at later time points due to aqueous instability of the ligand further supports a non-internalization model of this apparent targeting. The association of RVG29-modified nanoparticles with the cell surface appears to be temporary.

Prior studies demonstrated the ability of RVG29 to improve the CNS efficacy of encapsulated or tethered nucleic acids and proteins [136–148]. In contrast, evidence for functional enhancement of small molecules via RVG29 remains minimal. Enhanced in vitro and brain uptake of the small molecule antifungal agent itraconazole was observed for RVG29-modified albumin nanoparticles [148], although this study did not evaluate therapeutic potency of the targeted formulation in vivo. Thus, the initial motivation for the studies described here was to determine whether RVG29 modification of nanoparticles would improve therapeutic efficacy of the chemotherapeutic agent CPT. CPT is a topoisomerase I inhibitor that is effective at killing cancer cells but is also hydrophobic, poorly bioavailable, and highly toxic [165]. The opportunity for improved therapeutic efficacy of CPT rests either on improving its tolerability, which would enable a higher dose, or improving its delivery, which would increase potency in target tissue. To deliver drug to tumor cells that do not reside in the leaky tumor core, nanoparticles would need to engage in prolonged interaction (either by uptake or surface residence) with cells to be effective. In accordance with prior work, we achieved a high loading of CPT in PLGA, which was sufficient to slow the growth of intracranial GL261 tumors when nanoparticles were administered systemically [33]. However, we did not observe any evidence that RVG29 enhanced CPT efficacy. There were no differences in either median survival or tumor growth between the targeted and non-targeted group. Although it is possible that small differences in tumor growth are masked by variability inherent in bioluminescent measurement, any such differences did not ultimately affect overall survival. Further analysis leads us to two important points of discussion: first, a critical examination of common methods used for evaluating new nanoparticle designs, and, second, insight into the

mechanisms by which brain-specific delivery of encapsulated small molecules appears to be achieved.

The most direct method for measuring the delivery of drugs from nanocarriers would be pharmacokinetic analysis of actual drug levels in tissue. Alternatively, fluorescent or radioactive labeling strategies can permit direct tracking of the nanoparticle itself [35,166]. Evaluation of new nanoparticle designs would ideally incorporate both measurements, since the techniques provide complementary information. However, these methods are not widely applied in tandem due to several important drawbacks. Both strategies require careful optimization of experimental approaches that are specific to drug or carrier. In the case of the direct labeling strategy, it is extremely important to validate that the label itself is stably attached to the carrier in a manner that does not alter the biophysical properties of the carrier. As an alternative to these expensive and difficult to implement strategies, nanocarrier vehicles are commonly loaded with small, fluorescent drug surrogates. Measurement of biodistribution is a comparatively simple technique that proceeds with one of two expectations: either, that the freely loaded small molecule is well-retained within the carrier, or, if it exits the nanoparticle, that its movement in tissue might be considered sufficiently typical of the drug of interest, possessing similar molecular weight or charge. Our data suggest that, in fact, these small molecule surrogates are not retained within polymer nanoparticles in vivo, and that their rate of delivery to tissue largely reflects their own ability move through biological environments. DiR, for example, experiences a highly deceptive accumulation in the brain, even in its free form. DiR and other carbocyanine dyes are commonly used to track delivery of nanoparticle formulations. Yet, their retention within or release from a nanocarrier would be expected to be highly specific to both the carrier and the lipid composition of its biological environment; the specific experimental approach of using carbocyanine dyes for biodistribution may need to be revisited. We suggest that certain biodistribution experiments may be useful to provide an indication of relative differences in nanoparticle residence time within single tissues of interest. However, it is clear that the distribution of a drug surrogate should only ever be interpreted in context with other measures of delivery.

We propose that different kinetics measured by different payloads can be explained by differences in the ability of molecules to transfer to and from biological membranes. NR is known to experience rapid cell to cell membrane transfer [167] whereas, as a carbocyanine family member, DiR is expected to be well-retained within lipid compartments [168]. Thus, NR delivered to cells would rapidly track the washout of nanoparticles from blood, whereas DiR would be relatively immobilized in cellular membranes, egressing slowly into the lipid rich environment of the brain. It has been proposed that small molecule delivery from nanocarriers is primarily mediated by direct transfer of payload from nanoparticle to cell in vitro, where the majority of small molecule delivery does not rely on active uptake of the nanoparticle [167,169]. Our in vivo data support this model, and suggest that apparent brain delivery may in fact reflect peripheral circulation of nanoparticles, either via direct transfer of encapsulated agent from nanoparticle to BBB cells or by enhancing drug source in the periphery.

Release of the active agent is an additional confounder that should be considered when using biodistribution measurements to interpret drug delivery [170]. For example, some molecules could release very quickly, before targeting effects become apparent, whereas others may be better retained, which could over-represent targeting as it would be expected for the actual drug. Ultimately, the release of an encapsulated molecule from its nanocarrier will depend on properties that are specific to the molecule, carrier, and its particular in vivo environment. Since in vivo measurement of drug release is not straightforward and cannot be directly predicted from in vitro data, this further complicates the use of drug surrogates in making decisions about nanocarrier design. As our data demonstrates, unexpected peculiarities of certain molecules could easily mislead (e.g., as evident in the brain accumulation of DiR). It is important to note that encapsulation of payload within a nanoparticle still provides drug delivery benefits that should be considered in the design of the nanoparticle (e.g., reduced toxicity, prolonged circulation time, etc.). This highlights the need for improved drug/drug surrogate retention in designing targeted formulations: slower release from long-circulating nanoparticle formulations will reduce drug clearance to enhance delivery in target tissue, whether this occurs by extracellular transfer or actual uptake of the carrier.

Targeted drug delivery to the brain has not yet achieved widespread success. Our results support a model of nanoparticle-mediated brain delivery whereby molecules are transferred non-specifically from nanocarriers to the brain in absence of significant internalization of the nanoparticle [167,169]. For the conditions tested, our data support a model whereby RVG29 enhances delivery of small molecules from PLGA nanoparticles due to transient enhancement in affinity of the nanoparticle for the surface of the BBB. It is possible that further engineering of the nanoparticle (e.g., different modification density, alterations to the peptide structure) could alter ligand functionality. By bringing nanoparticles in closer proximity to endothelial cells, payload gains a better ability to transfer directly into cells. Delivery is thus fundamentally driven by the particle to cell transfer and clearance processes that are unique to each small molecule payload of interest. These observations emphasize the challenge and importance of achieving substantial internalization of PLGA nanoparticles in target cells in vivo and also highlight major experimental considerations for evaluation of targeted drug carriers in tissue. We focused here on confounders in the analysis of PLGA nanoparticle biodistribution. However, these concerns may also apply to carriers (liposomes, micelles, etc.) where the drug surrogate being tracked is not covalently linked to the carrier and retention of the surrogate in the carrier has not been demonstrated in target tissue. We argue that functional evaluation of drug efficacy in the appropriate disease model would be best initiated at early stages of nanoparticle engineering.

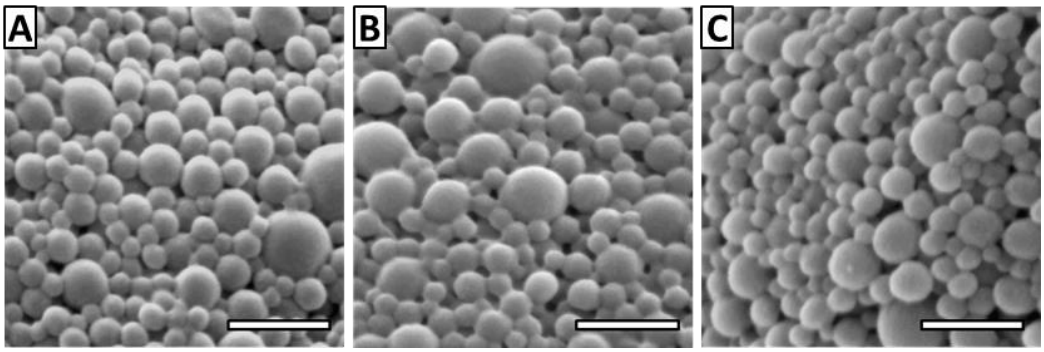

***Figure 2**: Nanoparticles were spherical and exhibited a smooth morphology. (A) RVG-PLGA-CPT and (B) Biotin-PLGA-CPT had an average diameter of 138±10 nm (n=3 batches). (C) RVG-PLGA nanoparticles had an average diameter of 156±36 nm (n=3 batches). Standard deviation represents variation between batches. Scale bar = 500 nm*

				SEM		DLS		
Name	Payload	Loading	EE[1]	Size[2] (nm)	PD[3]	Size (nm)	PD[3]	Zeta Potential (mV)
RVG-PLGA-DiR	DiR	0.26%	38.1%	129	36	188	44	0.36±1.76
Biotin-PLGA-DiR				141	31	238	56	1.69±0.95
RVG-PLGA-NR	NR	0.87%	54.6%	132	33	162	64	-0.88±2.98
Biotin-PLGA-NR				111	37	182	40	-3.35±1.89
RVG-PLGA-CPT	CPT	6.87±0.9%	80.3±7%	142±10	47	204	45	-2.50±1.19
Biotin-PLGA-CPT				134±10	43	252	31	-2.18±1.19
RVG-PLGA	None	N/A	N/A	156±36	64	253	69	-2.71±1.33

[1]Encapsulation Efficiency
[2]Error expressed as standard deviation of three batches
[3]Polydispersity (PD) expressed as standard deviation of the size distribution, averaged across experimental repeats

***Table 1**: Characteristics of nanoparticles used in biodistribution and treatment studies*

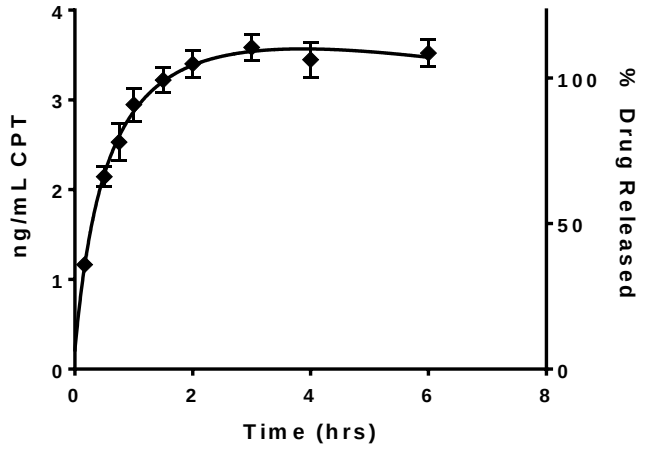

***Figure 3**: Camptothecin is released from RVG-PLGA-CPT nanoparticles within 3 hours. Error bars for individual time points represent standard deviation of three independent measurements.*

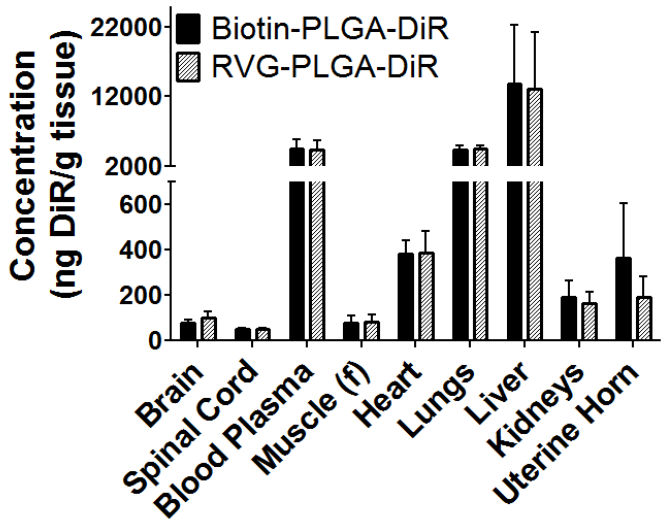

***Figure 4**: Biodistribution of Biotin-PLGA-DiR and RVG-PLGA-DiR nanoparticles in peripheral organs two hours post-injection. Error bars represent standard deviation (n=6 mice/group). (f) = femur*

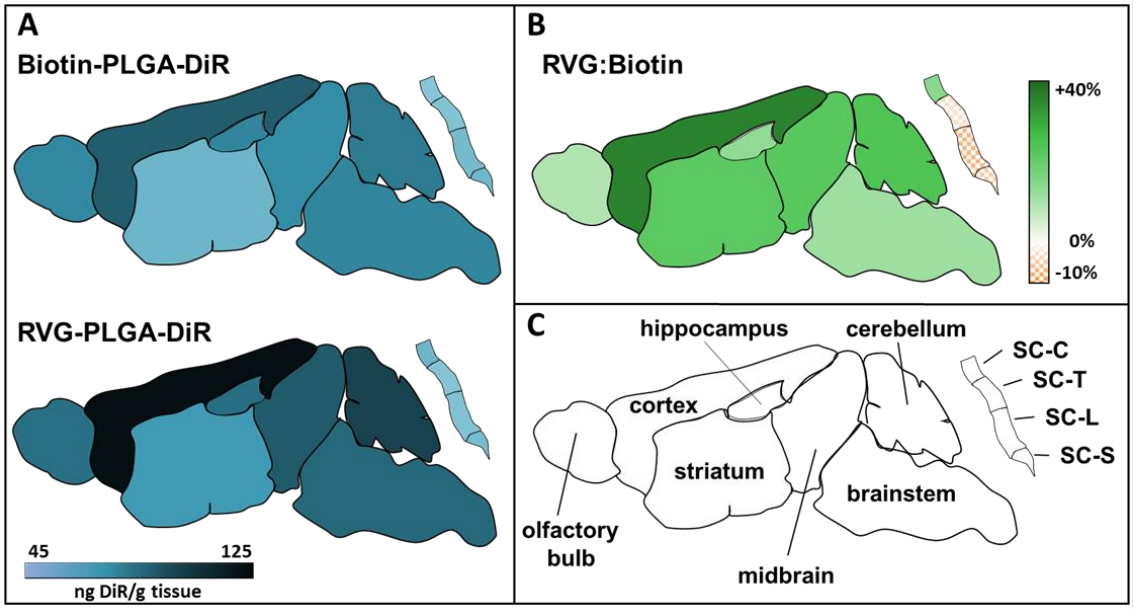

***Figure 5**: The distribution of targeted and non-targeted DiR nanoparticles varies by brain region. (A) Average total payload delivered to each brain and spinal cord region (ng DiR/g tissue) (n=6 per group). (B) Overall targeting effect of RVG-PLGA-DiR relative to Biotin-PLGA-DiR. (C) Map of brain and spinal cord regions, sagittal view. SC=Spinal Cord; C=Cervical, T=Thoracic, L=Lumbar, S=Sacral.*

Region	Biotin[1] (ng/g)	RVG[1] (ng/g)	Targeting[2]
Whole Brain	79.5 ± 10.8	101 ± 25.1	27.0%
Striatum	55.9 ± 10.7	67.9 ± 27.0	21.4%
Midbrain	73.9 ± 22.3	90.4 ± 25.8	22.4%
Olfactory Bulb	76.4 ± 13.0	83.2 ± 23.2	8.94%
Brainstem	76.9 ± 17.3	85.6 ± 14.5	11.3%
Cortex	89.6 ± 16.7	123 ± 36.4	36.8%
Hippocampus	62.9 ± 5.74	71.1 ± 16.2	13.0%
Cerebellum	79.9 ± 15.3	98.8 ± 13.1	23.6%
Whole Spinal Cord[3]	49.6 ± 4.18	51.4 ± 2.81	0.04%
SC-C	48.7 ± 8.69	55.8 ± 6.34	14.5%
SC-T	49.9 ± 3.89	48.5 ± 2.86	-2.74%
SC-L	53.2 ± 8.24	49.5 ± 5.89	-6.86%
SC-S	55.1 ± 2.07	52.4 ± 6.20	-4.93%

[1]Average ± SD, n=6 mice per group
[2]Targeting is defined as the percent increase or decrease in RVG average relative to biotin
[3]SC=Spinal Cord; C=Cervical, T=Thoracic, L=Lumbar, S=Sacral.

***Table 2**: Concentration of DiR as delivered from RVG29- and biotin-modified nanoparticles, measured within specific regions of the CNS*

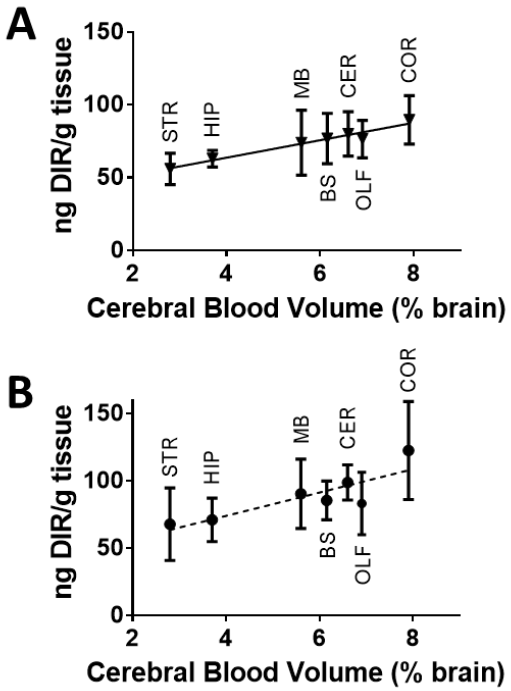

***Figure 6**: Regional blood volume correlates with payload distribution in the brain delivered by (A) RVG-PLGA-DiR and (B) Biotin-PLGA-DIR. Cerebral blood volume represents percent volume of blood per volume of brain tissue, obtained from published data for the mouse* [154]. *STR=Striatum, HIP=Hippocampus, MB=Midbrain, BS=Brainstem, CER=Cerebellum, OLF=Olfactory Bulb, COR=Cortex.*

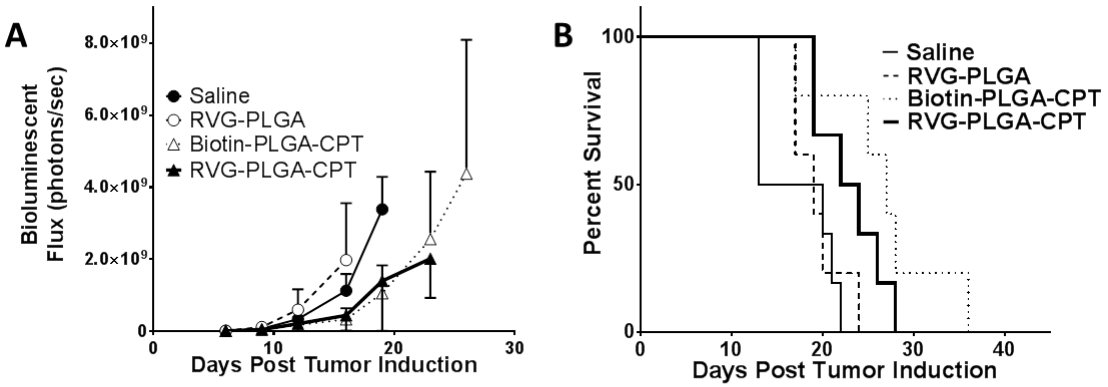

C

Group	Subjects (n)	Tumor Doubling Time (days [95% CI])	Median Survival (days)
Saline	6	2.46 [2.41, 2.52]	16.5
RVG-PLGA	5	2.50 [2.38, 2.64]	19
Biotin-PLGA-CPT	5	3.14 [3.01, 3.29]	27
RVG-PLGA-CPT	6	3.15 [2.99, 3.34]	23

***Figure 7**: PLGA nanoparticles encapsulating camptothecin slow tumor growth and prolong survival in vivo. (A) Normalized growth of GL261-Luc2 brain tumors monitored by IVIS, represented in photons/second. (B) Kaplan-Meier survival curve. (n=5-6 per group). (C) Summary of treatment study results. Tumor doubling time is represented in days with 95% confidence intervals shown in brackets.*

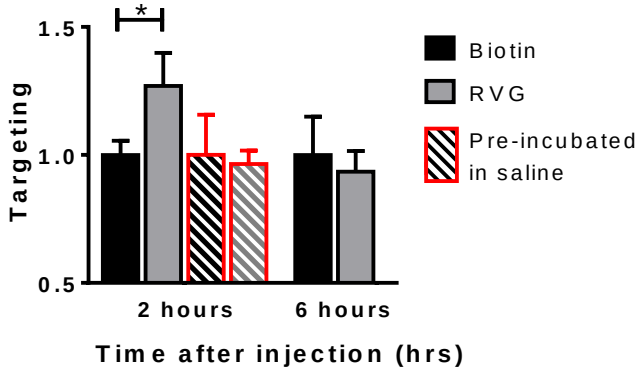

***Figure 8:** Loss of apparent targeting is observed after two hours in solution or in circulation. RVG-PLGA-DiR or Biotin-PLGA-DiR was injected via tail vein immediately after resuspension and measured in the brain after two or four hours in circulation (solid bars). In a separate group of mice, RVG-PLGA-DiR or Biotin-PLGA-DiR was resuspended in saline and incubated at 37°C for four hours, then injected into the tail vein and measured two hours later, for a total of six hours in solution (striped bars). n=5 mice per group. Ratios are normalized to biotin control for each condition measured.*

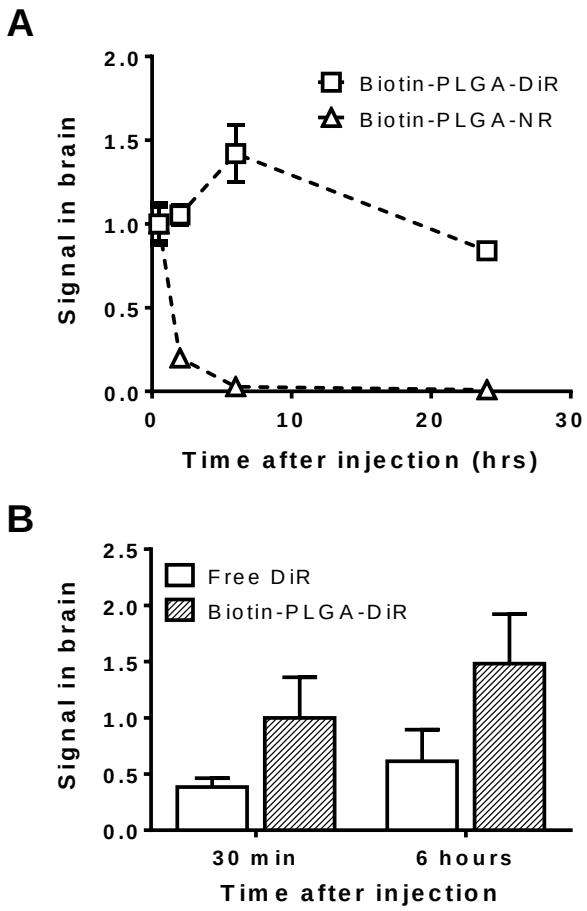

Figure 9: *Different nanoparticle payloads yield different apparent brain delivery kinetics. (A)NR or DiR loaded nanoparticles were administered to healthy mice and fluorescent signal was measured in brain homogenate. (B) When free DiR is administered to healthy mice, accumulation is observed in the brain, which accounts for ~40% of the signal detected for mice provided with an equivalent dose of DiR loaded nanoparticles. The same data are represented in each panel for the Biotin-PLGA-DiR group. Plots shown mean with error represented as standard error with 6 mice/group for Biotin-PLGA-DiR and 3 mice/group for all other conditions.*

CHAPTER 3

DESIGN, EXPRESSION, AND TESTING OF AN ANTI-CD3/CHLOROTOXIN T CELL ENGAGING MOLECULE, ACDClx, PRODUCED *IN PLANTA*

3.1. Abstract

Therapeutics capable of selectively enhancing destruction of malignant cells are desperately needed to improve patient survival and wellbeing within the setting of GBM. Clinical studies have observed that an anti-tumor immune response can be initiated following treatment with immunotherapies, however, this response is not prolonged due to rapid evolution of the tumor away from therapies designed to target antigen expressed on only a small population of tumor cells. To enhance immune cell recognition and killing of the majority of GBM cells, we have designed a bispecific T cell engaging fusion protein composed of an anti-CD3 variable fragment domain for engaging T cells and a chlorotoxin domain for engaging GBM cells, known as anti-CD3/chlorotoxin, or ACDClx. Chlorotoxin has been shown in preclinical studies to selectively bind GBM cells relative to healthy tissues and is in clinical development for GBM therapy and imaging. Here, we describe the design and expression of ACDClx in the plant host, *Nicotiana benthamiana.* ACDClx consistently expresses as an insoluble protein regardless of the addition of solubility-enhancing modifications, including N-glycosylation and fusion with cholera toxin subunit B. Purified, refolded ACDClx was shown to induce selective T cell activation only when co-incubated with GBM cells *in vitro*. These results indicate that further development and testing of ACDClx as an immunotherapy is warranted.

3.2. Introduction

Glioblastoma is a fatal form of brain tumor for which no curative treatments are available. Patients diagnosed with GBM have a mere 5% chance of surviving 5 years, and most patients receiving standard of care treatment (surgery, radiation, chemotherapy) will suffer from recurrent GBM one or more times before ultimately succumbing to the disease. The poor outcomes are mainly due to the rapid evolution of chemotherapy-resistant malignant cells within the tumor population, the well-characterized invasion of cells into healthy peripheral brain tissue, and the inability for most chemotherapeutics to cross the blood-brain barrier. Extensive research over

decades has thus far resulted in only a meager increase in life expectancy and quality for patients.

Recent progress in immuno-oncology has revealed the intricate involvement of the immune system in cancer. For GBM, the interplay of the immune system with malignant cell growth is consistently characterized as being overwhelmingly immune suppressive, resulting in a pro-tumor state where the tumor microenvironment favors neoplastic growth [45,55]. Although the immunosuppressive state observed in many GBM patients is thought of as an inability of the immune system to control tumor growth, this state can also be rationalized from an immune perspective of host defense. While GBM ultimately kills the host, the immune system is also ensuring that surrounding delicate brain tissue is not obliterated by an overeffective anti-tumor immune defense. The immune system accomplishes this by swaying the immune response from tumor cell killing to host-protective by reducing inflammation and recognition of target cells and promoting the survival of Tregs, which can ultimately kill or disable tumor-specific cytotoxic T cells [68–70]. Immune regulation in this context serves to preserve healthy tissue; unfortunately, GBM is well-known to co-opt the mechanisms used by regulatory cells and may even be responsible for initiating the process [11]. Overcoming immunosuppression while sparing healthy tissue and destroying malignant cells is thus the ultimate goal of GBM immunotherapy.

Several immunotherapies for GBM are being evaluated in clinical trials. Immune checkpoint blockade has been successful for many hematological and solid tumors, but results from clinical trials testing generalized blockade of the immune checkpoint protein PD-1, expressed on T cells, have yet to show benefit to GBM patients towards progression-free survival [21,22]. Targeted immunotherapies have also been tested, specifically against the tum or-specific antigen, EGFRvIII, a constitutively active mutant of EGFR expressed on the surface of a subpopulation of GBM cells in 30-40% of patients. Clinical trials evaluating the efficacy of an EGFRvIII vaccine [16,17,85] and a CAR T cell specific for EGFRvIII [19] have made strides in demonstrating that an anti-GBM immune response can be produced. However, both candidates have effectively failed following selective pressure on the EGFRvIII antigen within the tumor, resulting in targeted antigen loss and tumor recurrence. An additional immunotherapy platform for

targeting tumor antigens has also been developed for EGFRvIII and is based on the concept of a bispecific T cell engager (BiTE®, Amgen) [171]. BiTEs are composed of two opposing antibody-derived single chain variable fragments (scFv) expressed as a single polypeptide that serve to enhance T cell recognition of target cells via direct linkage irrespective of TCR specificity. This is accomplished by engaging T cells via CD3 within the TCR complex directly to the tumor cell target via a surface-expressed tumor antigen, inducing rapid and highly selective T cell-mediated killing of the target population. The EGFRvIII-specific BiTE® was first described by Choi *et al.* and was shown to be moderately effective in an immunocompromised mouse model of GBM [172]. Interestingly, they also investigated the effect of the BiTE® on Tregs and observed that these otherwise immunosuppressive cells could be redirected to kill GBM cells via the BiTE® due to CD3 engagement [173]. The results of these initial clinical and pre-clinical studies provide strong evidence that an immunotherapy-based approach is promising but that there is a significant need for targeting a more broadly-expressed antigen.

Chlorotoxin is a 36-amino acid peptide originally isolated from the venom of the deathstalker scorpion, *Leiurus quinquestriatus* and is non-toxic to humans. Chlorotoxin has been characterized as being highly selective for gliomas, especially GBM, while having no affinity for healthy tissues [92]. Although the receptor for chlorotoxin on GBM cells is unknown, it has been suggested that chlorotoxin binds GBM-specific chloride channels [174], MMP-2 [175], annexin A2 [176], or Nrp1 [177]. Regardless of receptor, the selective affinity for GBM and its capacity to bind over 95% of cells within GBM tissue samples [92] provide strong support for the use of chlorotoxin to enhance GBM therapeutics. Further support for its use as a therapeutic component comes from the stability of chlorotoxin, with the 36 amino acids forming a tight knotted structure stabilized by four disulfide bonds (PDB ID: P45639, see reference [178]), enabling chlorotoxin to be resistant to degradation in physiological conditions. These characteristics make chlorotoxin especially intriguing for development in pre-clinical and clinical research. As such, chlorotoxin is currently being developed for GBM-targeted radiotherapy and delivery of small molecules for treatment and tumor visualization.

The promise of immunotherapy for GBM combined with the exquisite selectivity of chlorotoxin inspired me to design a novel T cell engaging molecule, anti-CD3/chlorotoxin (ACDClx), that could enhance T cell recognition and killing of all or most cells within a GBM. Smaller than a traditional 50 kDa BiTE® due to the compact nature of chlorotoxin, this 32 kDa fusion protein may enable better penetration into solid tumor masses and consists of a scFv specific for the TCR complex protein, CD3ε, attached through its C-terminus via a flexible Gly_4Ser linker to chlorotoxin. To facilitate in the formation of the six disulfide bonds within ACDClx, we opted to transiently express ACDClx as an ER-targeted protein in *Nicotiana benthamiana*. This tobacco relative was previously demonstrated to support the expression, correct folding, and accumulation of recombinant disulfide-bonded proteins (e.g. antibodies [114,179] and human enzymes [180,181]). Plant expression systems have gained interest as promising platforms for production of various biologics offering several advantages including lower production costs compare to other eukaryotic systems, safety, flexibility and scale-up [111]. Here, we describe the expression, purification, and initial functional testing of ACDClx transiently expressed in the leaves of *N. benthamiana.*

3.3. Methods

3.3.1. Codon optimization and cloning of ACDClx into Geminiviral vectors for expression in plants

Optimization of the codons utilized within all ACDClx constructs was performed according to Geyer et al. [181] to ensure efficient expression in plants by using the codon table for *N. benthamiana*. Briefly, codon usage within the genes encoding for ACDClx constructs were modified as necessary to remove rare codons and maintain an average codon adaptation index (CAI) of 0.8 to improve the translation efficiency of mRNA transcripts. The resulting gene sequence was then manually checked for the presence of unwanted elements, such as poly-A signals, intron splice sites, and common restriction sites.

The gene encoding the original construct, ACDClx-His, was synthesized by GenScript with flanking NcoI and SacI restriction sites and provided in a pUC57 plasmid (pTM 1005). The

NcoI-SacI fragment containing ACDClx-His was isolated by restriction digest and gel purification and subcloned into a modified Geminiviral vector backbone [119] (XbaI-pBYR2eK2Mc-SacI) via triple ligation with nucleotides encoding for endoplasmic reticulum translocation (XbaI-BAA-NcoI), resulting in pBYR2eK2Mc-BAA-ACDClx-His. The construct was sequence-verified at the Arizona State University sequencing facility.

The genes encoding later ACDClx variants with the BAA signal peptide were synthesized as gBlocks® (Integrated DNA Technologies) with XbaI and SacI restrictions sites on the 5' and 3' ends, respectively. The GeneBlocks were subsequently digested with XbaI and SacI and ligated into pBYR2ek2Mc [119]. The resulting plasmids were transformed into *E. coli* DH5α and screened by PCR [30 cycles of: 15 sec at 95°C, 30 sec at 52°C and 1-2 min at 72°C (1 min per kilobase)], using primers oTM 878 and oTM 971, Table 3) and diagnostic digest to confirm correct cloning. The gene for anti-CD3 scFv was amplified by PCR using Ngly-His-ACDClx (pTM 1020) (primers oTM 971 and aCD3L-R) followed by restriction digest with XbaI and and SacI and ligation into the pBYR2eK2Mc backbone, to produce Ngly-His-aCD3_scFv. The primers used for colony screening and cloning are shown in Table 3.

3.3.2. Transient expression in N. benthamiana

Constructs encoding for ACDClx variants were transformed into the EHA105 strain of *Agrobacterium tumefaciens* and grown for two days on YENB-agar plates containing kanamycin (Kan, 50 µg/mL) for plasmid selection and rifampicin (Rif, 1.25 µg/mL) to inhibit *E. coli* growth. Colonies were screened by PCR to identify transformed clones. Liquid cultures were inoculated from a well separated clone into 10 mL of YENB/Kan/Rif and grown overnight with vigorous shaking (170 rpm) at 30°C. The next day, cultures in mid-log phase (OD_{600} = 0.6-0.9) were centrifuged (4,500 x*g,* 23°C, 20 min) and cells were resuspended in infiltration buffer (10 mM MES, 10 mM magnesium sulfate heptahydrate, pH 5.5 using KOH) to obtain a final OD_{600} of 0.2. Leaves from 6-week old *N. benthamiana* plants (grown at 24°C, 16/8 hr light/dark cycle) were infiltrated with the plasmid-containing agrobacteria suspension using a needleless syringe and

returned to a 30°C growth chamber. Leaf samples were collected once a day until necrotic (5 days) and analyzed for protein expression by immunoblot analysis (see below).

3.3.3. Extraction, purification, and refolding of ACDClx from plant tissue

To determine solubility, plant tissue was extracted in three consecutive steps. First, tissue was homogenized in a Waring blender in the presence of plant extraction buffer (PBS containing 10 mg/mL sodium ascorbate and 1 mM phenylmethylsulfonyl fluoride, PMSF) at 1 g of fresh plant material per 4 mL. The homogenate was then centrifuged at 17,000 *xg* at 4°C for 20 min to separate cell wall debris, membranes and other insoluble material in the pellet from water-soluble proteins in the supernatant fluid. The resulting pellet was subsequently resuspended in PBS containing 1% (v/v) Triton X-100 and recentrifuged to obtain membrane-associated proteins in the supernatant. Finally, this pellet was resuspended in 1x reducing sample buffer (SB, see next section) to solubilize the remaining insoluble protein fraction.

Upon realization that the recombinant ACDClx protein is insoluble in the presence of Triton X-100, we have attempted several different methods were used to solubilize the target protein. In Method I, leaf tissue was homogenized in plant extraction buffer supplemented with 1% (w/v) Triton X-100. Centrifugation separated water-soluble and detergent-soluble proteins (in the supernatant) from detergent-insoluble material in the pellet that contained almost all of the recombinant ACDClx protein. The pellet was then resuspended in denaturing/reducing buffer (500 mM NaCl, 8 M urea, 10 mM DTT, and 50 mM Tris, pH 8).

In Method II, the triton-X-100 insoluble pellet was resuspended in denaturing/reducing/S-sulfonating buffer (500 mM NaCl, 6 M guanidine-HCl, 150 mM sodium tetrathionate, 200 mM sodium sulfite, and 50 mM Tris, pH 8). Urea was replaced by guanidine in later studies due to the potential for urea-mediated protein modification (carbamylation) during long extractions [182].

For purification and on-column refolding of ACDClx-His, we followed Method III. Leaf tissue was homogenized in plant extraction buffer then centrifuged (20 min at 14,000 x*g,* 4°C). The pellet was resuspended in PBS containing 1% Triton X-100 and the sample was centrifuged again. The pellet was then resuspended in denaturing/reducing buffer. The supernatant was

incubated at 4°C on a rotator for 3 hours with a 2 mL column volume of Roche cOmplete™ nickel resin pre-equilibrated with 8 M urea, 50 mM Tris pH 8, 0.5 M NaCl and then purified/refolded based on a protocol adapted from Zhai *et al* [183]. Briefly, the column was washed with 10 mL 8 M urea in equilibration buffer, followed by 10 mL 8 M urea, 5 mM imidazole in equilibration buffer to assist in removal of contaminating proteins. ACDClx was then allowed to refold on-column by gradually lowering the urea concentration by washing with 40 mL each of refolding buffer (50 mM Tris pH 8, 0.5 M NaCl, 5 mM reduced glutathione, 0.5 mM oxidized glutathione) containing 3 M urea followed by a wash with refolding buffer containing 1.5 M urea. The His-tagged protein was then eluted with sequential addition of concentrated imidazole in 50 mM Tris pH 8, 0.5 M NaCl: first 2 mL at 500 mM imidazole, then 3 x 2 mL at 850 mM imidazole. Eluted fractions (2 mL each) were collected and the second fraction was dialyzed for 48 hours in PBS at 4°C using a Slide-A-Lyzer 3.5 kDa G2 cassette for functional testing.

Ngly-His-ACDClx was purified and refolded following Method IV which was similar to Method III used for ACDClx-His with the following exceptions: Leaf tissue was homogenized and then extracted overnight at 4°C directly in denaturing/reducing/S-sulfonating buffer that was supplemented with 10 mM sodium ascorbate, 1 mM PMSF. Supernatant was collected following centrifugation at 17,000 x*g* to remove insoluble components and was incubated at 4°C on a rotator with nickel resin overnight. Refolding proceeded as described above for Method III except that an additional refolding wash containing no urea was added following the 1.5 M urea wash, and protein was eluted with 4 x 1 mL volumes each of 50 mM, 200 mM, 500 mM, and 850 mM imidazole in 50 mM Tris pH 8, 0.5 M NaCl.

3.3.4. Protein analysis

Proteins samples in reducing SB (100 mM DTT, 5% glycerol, 1.67% SDS, 2% bromophenol blue, 60 mM Tris pH 8) were incubated for 5 min at 95°C and then briefly centrifuged to remove large aggregated material. For analysis under partial non-denaturing conditions samples were mixed with non-reducing SB that contained no DTT and the heating step was omitted.

Samples were then resolved by sodium dodecyl sulfate (SDS) polyacrylamide gel electrophoresis (PAGE) using hand-cast 12% polyacrylamide gels or Bio-Rad 4-15% stain-free TGX gels. Protein in gels were then visualized either by silver stain (Pierce silver stain kit, Thermo Fisher Scientific) or Coomassie stain (Coomassie Brilliant Blue G-250, Bio-Rad).

Immunoblot analyses were conducted on non-stained gels. SDS-PAGE-resolved proteins were wet transferred to polyvinylidene difluoride (PVDF) membranes for 1 hour at 100 V in a 4°C cold room or semi-dry transferred to nitrocellulose membranes for 15 minutes at 15 V at room temperature. Membranes were blocked for 15 minutes-overnight in 5% dry milk in PBST buffer (0.5% Tween-20 in PBS) and probed using mouse anti-6x-His (Sigma, H1029) and AffiniPure donkey anti-mouse conjugated to horseradish peroxidase (HRP, 715-035-150, Jackson ImmunoResearch) with three washes between each incubation. Blots were incubated with luminol reagent, exposed to film, and processed in an automated film developer. Expression of protein during time course studies was compared by loading leaf extracts at equivalent volumes from extractions performed at 4 mL buffer per gram of leaf material.

The concentration of purified ACDClx-His samples was determined by measuring A_{280} using the extinction coefficient (52090 M^{-1} cm^{-1} for bonded cysteines) that was calculated using the online ExPASy ProtParam tool (https://web.expasy.org/protparam/).

3.3.5. Cell culture

GL261-LucNeo cells (C57Bl/6 background) were cultured in DMEM + 10% fetal bovine serum (FBS) in a humidified incubator at 37°C with 5% CO_2. For calcium flux experiments, cells were trypsinized and prepared at a concentration of 0.5 x10^6 cells/mL in PBS. For CD69 experiments, cells were plated in 24-well plates and allowed to attach overnight before use.

3.3.6. In vitro *experiments*

Fresh splenocytes were obtained from C57Bl/6 mice immediately prior to calcium flux and CD69 experiments. Briefly, mice were euthanized via CO_2 asphyxiation followed by cervical dislocation. The spleen was then immediately dissected and placed in RPMI+ medium (RPMI,

Thermo Fisher Scientific, supplemented with 10% FBS) on ice, then mashed with a syringe plunger over a 70 µm strainer and washed with RPMI+. Red blood cells were lysed with Ack lysing buffer (Thermo Fisher Scientific) and splenocytes were washed twice with RPMI+, then counted and resuspended to a final concentration of 10^6 cells/mL in RPMI+. Splenocytes were loaded with calcium responsive dye via incubation of the cells with 5 µM Fluo-4 AM (Invitrogen) for 30 min at room temperature in the dark. Splenocytes were washed three times with RPMI+ to remove non-cytosolic Fluo-4 AM. During de-esterification of Fluo-4 AM to Fluo-4 (a process mediated by intracellular esterases, which slows the escape of the now charged molecule from the cells), the splenocytes were labeled with anti-CD4-FITC (eBiosciences) and anti-CD8-PerCP-Cy5.5 (eBiosciences) in FACS buffer (PBS + 1% FBS) at a 1:200 dilution for 15 minutes at room temperature, then washed twice with FACS buffer to remove unbound antibody. Finally, Fluo-4 loaded, labeled splenocytes were resuspended in FACS buffer at a concentration of $5x10^6$ cells/mL.

Intracellular calcium flux and CD69 expression were measured using flow cytometry on a BD LSR Fortessa. Before treatment, baseline calcium measurements of loaded cells (200 µL of $5x10^6$ cells/mL) were collected for 90 sec with the flow cytometer on “high” in the presence of 200 µL ($0.5 x10^6$ cells/mL) GBM cells or equivalent volumes of FACS buffer (final splenocyte:GBM ratio = 10:1). The flow cytometer was then placed on standby while the treatment was added and restarted for 105 sec of data collection. Calcium flux was measured for ~8 min. Calcium flux in CD4+ and CD8+ T cells was analyzed by gating the cell population on lymphocytes using side scatter/forward scatter (SSC)/(FSC) (small, low complexity). Lymphocytes were further gated based on CD4 or CD8 single marker positivity. CD69 MFI measurements were obtained using the same gating strategy in splenocytes co-incubated for 11 hours with GBM cells and 1 µg/mL ACDClx, PBS, or 1 µg/mL anti-CD3.

3.4. Results

3.4.1. Design and cloning of ACDClx

A T cell engager capable of selectively binding T cells and GBM cells was designed to be composed of anti-mouse CD3 variable fragments derived from hybridoma clone 145-2C11 (GenBank ID# AF000357.1 and AF000356.1) and expressed as a single polypeptide chain with the 36-amino acid peptide, chlorotoxin (Figure 10A). This fusion was designed with a flexible $(Gly_4Ser)_3$ linker between the anti-CD3 heavy (V_H) and light (V_L) variable fragments to allow for anti-CD3 binding without causing conformational stress. A single Gly_4Ser linker was also added to bridge the scFv and chlorotoxin such that T cell-GBM cells are maintained in close contact when bound. The original construct (ACDClx-His) was designed with a PreScission protease recognition sequence on the C-terminal end of chlorotoxin to assist with the removal of the 6x-histidine tag from the C-terminus, used for purification and detection (Figure 10A). In later iterations of ACDClx, the C-terminal His-tag was moved to the N-terminus (as an 8x-His tag) and a TEV protease recognition sequence was used in place of the PreScission protease sequence to enable use of a naturally occurring amino acid as the first codon following protease cleavage and to free the terminal arginine of chlorotoxin for potentially enhanced target binding [177]. For all constructs, a BAA signal peptide (SP) is encoded on the N-terminus for translocation to the ER to enable formation of disulfide bonds. ACDClx has a total of 6 predicted disulfide bonds, with one per antibody variable fragment and four within the 36-amino acid chlorotoxin peptide.

The DNA sequence of ACDClx was optimized for expression in plants by replacing rare codons and ensuring individual codons were not overused in succession, such as those for glycine in the case of four 4x-glycine repeats used within the two linker sequences. The codon adaptation index (CAI) for plant-optimized ACDClx-His was 0.82, which is expected increase expression relative to the non-plant optimized sequences reported in GenBank (CAI = 0.64 for plant codon usage) (Figure 10B) [181,184,185].

A geminiviral vector for transient expression of ACDClx-His was created by cloning the gene encoding ACDClx into the geminiviral backbone pBYR2ek2Mc (Figure 10C). The pBYR2eK2Mc backbone was modified by Diamos and colleagues, and contains multiple non-coding regulatory elements derived from other plant species and viruses found to enhance expression of the inserted gene of interest, as described in detail in [119]. This construct was

used for production and *in vitro* studies (Figures 11, 12-A-D, 15) described hereafter, but was later found to contain an arginine->lysine mutation (ACDClx_K270R-His) in the original gene design. The mutation was later corrected and is used in Figures 12E and 14A.

3.4.2. Expression of ACDClx in N. benthamiana

Geminiviral expression vectors drive accumulation of recombinant proteins to a maximum relatively faster than other plant-virus assisted expression systems, however the peak day itself has to be determined empirically for every target. To determine the peak leaf accumulation of ACDClx we collected infiltrated leaf samples daily for 5 days. The relative levels of the recombinant protein were determined in total protein extracts by resolving the proteins by SDS-PAGE and immunoblotting using the His-tag as a detection marker. Interestingly, peak expression of ACDClx from the ACDClx-His vector was determined to be 4-5 days post infiltration (DPI) (data not shown). Because necrosis was already quite substantial at 5 DPI (Figure 11), 4 DPI was chosen as the day for extraction for future experiments as a compromise between expression and necrosis, which can result in incomplete extraction, aggregation, and proteolysis.

3.4.3. *Solubilization, purification, and refolding of ACDClx*

Initial separation of the ACDClx homogenate into aqueous-soluble and insoluble fractions revealed that insolubility of ACDClx would be a major challenge. Differential fractionation using PBS, Triton X-100, and urea revealed that ACDClx was completely insoluble in neither aqueous solutions (PBS) nor could it be solubilized by detergent (Triton X-100) , while it came only modestly soluble in urea, with or without 1 hour incubation plus sonication (Figure 12A). Due to the presence of 6 disulfide bonds within ACDClx, the reducing agent dithiothreitol (DTT) was tested for its ability to solubilize ACDClx alone, with little success (Figure 12B). However, when denaturant combined with reducing agent was used to solubilize ACDClx for an hour with sonication, >90% of protein was solubilized (Figure 12C). These results indicated ACDClx was likely forming insoluble aggregates during expression due to the formation of intermolecular

disulfide bonds, even though ACDClx was designed with an ER signaling peptide to enable correct intramolecular disulfide bond formation *in planta*.

Refolding of ACDClx was then necessary to reform the secondary structure and form disulfide bonds within the protein fusion. ACDClx was initially purified via cobalt-based metal affinity chromatography (TALON® resin) but required refolding by dilution prior to purification due to the incompatibility of the resin with the reducing agents used for solubilization. Subsequent purification and refolding of ACDClx was thus performed using Roche cOmplete™ nickel resin, which is compatible with high concentrations of reducing and denaturing agents. This allowed for binding of ACDClx to the resin in denaturing/reducing conditions and refolding on-column, an approach which resulted in a 1+ day reduction in the time necessary to produce purified, refolded protein. Refolding on-column was accomplished by gradual reduction of denaturant in a GSH/GSSH redox system. Elution of refolded protein resulted in three separate isoforms when analyzed in non-reducing conditions compared to one isoform in reducing conditions, providing strong evidence that different disulfide bond combinations were forming during the refolding process (Figure 12D). Overall yield of pure ACDClx produced using the ACDClx-His vector was spectroscopically (A_{280}) determined to be 17.8 mg/kg fresh tissue and the final preparation was estimated to be >99% pure based on silver stained gels (Figure 12D).

3.4.4. *S-sulfonation improves extraction efficiency of ACDClx*

Overnight extraction of ACDClx from the insoluble protein pellet consistently resulted in highly aggregated protein multimers, which often reduced the overall soluble fraction available for purification and refolding. We hypothesized that this was due to breakage and reformation of mixed disulfides between molecules of ACDClx and tested the capacity for S-sulfonation of cysteine residues to reversibly block disulfide bond formation during extraction. The addition of a sulfite group to each cysteine following S-sulfonation was successful as evidenced by the near-complete solubilization of ACDClx compared to reduction with DTT (Figure 12E). As observed by others [186], the extraction of ACDClx with S-sulfonation resulted in a slower migration pattern on

SDS-PAGE in non-reducing conditions in comparison to its reduced counterpart (data not shown), further confirming successful S-sulfonation.

3.4.5. *Design of new constructs for improving yield and solubility of ACDClx*

Improvements in solubilizing ACDClx expressed from the ACDClx-His construct improved relative yield, but the total yield was still too low for efficient production for functional studies. To address this problem, we designed three new constructs and analyzed their solubility in aqueous buffer and compared their relative yields. An additional construct was also created to determine the solubility of the anti-CD3 Fv domain alone. All four constructs (Figure 13) contain the BAA ER signaling peptide, and the three ACDClx constructs have a free C-terminus, as others have reported that chlorotoxin may need a free C-terminal arginine residue for efficient target binding [177]. Furthermore, the PreScission protease recognition site was replaced with a tobacco etch virus (TEV) protease recognition site in order to leave native amino acid residues at the N-terminus following protease cleavage. The first construct, His-ACDClx, was designed to have an 8x-His tag and TEV site, distinguishing itself from ACDClx-His by moving the His tag from the C- to the N-terminus. The second construct, Ngly-His-ACDClx, contains a single N-glycosylation site immediately before the 8x-His tag, which has been reported to improve yield and solubility and reduce toxicity to plant tissue [187]. The third construct, CTB-ACDClx, contains the gene for cholera toxin subunit B (CTB) on the N-terminus followed by the TEV protease recognition sequence. This construct contains no distinct histidine repeat sequence within the primary structure, as expressed CTB is known to exist as a pentamer which naturally forms a metal-affinity binding site akin to a His-tag that can be used for purification [188]. CTB is also expressed as a CHAPS-soluble protein in *N. benthamiana*, thus we also expected that it may improve solubility as a fusion with ACDClx.

Following expression, extraction of these three new ACDClx constructs in aqueous solution revealed that ACDClx remained insoluble, regardless of modification (Figure 14A). His-ACDClx was found to express at higher levels than ACDClx-His, indicating that placement of the His-tag impacted expression. Ngly-His-ACDClx, however, expressed at significantly higher levels

in comparison to both ACDClx-His and His-ACDClx and resulted in virtually no plant toxicity, confirming the utility of N-glycosylation for improving expression of recombinant proteins in plants. Thus, Ngly-His-ACDClx was chosen as the optimal construct for further studies. Purification of Ngly-His-ACDClx via metal affinity chromatography was successful for enriching ACDClx in purified fractions, however, Coomassie stain of total protein content in the purified fractions revealed that the primary protein in these fractions was a contaminant ~55 kDa, most likely the large subunit of RuBisCo, which has a molecular weight of 56 kDa and is thought to be the most abundant protein on Earth, comprising 20-25% of total plant protein (Figure 14C and D). Furthermore, on-column refolding of Ngly-ACDClx resulted in a highly multimeric and aggregated form; monomeric refolded ACDClx was not detected by an anti-His antibody in non-reducing conditions, indicating that the N-terminal His-tag was not accessible following refolding (Figure 14C). Interestingly, expression of the anti-CD3 scFv alone without co-expression with chlorotoxin resulted in protein product that was primarily insoluble in aqueous solution and only modestly soluble in Triton X-100 (Figure 14E). Even though only two disulfides are predicted to be present, the anti-CD3 scFv is still mostly insoluble, indicating that at least a portion the insolubility observed for ACDClx may be unexpectedly due to the antibody variable fragments.

3.4.6. *Testing ACDClx functionality* in vitro

ACDClx-His was tested for the capacity to selectively activate T cells in the presence of GBM cells. To test T cell activation, two stages of T cell activation were assayed to confirm that activation was initialized, and that activation was sustained via signaling transduction pathways in the appropriate context. To measure activation instantaneously, intracellular calcium flux was measured, which is known to increase within seconds following target engagement by the TCR. Early T cell activation antigen (CD69) expression was chosen as the later marker of T cell activation (relative to calcium flux), which is known to be expressed on the cell surface 2-72 hours after target engagement.

Consistent with my hypothesis that ACDClx would activate T cells only in the presence of GBM cells, intracellular levels of calcium as measured by Fluo-4 fluorescence significantly

increased in CD8+ and CD4+ lymphocytes above baseline following addition of ACDClx to a mixture of splenocytes and GBM cells (Figure 15A and B). In contrast, addition of ACDClx to splenocytes alone, or addition of mock-purified protein to splenocytes and GBM cells resulted in no increase in intracellular T cell calcium levels. Calcium levels were sustained in the ACDClx/splenocyte/GBM group for the duration of measurement following addition of ACDClx (approximately 6.5 minutes), whereas levels drastically increased and then returned to baseline within 2 minutes for the positive control treatment, ionomycin, both consistent with the mode of calcium flux in their respective settings.

Similar effects were observed with CD69 upregulation 11 hours post-treatment (Figure 15C and D). MFI for CD8+ and CD4+ T cells within splenocytes co-incubated with GBM cells and treated with ACDClx was 2081.1 and 3387.1, respectively, while co-incubated cells treated with medium were 326.4 and 207.8 for CD8+ and CD4+ T cells, respectively. In contrast, cells co-incubated with GBM cells and treated with the positive control (full-length anti-CD3 antibody, clone 145-2C11) displayed a MFI of 16886 and 18591 for CD8+ and CD4+ T cells, respectively. For CD8+ T cells, 3%, 71%, and 93% were CD69-positive when treated with media, 1 µg/mL ACDClx, or anti-CD3, respectively. For CD4+ T cells, 4%, 85%, and 93% were CD69-positive when treated with media, 1 µg/mL ACDClx, or anti-CD3, respectively.

3.5. *Discussion*

Here, we describe the first production and testing of a novel immunotherapy utilizing anti-CD3 antibody fragments and chlorotoxin for enhancing T cell recognition and killing of GBM cells without requiring TCR specificity for GBM. Other groups have previously described the use of variously designed BiTEs for treating GBM that were shown to be highly effective against cells expressing the single antigen that is targeted [172,189]. However, these antigens are typically expressed on only a subset of cells within a tumor [18]. Studies have shown that targeting a single antigen within a population of GBM cells eventually results in antigen loss and tumor recurrence [19,85]. We therefore decided to focus on a binding partner that could bind the vast majority of malignant cells. Chlorotoxin has been shown to selectively bind >95% of GBM cells

within a tumor without affinity for healthy tissue [92]. We thus designed a novel fusion protein utilizing chlorotoxin as the GBM-targeting domain of a T cell engaging molecule, expecting that such a molecule could be highly effective at enhancing T cell recognition of all or most GBM cells within a tumor. To our knowledge, this is also the first BiTE-like molecule to use a peptide as the tumor-binding domain in place of a scFv.

Functional recombinant proteins containing disulfide bonds have been successfully produced to high yields in the tobacco relative *N. benthamiana* when targeted to the ER, providing the rationale for expressing ACDClx in plants. While we successfully expressed ACDClx in plants, the accumulated protein was found to be aggregated upon its extraction from leaves. This finding was consistent across different gene constructs utilizing alternately placed terminal histidine tags, an N-glycosylation site, as well as a fusion protein for use as a chaperone for protein folding. Intermolecular disulfide bonds formed during expression between the 12 cysteine residues within ACDClx initially appeared to be the cause of aggregation which required simultaneous denaturation and reduction for sufficient solubilization. However, later data suggested that even the anti-CD3 domain expressed alone was also generally insoluble, indicating that ACDClx contains more than one insoluble component and that the disulfide bonds are likely not the sole cause for insolubility.

The disulfide-mediated insolubility of chlorotoxin has been reported for expression in *E. coli* in the context of 6xHis-chlorotoxin, GST-6xHis-chlorotoxin, and a chlorotoxin-Fc fusion protein, all of which required high concentrations of the denaturant guanidine hydrochloride in combination with S-sulfonation or reduction with beta-mercaptoethanol [190,191]. Denaturation and DTT-mediated reduction of ACDClx resulted in a mixture of soluble and insoluble protein, with the soluble fraction present in higher-order multimers, likely due to the rapid reformation of disulfide bonds in the context of an oxidative environment and the natural instability of DTT. In comparison, reversible modification of the cysteine residues via S-sulfonation resulted in a monomeric soluble fraction of over 90%, indicating that the addition of a sulfite group to each of the cysteine residues prevented reformation of disulfide bond-mediated aggregation. Sulfite

groups can then be removed in reducing conditions to allow for proper disulfide formation in an appropriate refolding environment.

Ultimately, oxidative refolding of purified ACDClx-His resulted in three isoforms. Previous studies have reported that removal of the 6xHis-tag of S-sulfonated chlorotoxin was sufficient for refolding into a single isoform. Due to the overall low yields of ACDClx-His prior to protease-mediated removal of the histidine tag, attainment of a detectable and sufficient yield of cleaved ACDClx was not achieved (data not shown). To enable higher yield and/or solubility, we re-designed the genetic constructs for ACDClx, which resulted in three new expression vectors: His-ACDClx, Ngly-His-ACDClx, and CTB-ACDClx. Protein expressed from these vectors was still completely insoluble, however, protein yields were higher than that expressed from the original ACDClx-His vector. Of note, the CTB-ACDClx fusion resulted in protein which was present in a primarily monomeric form, however, CTB was tested for its ability to improve solubility, of which it failed. In comparison, however, the N-glycosylated form of ACDClx resulted in a significantly higher yield than ACDClx-His and His-ACDClx. We thus chose Ngly-His-ACDClx for further investigation due to the need for a sufficient amount of protein for functional studies. N-glycosylation has been demonstrated to improve yield and solubility while also reducing toxicity in plants, which may then result in reduced protein degradation [187]. This effect is hypothesized by Harmorsky *et al.* to be a result of reduced ER stress via assistance from lectin chaperones, which might serve to reduce a toxic unfolded protein response in the plant cell lumen. As expected, N-glycosylation of ACDClx resulted in a significantly higher yield and a striking reduction in leaf necrosis, however, purified N-glycosylated ACDClx contained a dominant contaminant around 55kDa, with the most likely candidate being the abundant plant protein, RuBisCo. Contamination in these samples was likely higher as a result of direct extraction of leaf tissue into denaturing/S-sulfonating buffer and thus may be improved by sequential extraction as previously described.

BiTEs are designed to induce selective T cell activation against their target cells and avoid spurious activation of T cells when not in the presence of their target cells. This indication is important in the context of tumor therapy, where activation of T cells when not selectively bound to their tumor target can result in overproduction of inflammatory cytokines that are harmful in

high quantities, a condition known as cytokine release syndrome. Improper activation of T cells can also ultimately result in T cell anergy, a state of T cell dysfunction. We thus tested ACDClx for the capacity to selectively activate T cells in the presence of GBM cells and found that activation was only observed when all three components necessary for activation were present (T cells, GBM cells, and ACDClx). Removal of GBM cells or ACDClx resulted in no T cell activation. These results are encouraging and indicate that ACDClx merits further evaluation as a possible GBM immunotherapy.

The ultimate goal of any cancer therapy is to destroy malignant cells while reducing damage to healthy tissue. For GBM, this goal is rife with obstacles, but will be assisted by the use of a pan-GBM selective moiety such as chlorotoxin. We have demonstrated that an anti-CD3/chlorotoxin T cell engaging fusion protein is capable of being expressed and refolded as a functional protein in low levels in *N. benthamiana,* that yield can be improved by the simple addition of an N-glycosylation site, and that ACDClx is functionally capable of enhancing T cell recognition of GBM cells that results in T cell activation. Further improvements in the yield of functional ACDClx will be required for the thorough investigation into the ability of ACDClx to selectively induce GBM cytotoxicity and produce inflammatory cytokines for enhancing an anti-tumor response *in vitro* and *in vivo*. This may be achieved by production in alternative expression systems that maximize total yield for purification and refolding, such as *E. coli*, or systems that are predicted to be naturally capable of producing a properly folded protein product, such as insect or mammalian cell lines.

Table 3: Oligonucleotides used for colony screening and cloning of plant constructs		
Primer	Description	Sequence (5'-3')
oTM 878	pBYR backbone R	GCATAAAGGCAGTTATGCAATTTGC
oTM 971	XbaI-BAA F	GCATATCTAGAACAATGGCTAACAA
aCD3L-R	SacI-Anti-CD3 V_L R	aggGAGCTCTTATGATCCTCCTCCTCCCCTCTTGATCTC

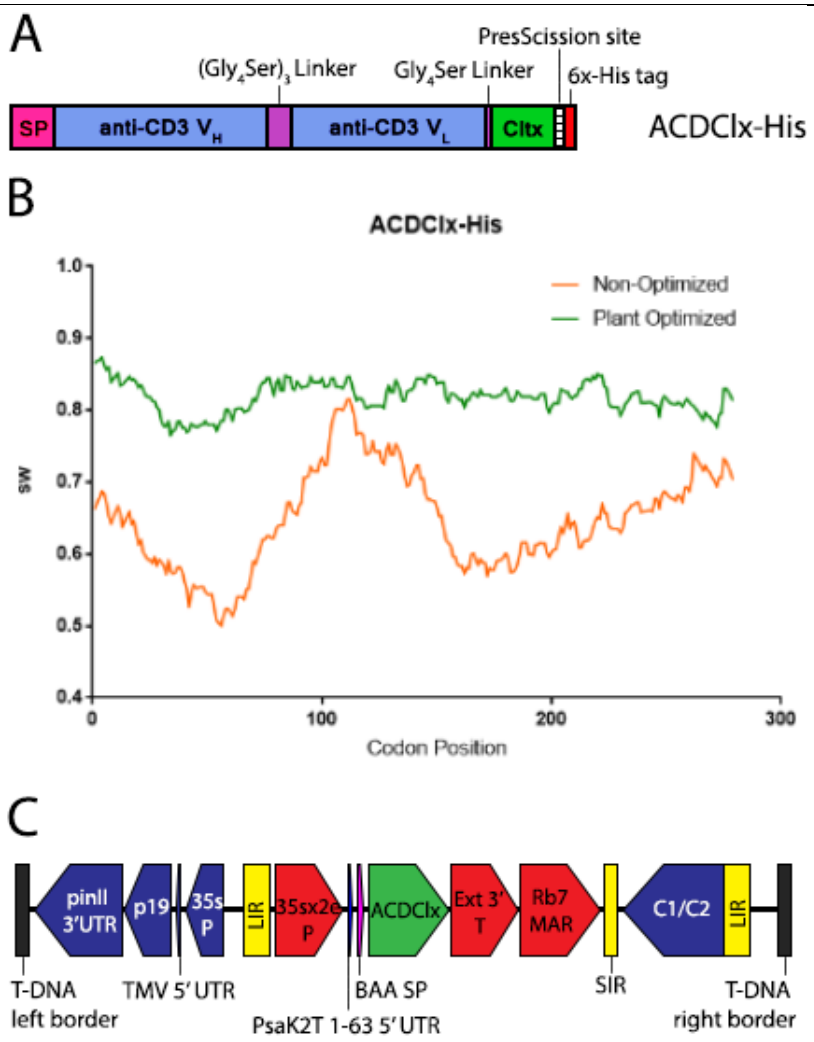

Figure 10: Design and optimization of the ACDCIx expression cassette. (A) A schematic of the linearized ACDCIx polypeptide expressed with the BAA signal peptide (SP). (B) The sliding window plot depicting average codon usage based on highly expressed proteins in *N. benthamiana* before and after codon optimization. (C) The transfer DNA (T-DNA) region of the modified geminiviral vector, pBYR2eK2Mc, used to express ACDCIx *in planta*. pinII: potato proteinase inhibitor II; UTR: untranslated region; TMV: tobacco mosaic virus; P: promoter; LIR: long intergenic region; PsaK2T: *N. benthamiana* homolog of photosystem I reaction center subunit K from *Arabidopsis thaliana;* Ext: extensin from *N. benthamiana*; T: terminator; MAR: matrix attachment region; SIR: short intergenic region; C1/C2: Rep/RepA viral replication proteins from bean yellow dwarf virus.

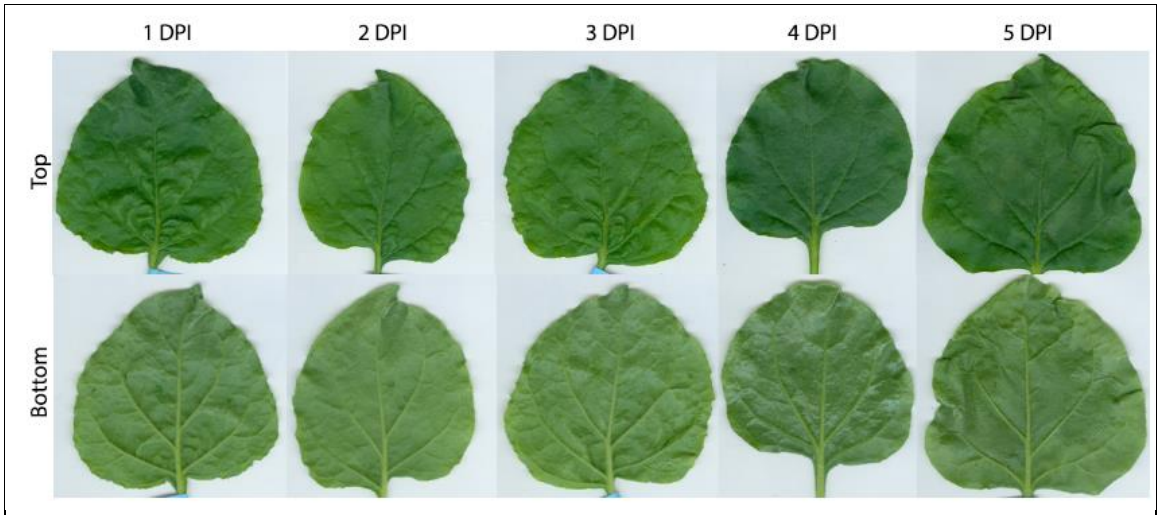

Figure 11: Kinetics of ACDClx-His expression in *N. benthamiana*. 6-week old *N. benthamiana* plants were infiltrated with OD 0.2 of pBYR2ek2Mc-ACDClx-His and leave samples were taken every 24 hours thereafter to monitor for expression and necrosis. Leaf samples show necrosis on day 5, as evident by brown patches and loss of turgor near the leaf edges.

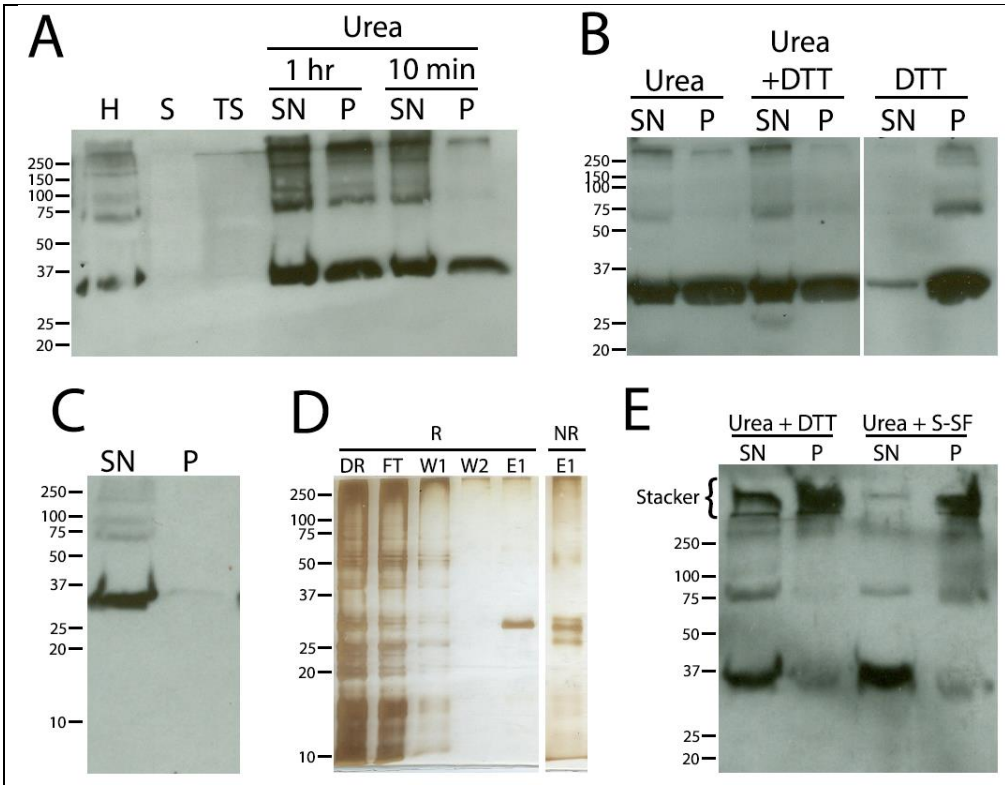

Figure 12: ACDClx is solubilized in reducing and denaturing conditions and purified via metal affinity chromatography. (A) Leaf tissue was homogenized (H) and sequentially solubilized into PBS (S = soluble), 0.1% Triton X-100 (TS = Triton soluble). The final insoluble fraction was divided in half and incubated with buffered 8 M urea for 10 minutes or 1 hour. This sample was centrifuged to obtain the urea soluble fraction from the supernatant (SN) and the remaining pellet was solubilized with 1X SDS sample buffer. (B) Buffered 8 M urea, 10 mM DTT + 8 M urea, or 10 mM DTT was incubated with PBS/Triton X-100-insoluble protein for 10 minutes to determine solubility in each buffer. (C) Extracting the PBS/Triton X-100-insoluble fraction for 1 hour with sonication every 10 minutes resulted in near complete solubilization of ACDClx-His. (D) ACDClx-His extracted in denaturing/reducing (DR) buffer was purified using Roche cOmplete His-tag purification resin. The unbound fraction was collected in the flow-through (FT) and washed with 2x10 mL each of buffered 8 M urea (W1 and W2). Remaining bound protein was refolded on column using sequential washes with decreasing concentrations of urea with 5 mM reduced glutathione and 0.5 mM oxidized glutathione. Protein was then eluted with 850 mM imidazole (E1) and analyzed via silver stain in reducing (R) and non-reducing (NR) conditions. (E) PBS/Triton X-100-insoluble protein was divided in half and solubilized with either 8 M urea + 10 mM DTT denaturing/reducing buffer or 8 M urea + 200 mM sodium sulfite + 150 mM sodium tetrathionate denaturing/S-sulfonating (S-Sf) buffer. Solubilized (SN) protein was separated from insoluble (P) protein and analyzed via SDS-PAGE and western blot, maintaining the stacker region of the acrylamide gel to show the proportion of highly aggregated protein unable to enter the resolving gel.

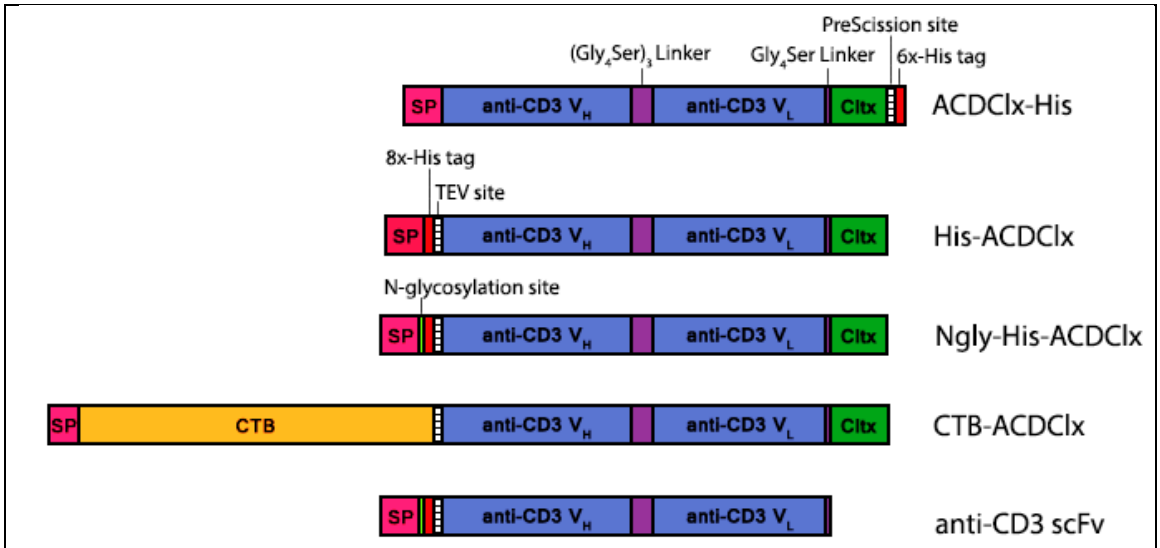

Figure 13: Schematics of new constructs designed to improve yield and solubility. The original ACDCIx-His construct is shown at the top for comparison to the new constructs. His-ACDCIx contains an N-terminal 8x-His tag following the BAA signal peptide (SP). A TEV protease recognition sequence is placed on the N-terminal side of ACDCIx for later removal of the His-tag and N-glycosylation site or CTB fusion. CTB = cholera toxin subunit B.

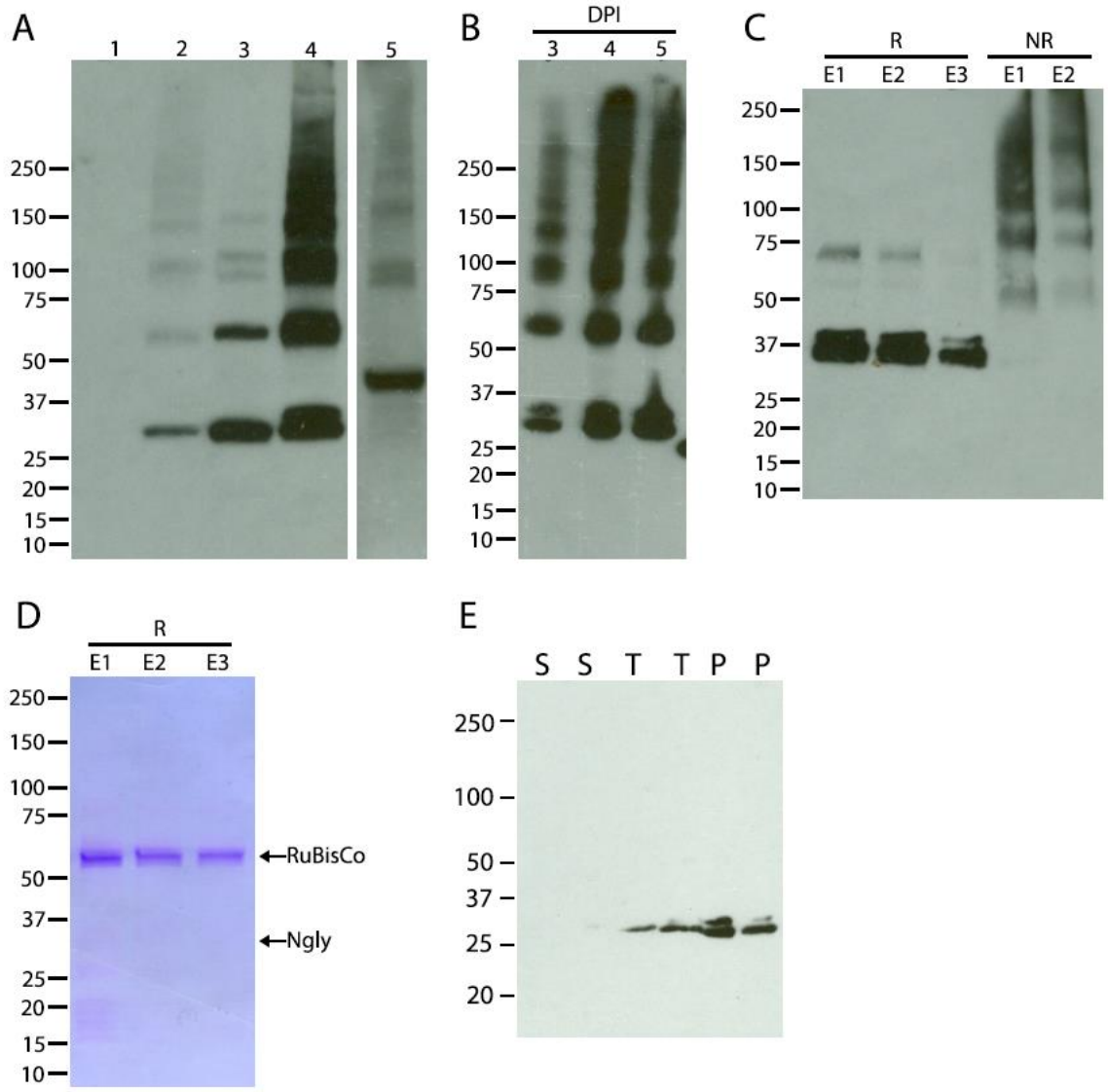

Figure 14: **Expression of ACDClx using new constructs still results in insoluble protein, but with greater overall yield.** (A) Expression comparison of constructs in the insoluble fraction at day 3 post-infiltration. Lane (1) Mock-infiltrated tissue (2) ACDClx-His (3) His-ACDClx (4) Ngly-His-ACDClx (5) CTB-ACDClx. Lanes 1-4 were probed with mouse anti-6xHis primary antibody goat anti-mouse secondary antibody. Lane 5 was probed with goat anti-CTB primary antibody and rabbit anti-goat secondary antibody, thus lane 5 cannot be directly compared to lanes 1-4. (B) Anti-6x-His western blot of expression kinetics of insoluble Ngly-His-ACDClx. (C) Anti-6x-His western blot of on-column purification and refolding of Ngly-His-ACDClx. (D) Coomassie stain of total protein following purification of Ngly-ACDClx; E1-E3 are the same samples as E1-E3 from (C). (E) Anti-6x-His western blot showing solubility of anti-CD3 scFv expressed without chlorotoxin. Lane markers are in kilodaltons. DPI = days post-infiltration. R = reducing conditions. NR = non-reducing conditions. E = elution. S = PBS-soluble. T = Triton X-100-soluble. P = Insoluble pellet.

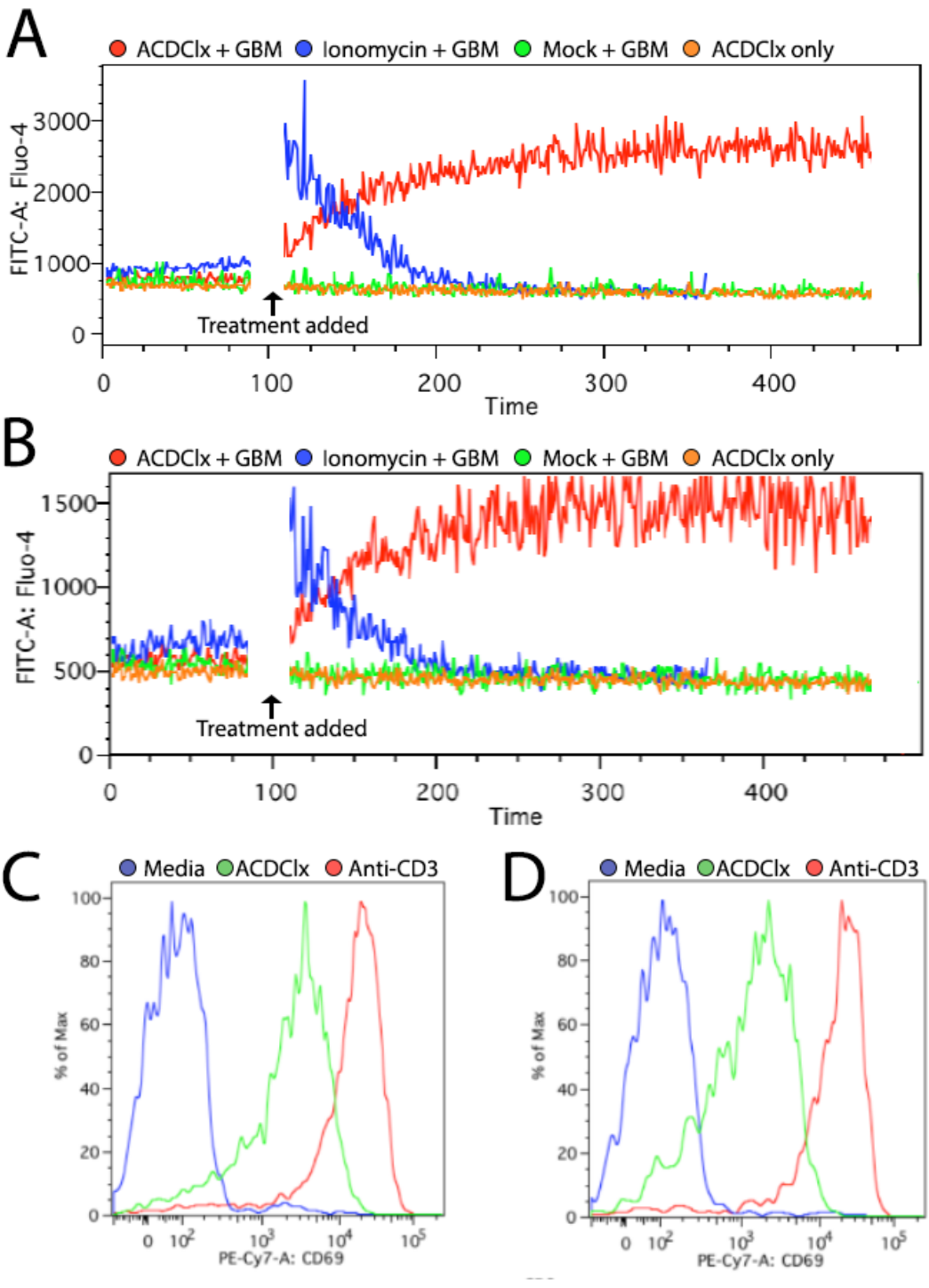

Figure 15: ACDClx-His can selectively activate T cells *in vitro.* Calcium flux as measured by Fluo-4 in (A) CD4+ and (B) CD8+ T cells following treatment with ACDClx or controls with or without co-incubation with GBM cells. Time scale = seconds. CD69 expression of (C) CD4+ and (D) CD8+ T cells following treatment with ACDClx, PBS, or full length anti-CD3 control for 11 hours with or without co-incubation with GBM cells.

CHAPTER 4

DESIGN, EXPRESSION, PURIFICATION, AND TESTING OF ACDClx PRODUCED IN *ESCHERICHIA COLI*

4.1. Abstract

There are many challenges in the process of developing an effective therapeutic for treating glioblastoma (GBM), which has resulted in a stagnating median and 5-year survival of 15 months and 5 years, respectively. Effective therapies must be able to bypass the blood-brain barrier (BBB) to reach malignant cells that have invaded into healthy brain tissue and must also be able to destroy a significant proportion of the ever-evolving tumor cell population to prevent tumor recurrence. We have previously described the design and initial testing of a GBM-selective immunotherapy for engaging and mediating T cell killing of GBM cells, regardless of T cell receptor specificity. This immunotherapy is a fusion of an anti-CD3 single chain antibody variable fragment and chlorotoxin, a small peptide known to bind >95% of GBM cells, known as anti-CD3/chlorotoxin, or ACDClx. Previous studies have shown that ACDClx is expressed in low yields as an insoluble aggregate in the plant host *Nicotiana benthamiana* regardless of solubility enhancing modifications, thus we sought to express ACDClx in higher quantities as an insoluble protein in the inclusion bodies of *E. coli* and designed two new variants to attempt to produce ACDClx in a more soluble form. Expression in *E. coli* was capable of producing much higher yields in comparison to production in plants, which required refolding by dilution instead of conveniently refolding on column. A periplasm-targeted fusion of disulfide bond isomerase C to ACDClx was unable to produce soluble ACDClx, nor was a truncated variant (ACDClxΔ15) which was predicted to contain three fewer disulfide bonds than full-length ACDClx. However, due to the extreme insolubility of ACDClx and its variants, a new method of purification was designed to enable purification without requiring metal affinity chromatography. This new method is based on utilizing denaturant to remove protein contaminants while ACDClx, requiring denaturing reducing buffer, can be enriched by centrifugation. Furthermore, though initially insoluble, we demonstrate for the first time that ACDClxΔ15 binds GBM cells *in vitro*. Future work will include further

functional testing of both ACDClx and ACDClxΔ15 and continued development in the production of soluble protein.

4.2. Introduction

The prognosis for glioblastoma (GBM) patients who receive standard of care treatment is considered one of the worst among all tumor types, with only 5% of patients surviving 5 years following diagnosis, and only 50% of patients surviving longer than 15 months. Standard of care after initial diagnosis includes surgical resection of bulk tumor, radiation, and chemotherapy with temozolomide. Aside from its sensitive location which limits aggressive surgical and therapeutic strategies, successful treatment of this invasive form of primary brain tumor is also significantly hindered by the BBB, heterogeneous expression of targetable cell surface markers, and genetic mutation enabling treatment resistance. The development of drugs or alternative treatments capable of bypassing the BBB and targeting the entirety of the malignant cell population without harming healthy tissue are thus in high demand.

Capitalizing on recent advances in immuno-oncology, we have designed an immunotherapeutic fusion protein for the purpose of enhancing T cell recognition and killing of GBM cells. This fusion protein, anti-CD3/Chlorotoxin, or ACDClx, is designed to target the majority of GBM cells within a tumor via chlorotoxin, a non-toxic, 36-amino acid peptide found in the venom of the deathstalker scorpion, *L. quinquestriatus*. Chlorotoxin is characterized for having unique selectivity for GBM cells relative to healthy tissue [92] and is currently in clinical trials for improving detection of malignant cells during surgical resection [97]. ACDClx is thus expected to tag GBM cells via its chlorotoxin domain while engaging CD3, a protein expressed on the surface of all T cells, via its anti-CD3 single chain variable fragment (scFv) domain. Direct cell-cell engagement is then expected to induce selective T cell killing of the bound GBM cell, which is the primary mechanism for bispecific T cell engagers (BiTEs) used for treatment of B cell malignancies [192].

We have previously demonstrated that ACDClx is capable of selectively activating T cells when simultaneously bound to both cell types. The initial activation of T cells observed in these

studies is the first step in an orchestrated signaling cascade that spurs the release of cytotoxic granules into the bound target cell, resulting in caspase-3 mediated cell death. The production of ACDClx, however, has proven to be challenge for furthering functional characterization of this unique fusion protein.

scFVs are known to aggregate during production or storage, and much effort has been put into developing expression strategies that minimize aggregation. In the initial characterization of ACDClx solubility following expression in the plant host *N. benthamiana,* we observed that the fusion was completely insoluble even when produced with modifications known to enhance solubility for other proteins. We speculated that the insolubility was likely due to the 12 cysteine residues for the formation of 6 disulfide bonds within ACDClx, however, following expression of the anti-CD3 scFv alone in the absence of chlorotoxin, the scFv was still mostly insoluble. This, combined with the need for a reducing agent in the solubilization of ACDClx, indicated that challenges in the solubility were likely due to both scFv-mediated aggregation and the formation of intermolecular disulfide bonds.

Given the inability to produce ACDClx as a soluble protein in *N. benthamiana* and the relatively low yield of insoluble ACDClx expressed compared to other recombinant proteins expressed in the same host and with a similar vector [119], we hypothesized that production of ACDClx in the insoluble form may be more efficient in the common laboratory protein production workhorse, *Escherichia coli*. *E. coli* is well known for its ease of transformation and its fast, low-cost production of recombinant proteins, but is often bypassed as a production host for clinical applications due to the inability to impart post-translational modifications, such as cysteine-cysteine bonds (also known as cystine or disulfide bonds) and glycosylation, that may be necessary for the stability and functionality of the protein of interest in its native form. ACDClx, in contrast to many scFv-containing therapeutics, is not predicted to be glycosylated, and is thus an excellent candidate for production in *E. coli*. Further, cystine formation for disulfide-rich peptides expressed in E. coli has been shown to be possible via co-expression with periplasmic-targeted disulfide bond isomerase C (DsbC). We thus also hypothesized that a fusion of DsbC to ACDClx might enable soluble expression and correct disulfide formation of ACDClx. Here, we describe the

design, expression, and biochemical analysis of genetic constructs for producing ACDClx as well as a new, more compact variant, ACDClxΔ15.

4.3. Methods

4.3.3. Codon optimization and cloning of ACDClx into pET-11a vectors for expression in E. coli

Amino acid sequences for producing His-tagged ACDClx (His-ACDClx) and a periplasm-targeted fusion of disulfide isomerase C (DsbC) to His-tagged ACDClx (DsbC-His-ACDClx) were designed based on prior constructs for producing ACDClx in the leaves of *N. benthamiana.* These constructs include a TEV protease recognition sequence between the His-tag and ACDClx, and were modified as necessary for the DsbC fusion to include a signal peptide for co-translation into the periplasm of *E. coli*, which was predicted to facilitate formation of disulfide bonds given the oxidative nature of the periplasm environment. Gene sequences for each construct were then optimized to ensure efficient codon usage in *E. coli* for the purpose of overexpression, and to prevent overuse of abundantly used codons within the ACDClx sequence. Special care was taken to distribute codon usage for glycine (Gly), serine (Ser), and cysteine (Cys), with Gly and Ser present in abundance within the linker sequences and with Cys being especially rare in *E. coli*. The sequences were designed for cloning into a pET-11a vector and thus included a 5' NdeI restriction site and a 3' BamHI restriction site for replacing the start codon and T7 tag present within the vector with the start codon and sequence for His-ACDClx or DsbC-His-ACDClx. Gene synthesis and cloning into the pET-11a vector was completed by GenScript (Piscataway, NJ) and sequenced to verify the accuracy of synthesis and cloning.

To produce non-His-tagged ACDClx, primers were designed to capture the regions containing only the ACDClx gene sequence without the His-tag or TEV protease recognition sequence. The forward primer (oTM 977) contained an NdeI restriction site prior to the sequence for anti-CD3 V_H and the reverse primer (oTM 976) contained an BamHI restriction site at the terminal end of the chlorotoxin sequence. Following PCR amplification of the ACDClx sequence, the purified PCR product was subcloned into the pET-11a backbone derived from DsbC-ACDClx digested with NdeI and BamHI via overnight ligation at 16°C mediated by T4 DNA ligase

(Promega). 2 µL of precipitated ligation reaction was used to transform DH5α *E. coli* via electroporation and grown overnight on LB/Carbinicillin plates at 37°C. The resulting colonies were screened using T7 forward and reverse primers and cultured overnight for plasmid preparation the next day, and the gene sequence was confirmed via Sanger sequencing. His-ACDClxΔ15 and non-His-tagged ACDClxΔ15 (ACDClxΔ15) was produced using the methods described for non-His-tagged ACDClx, but used primers oTM 115 and oTM 978 for His-ACDClxΔ15 and oTM 977 and oTM 978 for ACDClxΔ15, for PCR amplification of the gene products for cloning. Table 4 shows a list of all primers used.

4.3.4. Expression in E. coli

BL21(DE3) electrocompetent cells were transformed with plasmid DNA corresponding to His-ACDClx, DsbC-ACDClx, ACDClx, His-ACDClxΔ15, or ACDClxΔ15 and grown overnight at 37°C on LB/Carbinicillin plates. Colonies were screened using T7 forward and reverse primers present within the pET-11a backbone and flanking the gene of interest (GOI). A single positive colony was chosen and used to grow a 10 mL culture overnight at 30°C (a 37°C shaking incubator was not readily available for these studies). The next morning, the 10 mL culture was used to inoculate a 100 mL culture to an OD_{600} of 0.1. The 100 mL culture was grown to an OD of 0.6 and protein expression was induced by addition of IPTG. To determine optimal growth conditions, protein expression was induced with 0.3 mM or 1 mM IPTG and samples were collected at 1, 2, 3, 4, and 5 hours post-induction. Sample OD_{600} measurements were also taken at each time point. The collected sample was immediately centrifuged and supernatant discarded to obtain a cell pellet, which was frozen at -80°C until further analysis. For analysis, cell samples were normalized by concentration using OD_{600} measurements and via resuspension in 50 mM Tris pH 7, 150 mM NaCl, 5 mM EDTA, and 1 mg/mL lysozyme (25 µL per OD_{600} 0.6) These samples underwent four freeze-thaw cycles using dry ice and a 42°C heat block with vortexing between steps. Samples were then treated with DNAse I and centrifuged for 5 minutes at 12,000 *xg* at 4°C to obtain the soluble and insoluble protein fractions. Fractions were analyzed via SDS-

PAGE and Coomassie or stain-free imaging as described below. For purification purposes, expression was induced in a 1 L culture with 0.3 mM IPTG for 4 hours at 30°C. The culture was aliquotted into conical tubes containing 50 mL each, cells were pelleted by centrifugation (6,000 *xg* for 20 min at 4°C*)*, and pellets were frozen at -80°C until further use.

4.3.5. Extraction and purification of ACDClx from inclusion bodies

The protocol for isolating inclusion bodies containing ACDClx was adapted from Rodriguez-Carmona *et al.* Briefly, the cell pellet was thawed and resuspended in 1/5th the original aliquot volume in 50 mM Tris pH 7, 150 mM NaCl, 2 mM EDTA, frozen at -80°C, and re-thawed. PMSF was added to 0.5 mM and lysozyme to 1 mg/mL, then agitated for 45 minutes at 30-37°C. Triton X-100 was then added to 0.5% and incubated at room temperature for 45 minutes on an orbital shaker. Lastly, DNAse I was added to 3.75 units/mL and $MgSO_4$ to 750 µM and incubated at 30-37°C for 45 minutes. The resultant solution was centrifuged for 15,000 x*g* for 20 minutes at 4°C and the supernatant containing solubilized *E. coli* proteins, membrane, and DNA was discarded. The pellet containing *E. coli* inclusion bodies was washed with 50 mM Tris pH 7, 150 mM NaCl, 2 mM EDTA to remove any remaining soluble components. Inclusion bodies were then solubilized and cysteine residues were modified via S-sulfonation to reversibly prevent disulfide formation by overnight incubation in 6 M guanidine-HCl, 150 mM sodium tetrathionate, 200 mM sodium sulfite, 50 mM Tris pH 7, 150 mM NaCl, and 2 mM EDTA at 4°C while gently shaking.

For purification of His-ACDClx, DsbC-ACDClx, or His-ACDClxΔ15 from 50 mL culture aliquots solubilized inclusion bodies were centrifuged to remove insoluble aggregates (15,000 x*g*, 20 minutes, 4°C) and the supernatant was loaded onto 1 mL of Roche cOmplete nickel resin equilibrated with denaturing buffer (6 M guanidine-HCl, 50 mM Tris pH 7, 150 mM NaCl) and incubated overnight on rotation at 4°C. The next day, the flow-through (FT) was collected and the resin washed with 20 mL denaturing buffer to remove unbound protein. His-tagged protein was eluted from the column in 1 mL fractions using 850 mM imidazole in denaturing buffer. UV280 was measured for each fraction using denaturing buffer as a blank and was then

converted to concentration using the calculated extinction coefficient for the protein of interest (His-ACDClx: 52830 $M^{-1}cm^{-1}$; DsbC-ACDClx: 70250 $M^{-1}cm^{-1}$; His-ACDClxΔ15: 51340 $M^{-1}cm^{-1}$).

To purify untagged ACDClx or ACDClxΔ15, inclusion bodies were obtained as described above and the inclusion body pellet was washed twice with 3 M guanidine-HCl in 50 mM Tris pH 7, 150 mM NaCl, 2 mM EDTA to remove most contaminating proteins, leaving ACDClx insoluble or partially insoluble. ACDClx was then solubilized using denaturing S-sulfonation as described above.

4.3.6. Refolding, concentration, and buffer exchange

Denatured, S-sulfonated ACDClx was refolded by rapid dilution into renaturing, oxidizing buffer. Various buffers were tested to determine which conditions produced the highest proportion of refolded protein and are listed in Table 5. The optimized refolding protocol is as follows: Cysteines are reduced with 1 mM DTT at room temperature for 15 minutes to remove sulfite groups, followed by diluting the protein drop-wise 1:100 into a rapidly stirring solution of 0.5 M L-arginine, 2 mM oxidized glutathione, 100 mM Tris base, 2 mM EDTA, pH 10.3 at 4°C. The solution is stirred overnight-48 hrs, after which the protein is concentrated using an Amicon Ultra-15 centrifugal filter unit with a 3,500 Da cutoff to its original volume and exchanged into PBS using a PD-10 desalting column (GE Healthcare, Pittsburgh, PA). Refolded ACDClx in PBS is stored at 4°C for up to one week or -80°C until needed.

4.3.7. Protease cleavage of His-tag

Various conditions were tested for optimal AcTEV-mediated cleavage of the TEV protease recognition sequence located between DsbC-His and ACDClx and subsequent separation via metal affinity chromatography. For optimization, the starting protocol (10 units AcTEV, 20 µg fusion protein, 1 mM DTT, 0.5 mM EDTA, 50 mM Tris-HCl, pH 8) was tested along with various alterations. For most buffers, pH 7 buffer was used to avoid precipitation of DsbC-ACDClx (pI = 7.86) but still operate within the optimal pH of AcTEV, reported to be pH 6-9. Additional buffer alterations for optimization included (one variable at a time) the addition of 150

NaCl, using 5 mM DTT, using 50 units AcTEV, adding 5% or 10% glycerol, adding 0.1% Triton X-100, decreasing the mass of fusion protein used in the reaction, and adjusting reaction time (1-24 hours) and temperature (4°C, room temperature, 30°C). Separation of His-tagged AcTEV and DsbC-His from cleaved ACDClx was attempted using Roche cOmplete His-tag purification resin and TALON resin using gravity and centrifugal methods for obtaining flow-through.

4.3.8. Protein Analysis

Analysis of protein samples was performed using SDS-PAGE with Bio-Rad 4-20% stain-free TGX gels. Reducing samples were prepared using standard SDS sample buffer containing 10 mM DTT and boiled for 5 minutes at 95°C. Non-reducing samples were prepared using SDS sample buffer containing no DTT or other reducing agents without boiling. Total protein content was visualized using Coomassie Brilliant blue for early experiments, or by UV exposure of Bio-Rad stain-free gels for 3 minutes, followed by image capture using the SYBR-Green setting on a UVP Biospectrum 310. All proteins evaluated in this study contain Trp residues that are required for stain-free imaging, which utilizes 2,2,2-trichloroethanol to interact with Trp following exposure to UV light to produce fluorescence. Analysis of His-tagged protein was performed via western blot using the same electrophoresis protocol described above. When possible, the same gel was used for stain-free total protein imaging and western blotting. Following imaging, the protein was transferred from the gel to nitrocellulose in semi-dry conditions and blocked for 15 minutes-overnight in 5% dry milk in PBST (0.5% Tween-20 in PBS). The blot was probed using a monoclonal mouse anti-6xHis antibody (Sigma-Aldrich #H1029) for 15 minutes at room temperature, washed three times with PBST, and probed using a polyclonal donkey anti-mouse secondary antibody (peroxidase AffiniPure Donkey anti-mouse IgG (H+L), Jackson ImmunoResearch #715-035-150) for 15 minutes at room temperature followed by three additional washes with PBST. Blots were treated with luminol reagent, exposed to Amersham Hyperfilm ECL film (GE Healthcare), and processed using an automated film developer.

4.3.9. In vitro experiments

GL261-LucNeo cells were cultured in DMEM + 10% FBS + 1% P/S/G in a humidified incubator at 37°C with 5% CO_2. For CD69 experiments, cells were plated at 10,000 cells/well in a 96 well cell culture treated plate and allowed to grow overnight. The next day, fresh splenocytes were obtained from a C57Bl/6 mouse and red blood cells were lysed with ACK lysis buffer. At the time of treatment, media was removed from each well and replaced with a 10 µL volume containing the treatment (His-ACDClx, anti-CD3, or PBS) and 90 µL containing 500,000 splenocytes in RPMI + 0.5% FBS. Approximately 20% of splenocytes are T cells, thus the estimated effector: target cell ratio was 10:1 (20% of 500,000 splenocytes = 100,000 T cells, incubated with 10,000 GBM cells = 10:1). After 24 hours, the splenocytes were transferred to a round bottom 96-well plate, washed with FACS buffer (1% BSA in PBS with 0.1% sodium azide), stained with 1:200 dilutions of anti-CD4-APC, anti-CD8-FITC, and anti-CD69-PerCP-Cy5.5 for 30 minutes, 4°C, and analyzed for CD69 expression.

For His-ACDClxΔ15 binding studies, cells were plated at 400,000 cells/well in a 96-well plate and incubated with His-ACDClxΔ15 or mock-purified protein (treated with (RE) or without (NT) Triton X-114 to reduce endotoxin contamination), or FACS buffer (1% BSA in PBS with 0.1% sodium azide) for 30 minutes at 4°C, washed twice with cold FACS buffer, then incubated with mouse anti-6xHis-PE antibody (1:100 in FACS buffer) for 30 minutes at 4°C and washed twice more. The live cell population was gated and the resulting population was analyzed for anti-6xHis-PE positive cells.

4.4. Results

4.4.1. Design and cloning of ACDClx variants

A schematic of all variants used in this study are illustrated in Figure 16. In comparison to the original plant construct, ACDClx-His, His-ACDClx was designed to have an 8x-His-tag on the N-terminus for purification and detection, separated from ACDClx via a TEV recognition site. The use of a TEV site instead of the previously used PreScission protease site allowed for the use of the native start codon of the anti-CD3 V_H domain of ACDClx. For DsbC-His-ACDClx, a periplasm signal peptide native to *E. coli* DsbC was added to the N-terminus to target the DsbC-ACDClx

fusion to the oxidative environment of the periplasm to allow for disulfide formation. The addition of DsbC was based on previous reports of DsbC fusions being effective for proper folding and disulfide formation of small cysteine-rich venom peptides [194]. An 8x-His-tag was included on the C-terminal end of DsbC, followed by a TEV recognition site for later removal of DsbC-His-TEV from ACDClx.

Prior to gene synthesis, the sequence for ACDClx was optimized for expression in *E. coli* by replacing uncommonly used codons and ensuring that codons for frequently used amino acids within the sequence were not overused. The sequence for DsbC was kept in its native form given that DsbC is a native *E. coli* protein. The codon adaptation index for *E. coli*-optimized ACDClx was improved from 0.222 (plant-optimized) to 0.746 as shown in Figure 17. Both His-ACDClx and DsbC-His-ACDClx were cloned and sequenced by Genscript.

The His-ACDClx plasmid was then used as a template to create untagged ACDClx and tagged/untagged truncated forms of ACDClx (His-ACDClxΔ15 and ACDClxΔ15). ACDClxΔ15 was designed to contain only the first 14 amino acids of chlorotoxin linked to the anti-CD3 variable fragments, denoted as a deletion of chlorotoxin amino acids 15-36 (Δ15). This variation was created based on observations that truncated chlorotoxin may bind GBM cells with a higher affinity than full-length chlorotoxin [177]. Following cloning, all sequences were confirmed to be correct by Sanger sequencing at the Arizona State University sequencing facility.

4.4.2. Expression of ACDClx in E. coli

Constructs were found to be optimally expressed via induction with IPTG for 4-5 hours at 30°C (a 37°C shaking incubator was not readily available for *E. coli* growth) (Figure 18). The products of all constructs were found in the insoluble fraction during optimization. Expression at lower temperature (15°C) or in an *E. coli* strain known to improve disulfide formation (Origami) to improve production of soluble ACDClx was not successful (data not shown and Figure 18F). We also sought to determine if DsbC-His-ACDClx was present in the periplasm via the periplasm targeting sequence. Periplasm proteins were obtained via osmotic shock and analyzed via

western blot. DsbC-ACDClx was only detected in the non-periplasmic insoluble fraction (Figure 18C).

4.4.3. Purification of ACDClx

Purification of His-ACDClx, DsbC-His-ACDClx, and His-ACDClxΔ15 was accomplished using Roche cOmplete His-Tag purification resin (Figure 19, left box). His-ACDClx purification in non-denaturing conditions resulted in pure protein but over a long elution time, resulting in fractions of low concentration. With the addition of guanidine to the wash and elution buffers, the elution time was reduced and resultant fraction concentrations were significantly higher (Figure 20A and B). This indicated that the protein fusions were prone to aggregation when bound to the metal affinity resin, a common issue with scFvs [cite], which was mitigated by the addition of a denaturant. The yield of purified HisE was estimated to be 72.3 ± 17.1 mg per 1 liter of culture.

Due to the inherent insolubility of ACDClx, which requires both denaturant and reductant for complete solubilization, we expressed non-His-tagged ACDClx and ACDClxΔ15 with the goal of purifying by removing contaminating proteins via addition of denaturant in the absence of reducing agent (Figure 19, right box). Washing the inclusion body pellet with denaturant was found to be capable of removing the majority of native *E. coli* proteins from the inclusion bodies, resulting in a 99% pure solution of ACDClx (Figure 20C). The purity achieved using denaturing purification of inclusion bodies was found to be nearly equivalent to the purity achieved following metal affinity purification of His-tagged ACDClx (Figure 20C). Denaturing purification inconsistently removed up to 50% of ACDClxΔ15 during the 6 M guanidine wash, thus metal affinity purification of His-ACDClxΔ15 was chosen for future experiments to obtain maximum yield.

4.4.4. His-tag removal via AcTEV protease

His-ACDClx, DsbC-His-ACDClx, and His-ACDClxΔ15 were all designed to include a TEV protease recognition sequence for removal of the 8x-His tag (and DsbC) following purification.

Optimization of AcTEV-mediated cleavage of the DsbC-8xHis-TEV sequence from ACDClx was attempted first due to the expected ease of detecting successful cleavage products via SDS-PAGE (55.3 kDa cleaved to 25.4 and 29.9 kDa versus 32.0 kDa cleaved to 29.9 and 2.1 kDa for DsbC-His-ACDClx and His-ACDClx, respectively). AcTEV (Invitrogen) was chosen over native TEV due to its S219V mutation for prevention of autocatalysis as well as the built-in His-tag for detection and removal via metal affinity chromatography. AcTEV-mediated protein cleavage was attempted using various buffers, temperatures, and protease:target protein ratios. The greatest cleavage efficiency reached approximately 50% (Figure 21A), although visual identification of the protease and the cleavage products following gel electrophoresis was difficult due to the similarity of the expected molecular weights of each (25.4 kDa for DsbC-His-TEV, 29.9 kDa for ACDClx, and 27 kDa for AcTEV) (Figure 21C). Maximum scission was observed using 20 µg fusion protein, 50 units AcTEV, 50 mM Tris pH 7, 0.5 mM EDTA, and 1 mM DTT incubated at 30°C overnight. Separation of the His-tagged AcTEV and His-tagged DsbC components from ACDClx by metal affinity chromatography, however, was unsuccessful. 100% capture of the AcTEV and DsbC fragments on the metal affinity resin was not achieved, and attempted isolation of ACDClx in the purification flow-through was present at very low concentration and equally contaminated with AcTEV and DsbC (Figure 21A and B). The inability to remove AcTEV from the cleaved fraction prompted me to move forward with utilizing His-ACDClx, ACDClx, and His-ACDClxΔ15 for future experiments.

4.4.5. Refolding, concentration, and buffer exchange of ACDClx

Refolding of His-ACDClx was originally attempted on-column, which resulted in significant aggregation and multimerization following elution with imidazole (Figure 22A). This prompted me to investigate methods for refolding His-ACDClx by rapid dilution into renaturing, oxidizing buffer. Rapid dilution is often utilized for refolding proteins that have a tendency to aggregate, especially in the context of multiple cysteine residues that can form intermolecular disulfide bonds. The nature of dilution is expected to create the necessary space between protein molecules to enable self-refolding and intramolecular disulfide formation with a lower chance of

forming mixed disulfides. Four buffer compositions were initially chosen to test the capacity to refold ACDClx (Table 5). These buffers were based on those reported in literature for refolding molecules with similar properties, such as refolding of chlorotoxin, refolding of an Fc-chlorotoxin fusion, a GBM-specific BiTE, and a snake toxin containing multiple disulfides [172,190,191,195]. Following overnight incubation, buffers 1-3 were observed to have caused significant protein precipitation while the sample in buffer 4 (100 mM Tris, 0.5 M L-arginine, 0.9 mM oxidized L-glutathione, 2 mM EDTA, 1 mg/mL CHAPS, pH 10.3, 1:100 dilution) showed no signs of precipitation and resulted in two isoforms in non-reducing conditions (Figure 22B). Isoform 1 migrated at the same rate as reduced ACDClx, while isoform 2 migrated faster, indicating that this isoform may be the refolded form.

The conditions of buffer 4 were then tested to determine which components were necessary. It was determined that while CHAPS was not necessary, 0.5 M L-arginine was critical to refolding, as the absence of or a lower concentration (0.1 M) of L-arginine resulted in complete aggregation and the inability to migrate into the acrylamide gel during SDS-PAGE in non-reducing conditions, suggesting significant formation of intramolecular disulfides (Figure 22C). Interestingly, the addition of more reducing agent resulted in a lower fraction of isoform 2. This is contrary to refolding dogma, which often suggests that including a redox pair such as GSH/GSSH favors the formation of energetically stable disulfide bonds rather than incorrect, unstable disulfides. The addition of reduced L-glutathione in the refolding buffer or the use of additional DTT in the pre-reduction step all resulted in an increase in isoform 1, while reducing the concentration of DTT used for pre-reduction or increasing the concentration of oxidized L-glutathione resulted in a slight or negligible increase in isoform 2 (Figure 22D). Taking these results together, the optimized final refolding protocol resulted in pre-reduction of ACDClx with 1 mM DTT followed by 1:100 dilution into 100 mM Tris, 0.5 M L-arginine, 2 mM oxidized L-glutathione, pH 10.3 at 4°C overnight.

Following refolding by dilution, re-concentration was required to obtain usable concentration for downstream analysis. It was observed that most standard methods of protein concentration failed if His-ACDClx was first exchanged into PBS (Figure 22E, upper left panel).

However, if His-ACDClx was first concentrated in the refolding buffer via dialysis against high molecular weight PEG or Amicon concentrator tubes, concentration was successful, and the resultant concentrated protein could be successful exchanged into PBS after using a PD-10 desalting column (Figure 22E, upper right and lower panel).

4.4.6. Testing ACDClx functionality in vitro

To test the capacity of His-ACDClx to selectively activate T cells *in vitro*, mixtures of GBM cells and splenocytes or splenocytes alone were treated with varying concentrations of His-ACDClx, full-length anti-CD3 (positive control), or media (negative control). An increase in CD69+ CD4+ and CD8+ splenocytes were observed in His-ACDClx-treated samples co-incubated with GBM cells compared with treated splenocytes alone, though the percentage of CD69+ cells overall was relatively low, reaching 12% positivity at its peak (Figure 23A and B).

Initial studies were then performed to determine the capacity of ACDClxΔ15 to bind GBM cells. In this study, His-ACDClxΔ15 was purified with or without the addition of Triton X-114, a nonionic detergent used to solubilize and remove endotoxin from DNA and protein preparations [196]. Triton X-114 treated (TT) and untreated (NT) His-ACDClxΔ15 was found to bind GBM cells compared to mock-purified controls as measured by an anti-6xHis antibody (Figure 24). 19.6% of TT-His-ACDClxΔ15 and 34.7% of NT-His-ACDClxΔ15-treated cells were found to be positive for anti-6x-His-PE, compared with 0.9% of TT-mock and 0.5% of NT-mock, suggesting that His-ACDClxΔ15 was specifically bound to the cells. It was later determined that TT-His-ACDClxΔ15 and NT-His-ACDClxΔ15 were used at different concentrations (3.5 μM and 5.2 μM, respectively), which may partly explain the quantitative differences observed in positive cells.

4.5. Discussion

Here, several variations of ACDClx and methods by which to express, purify, refold, and concentrate these variations from *E. coli* inclusion bodies are described. Compared to expression in *N. benthamiana,* expression of His-tagged ACDClx in *E. coli* produced more protein at a faster

rate (72.3 ± 17.1 mg per 1 liter of culture 4 hours post-induction in *E. coli* versus 17.8 mg per 1 kg fresh leaf weight four days post-infiltration in *N. benthamiana).* Such low yields of antibody-like therapeutics observed from plant extraction are uncommon [119,197], but for ACDClx, lower yields were likely due to the tendency of the protein to aggregate following expression. ACDClx preparations were also generally more pure when extracted from *E. coli*. These observations can be attributed to the enrichment of recombinant protein in *E. coli* inclusion bodies and the absence of the world's most abundant plant-derived protein, RuBisCo, a common contaminant found in plant preparations of ACDClx. The higher yield of *E. coli*-produced ACDClx, however, complicated the process of refolding due to significant aggregation observed during the on-column purification and refolding protocol. Although the goal of producing higher yields of ACDClx was achieved during this study, post-expression processing was not simplified nor accelerated compared to the plant-based approaches.

Proteins recombinantly expressed in *E. coli* are typically expected to be packaged into specialized, high molecular weight compartments within the cytoplasm known as inclusion bodies if the goal is to achieve significant yield and overexpression. This process was anticipated to improve the purification of His-tagged and non-His-tagged ACDClx and ACDClxΔ15 via enrichment in inclusion bodies which can be easily separated from native soluble cytoplasmic and membrane-associated proteins. Purification of ACDClx variants from inclusion bodies was successfully achieved using metal affinity chromatography with acceptable yield. Interestingly, purification using metal affinity resin required denaturing conditions for efficient elution. This suggested that ACDClx was aggregating on the resin due to non-specific protein-protein interactions and not due to the high number of cysteine residues capable of forming mixed disulfides, as reducing agent was not required and the cysteine residues were modified to prevent disulfide formation via S-sulfonation. Following success with metal affinity chromatography, a more economic and expedited process was developed to purify ACDClx variants by taking advantage of its unique insolubility. We have previously demonstrated that ACDClx is largely insoluble unless extracted in a harsh buffer containing denaturant and reducing or S-sulfonating agents. We thus rationalized that because most proteins are soluble via denaturation alone,

impure ACDClx preparations could be purified by the simple addition of denaturant to solubilize contaminating proteins, leaving ACDClx in its aggregated, insoluble state. After removing solubilized contaminants, ACDClx can be isolated by centrifugation and solubilized in denaturing, reducing buffer. This purification process was successful, resulting in greater than 95% purity (Figure 20C). However, because some ACDClx is solubilized with denaturant alone, the overall yield decreased, thus this process may be better suited to highly insoluble proteins that might suffer from addition of a purification tag.

Several alterations to the original ACDClx construct were tested to improve the solubility of ACDClx in *E.* coli. Fusion of DsbC to venom peptides containing multiple disulfide bonds has been previously described to enable the correct folding and formation of disulfides when targeted to the oxidative environment of the periplasm [194]. Given the cysteine-rich sequence of ACDClx, especially within the chlorotoxin domain, we hypothesized that DsbC might improve production of soluble, correctly folded ACDClx. Contrary to expectation, DsbC-His-ACDClx was observed to be in the insoluble fraction following initial analysis of soluble and insoluble components, and extraction via osmotic shock revealed that DsbC-His-ACDClx was absent from the periplasmic fraction Figures 18B and C.) This indicated that the periplasm targeting peptide was not successful for translation into the periplasm and that further development of this construct is necessary for success. We then attempted to test the potential for TEV protease-mediated scission to remove the 8x-histidine tag and DsbC from the C-terminus Although some success was observed with a 5-fold higher concentration of AcTEV than recommended, no efficient separation of the His-tagged AcTEV and DsbC-His-TEV components from cleaved ACDClx was achieved (Figure 21). Due to the difficulties in producing high yields of pure, soluble, untagged ACDClx, further experiments focused on producing and testing correctly folded His-ACDClx and His-ACDClxΔ15.

Properly refolding a linearized polypeptide into a functional protein with native disulfide bonds and correct secondary structure has long been considered a laborious process requiring significant optimization. In general, insoluble proteins are denatured to improve solubility, a process which disrupts hydrogen-hydrogen bonds responsible for the secondary structure that

has a significant role in imparting protein functionality. To reform these bonds, denatured protein is commonly refolded by rapid dilution or sequential dialysis into a non-denaturing buffer. For proteins containing disulfide bonds, the refolding procedure becomes more complex with an increasing number of disulfides or with uniquely-placed bonds, and requires an oxidative environment for disulfide bond formation. The formation of disulfide bonds between the appropriate cysteine residues in their native configuration is thought to be enhanced by the presence of a redox pair (versus oxidizing only), where cysteine-cysteine bonds are constantly formed and rebroken until the correct, and thus most stable, configuration is formed. Though a redox environment was successful for refolding ACDClx on column following extraction from plant tissue, the addition of reduced glutathione to the refolding buffer following extraction from *E. coli* inclusion bodies resulted in the dominating presence of an isoform which migrated at the same rate as non-refolded, reduced ACDClx following SDS-PAGE (Figure 22D). While the goal of these studies was not to determine which isoform is correctly folded ACDClx, it is hypothesized that correctly folded protein is likely to be more compact than a misfolded isoform and would thus migrate faster in non-reducing conditions. It is then assumed in these studies that the appearance of an isoform that migrates faster in non-reducing conditions vs reducing conditions is more likely to be correctly folded. However, it should be noted that chlorotoxin alone migrates *slower* in non-reducing conditions (CITE), likely due to its abundance of positively charged residues resulting in an isoelectric point (pI) of 8.5. The pI of ACDClx is even greater than chlorotoxin alone (ACDClx pI = 8.78), though distinct bands migrating slower in non-reducing vs reducing conditions were never observed. In the case of ACDClx, migration of a correctly folded isoform may manifest as migration at the same rate as fully reduced ACDClx, where a balance is reached between a more compact structure that might result in faster migration and the abundance of positively charged residues that might result in slower migration. Further studies are required for confirmation of isoform identity; for preliminary *in vitro* experiments, the mixture of isoforms was used.

In the context of protein refolding, arginine has long been considered an essential additive to reduce the potential for protein aggregation during renaturation. The addition of 0.5M L-arginine to the renaturing buffer was determined to be a requirement for refolding ACDClx

without significant aggregation and was also found to assist with concentrating protein following the refolding dilution process (Figure 22C and E). Because some aggregation of ACDClx was still observed following refolding (visualized as a smear above the two distinct bands), the refolding buffer may benefit from increasing the concentration of arginine, which has been observed to increase the refolded fraction of other proteins [198]. In these experiments, especially in the case of filter-based concentration, arginine appeared to act as a blocking agent, preventing ACDClx from non-specifically binding the filter membrane during centrifugation which had previously resulted in protein loss and an inability to concentrate ACDClx. Given the success of using arginine as a refolding additive, it may be possible to use it as an additive during on-column refolding and purification to reduce aggregation and accelerate production of functional ACDClx.

The number of disulfides present with the chlorotoxin domain of ACDClx is seen as one of the major challenges in producing properly folded ACDClx. To address this issue, we designed a similar fusion protein, ACDClxΔ15, differing from full-length ACDClx by the deletion of the last 22 amino acids of the chlorotoxin domain (amino acids 15-36 of chlorotoxin). This truncation was modeled based on the observations of others that this truncated chlorotoxin may impart higher affinity binding to GBM cells [177]. As an additional benefit, three disulfide bonds are removed, leaving a total of three expected disulfides in ACDClxΔ15 compared to six in full-length ACDClx. ACDClxΔ15 was unexpectedly equally difficult to solubilize and refold (data not shown) but was found to successfully bind to mouse GBM cells in preliminary studies (Figure 24). Previous studies have observed that full-length chlorotoxin is capable of selectively binding GBM cells with no observed affinity to healthy tissue [92]. The significant differences in peptide composition between chlorotoxin and chlorotoxinΔ15 may change this selectivity, however, and studies must now be completed to determine if the GBM selectivity of chlorotoxinΔ15 over healthy tissue is retained.

These studies show that the current method of producing ACDClx and its variants in *E. coli* is complicated by their unique insolubility which requires sequential harsh solubilization techniques, purification, refolding, and concentration – a process that likely results in a small

fraction of functional protein (Figure 23). For any given recombinant protein therapeutic, the ideal method of production would be a simplified purification of excreted, correctly folded, functional protein. We have so far demonstrated that the unique structural features of ACDClx result in insoluble protein expression in both plants and *E. coli.* The production and purification of ACDClx would thus likely benefit from expression in a system capable of forming complicated disulfide bond configurations and secreting the resultant protein into a medium where it can be easily isolated and relatively free from the potential of proximity-induced aggregation.

Table 4: Oligonucleotides used for colony screening and cloning of *E. coli* constructs		
Primer	Description	Sequence (5'-3')
oTM 976	BamHI-Cltx	CATGGATCCTCAACGACACAGG
oTM 977	NdeI-aCD3_VH	GCATCATATGGAAGTTCAGCTGG
oTM 978	BamHI-CltxΔ15	GTATGGATCCTCAACGTGCCATCT
oTM 115	T7 forward	TAATACGACTCACTATAGGG
oTM 228	T7 reverse	GCTAGTTATTGCTCAGCGG

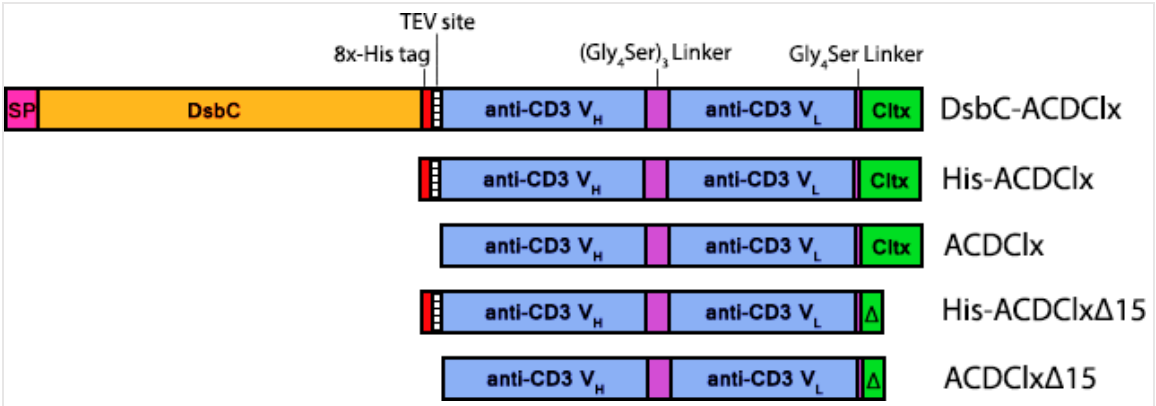

Figure 16: **Schematic of the five constructs used to express ACDClx and variants of ACDClx in *E. coli* from a pET-11a vector.** SP = *E. coli* native DsbC periplasm signal peptide. TEV = TEV protease recognition site. V_H = variable heavy fragment from anti-CD3, clone 145-2C11. V_L = variable light fragment from anti-CD3, clone 145-2C11. Cltx = chlorotoxin. Δ = chlorotoxin with residues 15-36 deleted.

Figure 17: **Codon optimization of the His-ACDClx sequence.** The His-ACDClx was originally codon-optimized for expression in plants. The sliding window values of codon usage was calculated for *E. coli* based on the plant-optimized sequence (orange, "Non-optimized") and following optimization for expression in *E. coli* (blue, "E. coli Optimized"). The average codon adaptation index (CAI) for the non-optimized sequence was 0.222, which was increased to 0.746 for the optimized sequence.

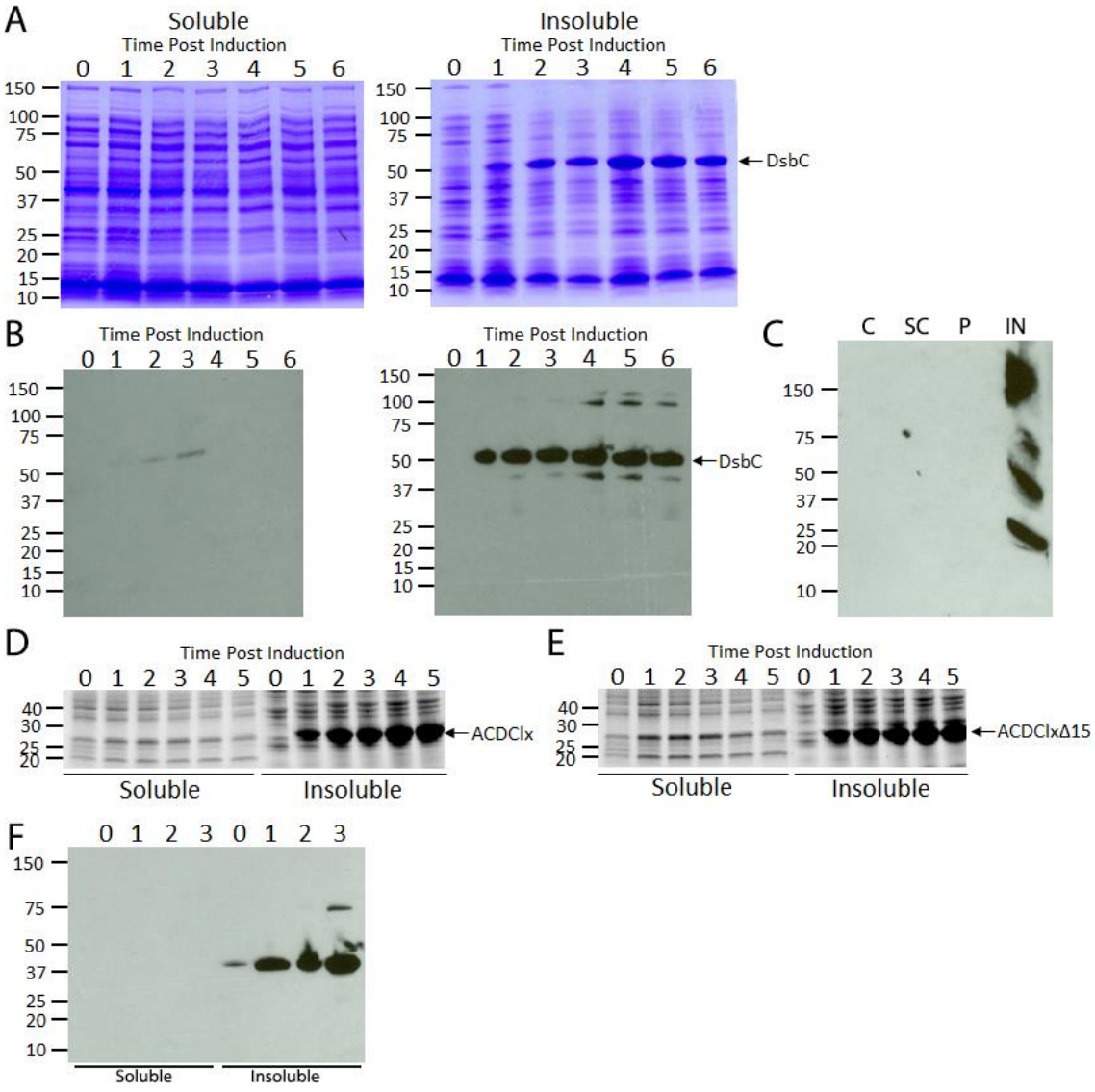

Figure 18: ACDClx expression kinetics in *E. coli* following IPTG induction. (A) Coomassie and (B) western blots of soluble and insoluble protein expression in *E. coli* transformed with a pET-11a plasmid encoding DsbC-His-ACDClx and induced with 1mM IPTG. (C) Periplasm extraction following expression of periplasm-targeted DsbC-His-ACDClx. C= culture supernatant; SC = sucrose supernatant following osmotic shock; P = periplasmic fraction; IN = insoluble fraction. Expression kinetics of untagged ACDClx (D) and untagged ACDClxΔ15 (E) following induction with 0.3 mM IPTG. (F) Expression of His-ACDClx in BL21 (DE3) Origami *E. coli*. All times indicated are in hours. Molecular weight markers are in kilodaltons.

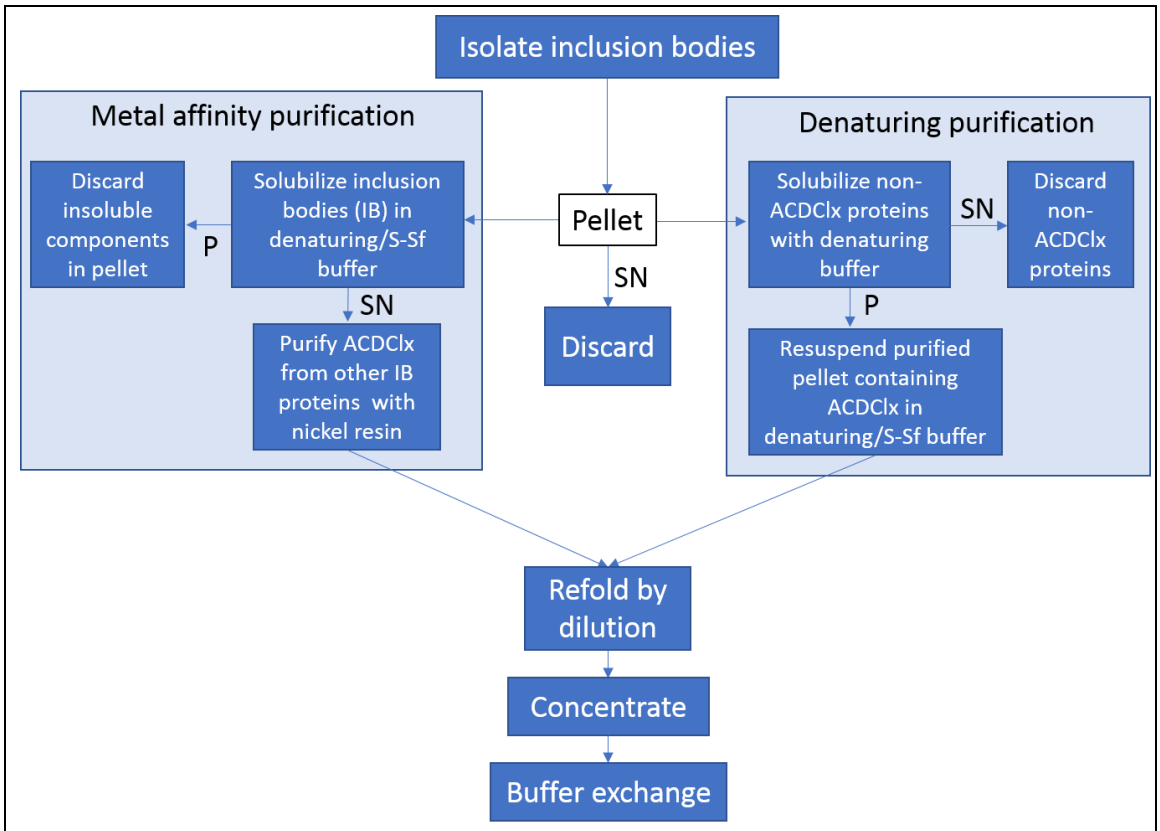

Figure 19: Schematic of the purification and refolding process. The unique insolubility of ACDClx allows for purification to be achieved with (left box) or without (right box) metal affinity chromatography (MAC). Purification via MAC is accomplished by allowing His-tagged ACDClx to bind to nickel resin and washing away non-His-tagged *E. coli* proteins, then eluting His-tagged ACDClx from the resin by competition with imidazole. Elution is most efficient using a denaturing buffer to prevent protein aggregation on the column. Purification without MAC is accomplished by solubilizing *E. coli* proteins via addition of denaturant and removing them from the supernatant (SN) following centrifugation. ACDClx is primarily soluble only in denaturant with reducing/S-sulfonating (S-Sf) buffer, thus it will be located in the pellet (P) following centrifugation in a purified form, where it can then be solubilized. For both purification processes, the resultant soluble ACDClx is then refolded by dilution overnight, concentrated by centrifugal molecular weight filters, and rapidly exchanged into a buffer of choice (i.e., PBS) using a desalting column.

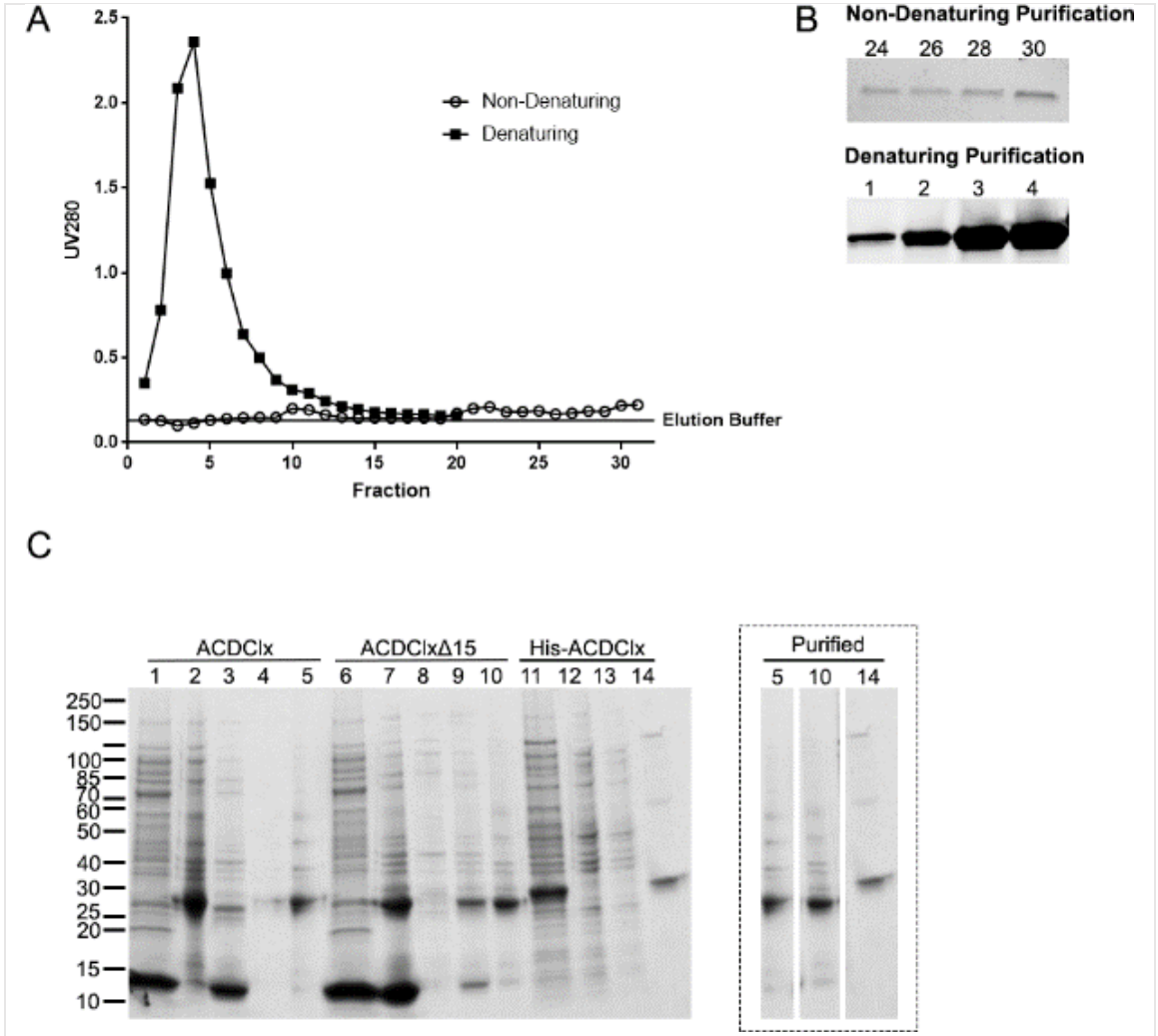

Figure 20: Purification of ACDClx is achieved using denaturing conditions, with or without metal affinity chromatography. His-ACDClx was purified in either non-denaturing conditions (50 mM Tris pH 7, 150 mM NaCl) or denaturing conditions (50 mM Tris pH 7, 150 mM NaCl, 6 M guanidine-HCl) and fractions were collected one column volume at a time with elution buffer (850 mM imidazole in the respective buffer). (A) UV280 spectrophotometer measurements were taken for each elution fraction after blanking with the respective buffer. The elution buffer measurement (0.131 for non-denaturing, 0.128 for denaturing) is marked as a line at 0.13 on the graph to indicate the maximum contribution of elution buffer components to the UV280 measurements. (B) Fractions representing the highest UV280 measurements were resolved via SDS-PAGE in reducing conditions on a stain-free gel and imaged following UV exposure. Gel fluorescence of the non-denaturing fractions were imaged following a 5 second exposure in order to visualize bands, whereas a 0.5 second exposure resulted in overexposure for the denaturing fractions due to the high protein concentration relative to the non-denaturing fractions. (C) ACDClx, ACDClxΔ15 were purified via denaturant-mediated removal of contaminating proteins and compared to His-ACDClx, which was purified via metal affinity chromatography. Lanes 1/6: soluble (non-inclusion body) *E. coli* fraction; lanes 2/7: inclusion bodies; lanes 3/8: protein solubilized during denaturant wash #1; lanes 4/9: protein solubilized during denaturant wash #2; lanes 5/10: fraction representing denaturant-mediated

purified protein, solubilized via denaturant + reduction/S-sulfonation; lane 11: denatured + reduced/S-sulfonated inclusion bodies prior to loading onto metal affinity resin; lane 12: unbound protein (flow-through); lane 13: wash #1 with denaturant; lane 14: eluted purified fraction. The dashed line box to the right represents the three purified fractions from lanes 5, 10, and 14 grouped together for comparison. Molecular weights of ACDClx, ACDClxΔ15, and His-ACDClx are calculated to be 30.0 kDa, 27.7 kDa, and 32.0 kDa, respectively.

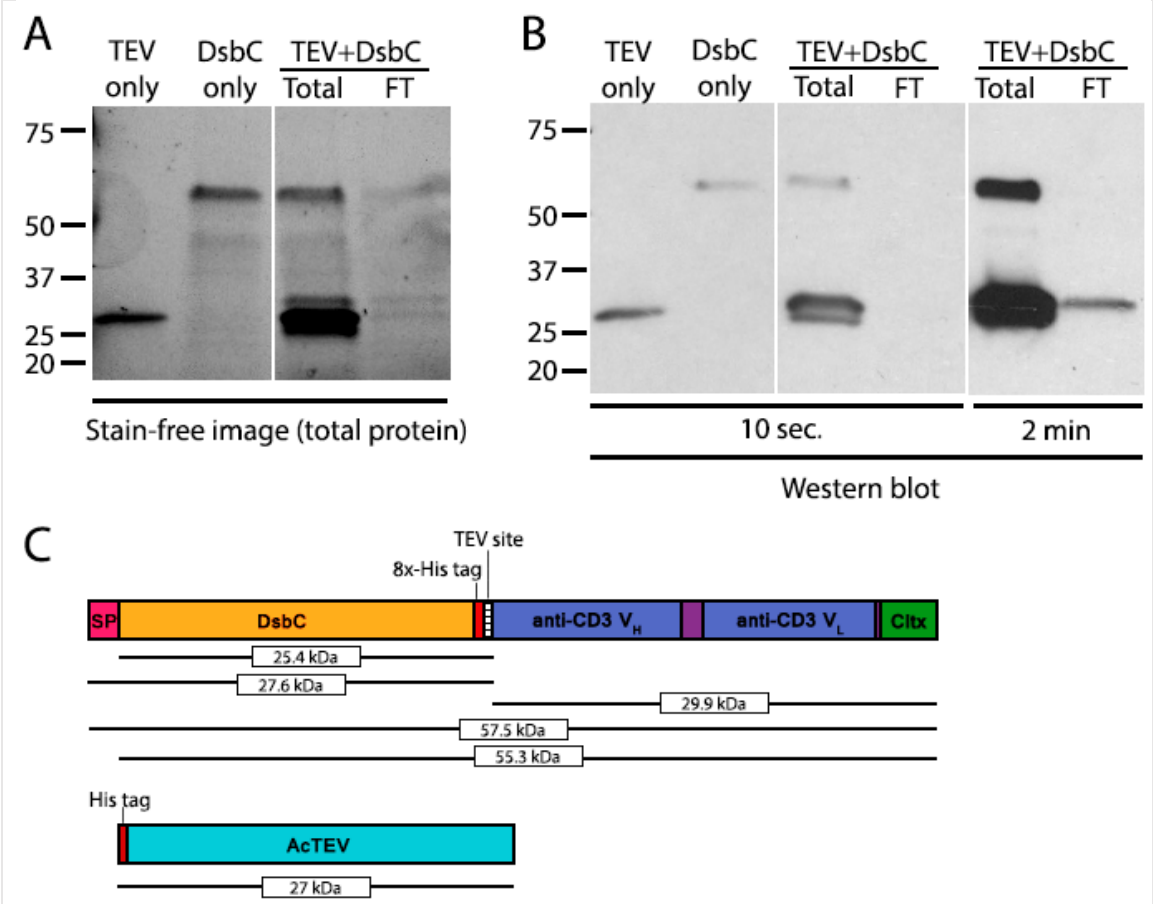

Figure 21: Removal of the DsbC-His fragment from ACDClx following TEV-mediated scission is inefficient. (A) Total protein gel of reactions containing TEV only, DsbC-ACDClx only, and TEV + DsbC-ACDClx. The last lane shows the flow-through (FT) of the TEV + DsbC-ACDClx reaction following incubation with metal affinity resin. (B) Western blot of the gel shown in (A), probed with anti-6xHis. A longer exposure of the TEV + DsbC reactions are shown to indicate the presence of His-tagged protein in the FT. (C) Schematic and calculated molecular weights of the various products that may be present on the gels in (A) and (B).

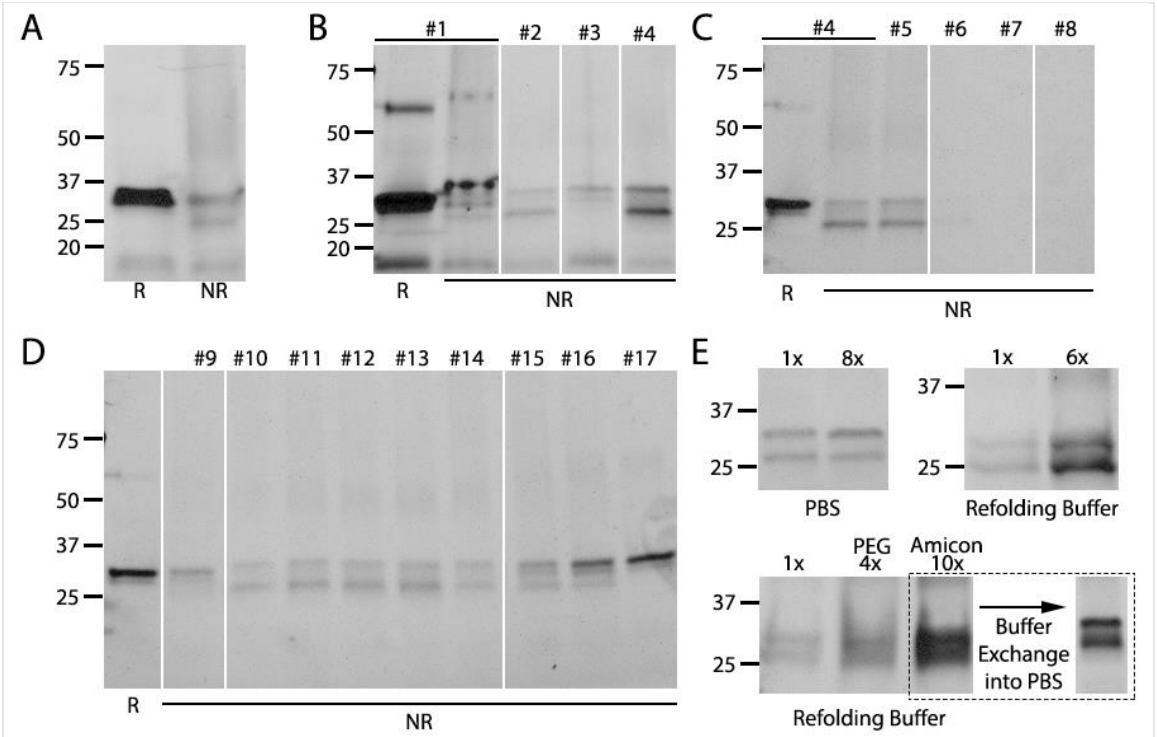

Figure 22: Refolding optimization for ACDClx. (A) Eluted His-ACDClx following refolding on column in reducing (R) and non-reducing (NR) conditions. (B) Refolding by dilution using buffers #1-4 (Table 5) previously successful for similar proteins. (C) Arginine is required for refolding while CHAPS is not essential. Buffer #5: #4 with no CHAPS; #6: #4 with no arginine; #7: #4 with no CHAPS and no arginine; #8: #4 with 0.1 M arginine instead of 0.5 M. (D) Optimization of redox conditions. Buffer #9: #5 pre-reduced with 50 mM DTT; #10: #5 (pre-reduced with 10 mM DTT); #11: #5 pre-reduced with 5 mM DTT; #12: #5 pre-reduced with 2.5 mM DTT; #13: #5 pre-reduced with 1 mM DTT; #14: #5 with 0.1 mM reduced glutathione added; #15: #5 with 0.9 mM reduced glutathione added; #16: #5 with 1.8 mM reduced glutathione added; #17: #5 with 9 mM reduced glutathione added. (E) Arginine is essential for protein concentration following refolding and monomers are retained following arginine removal using a desalting column. The top left image represents His-ACDClx exchanged into PBS (1x) and then concentrated 8-fold in an Amicon 3.5kDa centrifugal device (8x). The top right image represents His-ACDClx (1x) concentrated 6-fold in an Amicon device without exchange into PBS (6x). The bottom image represents His-ACDClx in refolding buffer (1x) concentrated 4-fold by dialysis against 35k MW dry PEG (PEG 4x) or concentrated 10-fold in an Amicon device (Amicon 10x). The Amicon 10-fold concentrated His-ACDClx was then successfully exchanged into PBS using a PD-10 desalting column. All images represent total protein resolved on stain-free gels. Protein refolded in buffers #1-8, 10, & 14-17 were pre-reduced with 10 mM DTT for 15 minutes at room temperature prior to dilution.

Table 5: Buffers used for initial refolding optimization		
Buffer	**Refolding conditions**	**Modified from**
#1	1:10 dilution into 0.5 M L-arginine, 1 mM EDTA, 2 mM oxidized glutathione, pH 8.5, 0.1% CHAPS	Wang *et al.* [190]
#2	1:20 dilution into 10 mM Tris pH 8.5, 0.1 M NaCl, 0.5 mM oxidized glutathione, 0.1% CHAPS	Kasai *et al.* [191]
#3	1:10 dilution into 0.4 M Tris pH 8, 1 mM EDTA, 2.5 mM reduced glutathione, 0.25 mM oxidized glutathione, 0.1% CHAPS	Bae *et al.* [195]
#4	1:100 dilution into 100 mM Tris, 0.5 M L-arginine, 0.9 mM oxidized glutathione, 2 mM EDTA, 0.1% CHAPS, pH 10.3	Choi *et al.* [172]

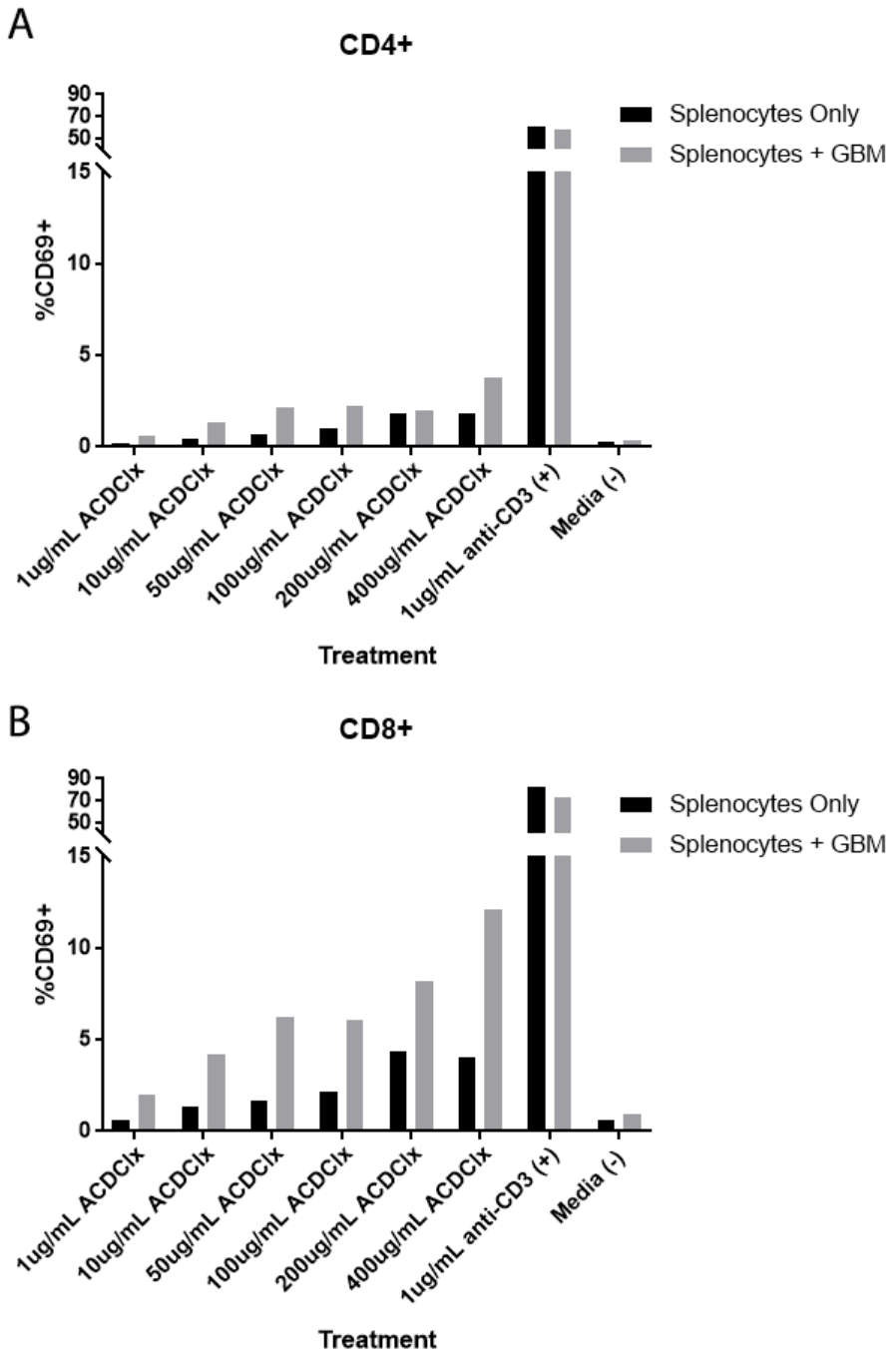

Figure 23: His-ACDClx produced in *E. coli* results in low-level T cell activation. Fresh splenocytes were incubated with varying concentrations of His-ACDClx, 1 µg/mL anti-CD3, or media for 24 hours, with or without GBM cells. Splenocytes were stained with anti-CD4-APC, anti-CD8-FITC, and anti-CD69-PerCP-Cy5.5 and analyzed via flow cytometry.

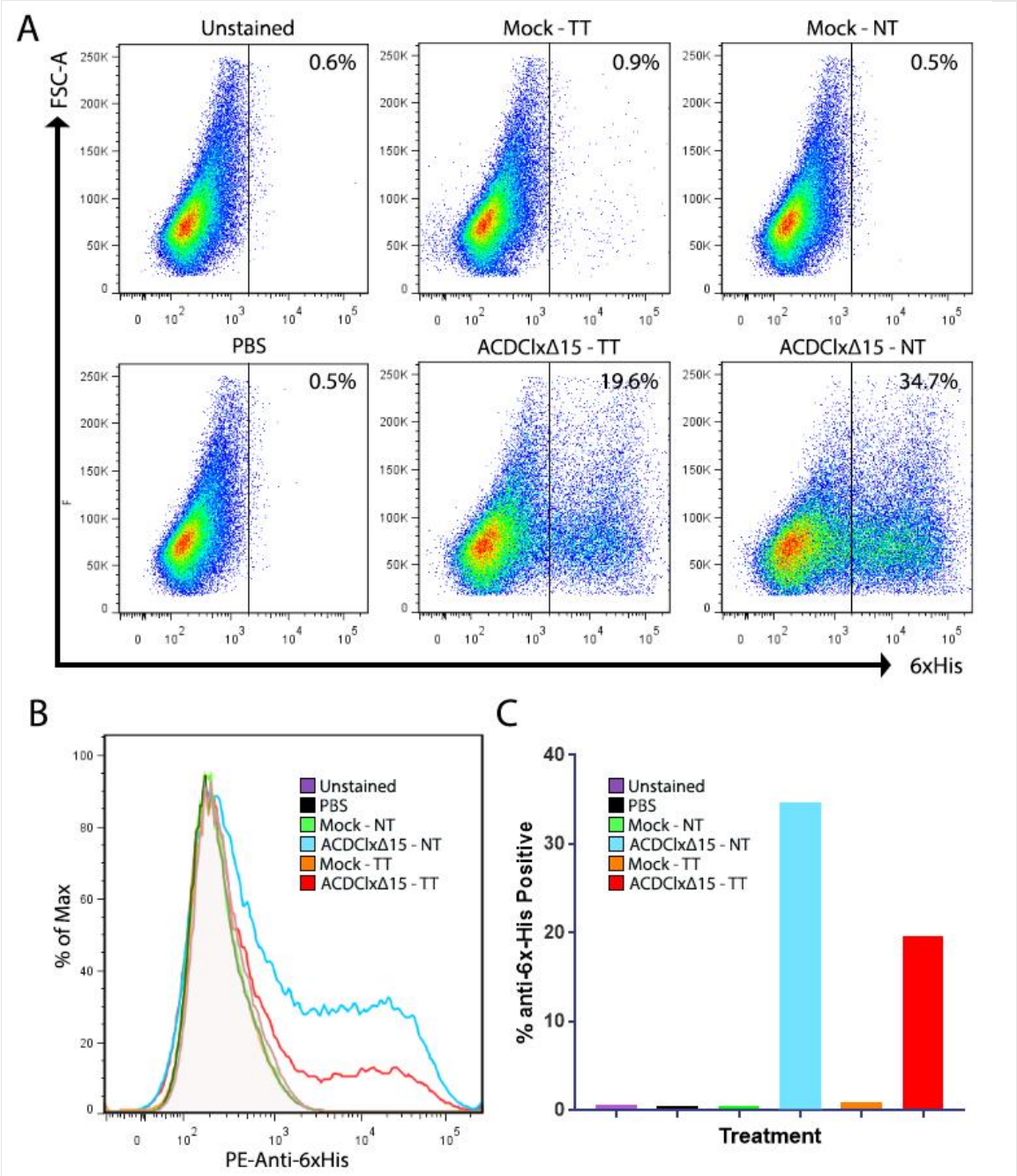

Figure 24: ACDClxΔ15 binds GBM cells *in vitro.* (A) Top left: Unstained GBM cells. Bottom left: Untreated GBM cells stained with anti-6xHis-PE. Top middle: Mock-TT-treated GBM cells. Bottom middle: ACDClxΔ15-TT-treated GBM cells. Top right: Mock-NT-treated GBM cells. Bottom right: ACDClxΔ15-NT-treated GBM cells. The line in each plot shows the cutoff for anti-6xHis-negative (left) and -positive cells (right) used for analysis in (C). (B) A histogram depicting the anti-6xHis-PE signal from dot plots shown in (A). (C) Percent anti-6xHis-positive cells for each treatment group. The vertical lines in the dot plots shown in (A) represent the cutoff for anti-6xHis negative/positive cells. TT = Triton X-114 treated during protein purification to reduce endotoxin levels. NT = No Triton X-114 treatment during purification.

CHAPTER 5

SUMMARY AND OUTLOOK

Treatment of GBM relative to other peripheral tumors is significantly hindered due to the gatekeeping of the BBB. Exploiting pathogenic strategies of gaining entry to the brain parenchyma to enhance drug concentration where invasive malignant cells lie is an intriguing alternative. The studies described in chapters 2-4 underscore specific difficulties in developing pathogen-inspired strategies for targeting GBM. We sought to explore the potential of two naturally-derived peptides to enhance treatment of GBM. The first peptide is derived from one of the most widely recognized neurotropic pathogens, the rabies virus. Entry into the CNS is mediated by a 29-amino acid peptide within the rabies virus glycoprotein, which was used in chapter 2 for the purpose of enhancing the concentration of chemotherapeutic-loaded nanoparticles in the brain. The second peptide, chlorotoxin, is a component of deathstalker scorpion venom that is often exploited by researchers for its capacity to selectively bind tumor cells. We investigated the potential of producing a chlorotoxin fusion protein for enhancing T cell recognition of brain tumors in chapters 3-4.

5.1. Summary of Chapter 2

Using a polymeric nanoparticle PLGA-based platform, we investigated the potential of RVG-29 to enhance delivery of dye or drug-loaded nanoparticles to the brain parenchyma in mice and to improve GBM-related outcomes. We were first interested to measure the distribution of payload delivered by RVG-29-modified particles in comparison to control biotin-modified particles to peripheral organs. However, we were especially interested in measuring delivery to major brain regions, given that brain entry via RVG-29 is thought to occur via motor neurons. We found that the lipophilic dye DiR was distributed to peripheral organs in similar quantities for both targeted and non-targeted formulations. Within the brain, we observed that the concentration of DiR or other small, hydrophobic payloads was increased in the brain when delivered by RVG-29-modified particles compared to control particles. Targeted delivery of DiR after 2 hours was

especially apparent in the cortex, and to a lesser extent, the cerebellum, midbrain, and striatum (36.8%, 23.6%, 22.4%, and 21.4% greater delivery via RVG-29 particles to these regions, respectively). We speculate that delivery to these regions is mediated by the higher proportion of $GABA_BR$ in these regions compared to others, which has been implicated as a receptor for RVG-29 by other researchers.

In contrast to targeting observed 2 hours after injection, targeting was not observed 6 hours post-injection. We hypothesized that peptide instability may be responsible for this affect. Data revealed that exposure of RVG-29 modified particles to an aqueous environment at 37°C for 4 hours pre-injection to emulate the environment encountered post-injection resulted in loss of targeting affect. This indicated that natural peptide instability, likely hydrolysis, was the primary cause of equivalent encapsulant found in the brain 2 hours post-injection in this experiment. Interestingly, we also uncovered the innate ability of DiR to accumulate in brain tissue over time compared to the hydrophobic dye Nile red. We argue that this observation is significant in the field of drug delivery, where experiments intended to measure the anticipated delivery of nanoparticles loaded with chemotherapeutics by substituting in a spectroscopically-measurable dye surrogate may be misleading due to confounding factors inherent in the chemical properties of the two payloads. In many studies for example, dye payloads are substituted for drug payloads strictly based on hydrophobicity or charge similarity between the two. However, our studies indicate that two dyes used as a hydrophobic surrogate display opposite kinetics within the brain, with a more lipophilic dye (DiR) being accumulated while the non-lipophilic dye (Nile red) was not.

These studies also provide evidence that supports the need for covalent attachment of payload to the slow release polymer to accurately measure nanoparticle uptake into tissue. In our experiments investigating brain uptake of nanoparticles encapsulated with dye (without covalent attachment), the differences in uptake observed between the two payloads indicated that payload was being transferred from nanoparticle to tissue versus actual nanoparticle uptake into tissue. I.e., if nanoparticles were entering tissue via RVG29-mediated uptake, similar accumulation should have been observed regardless of payload. To further support this, we observed that kinetics of brain uptake following injection of free dye (DiR) was similar to the kinetics of brain

uptake observed following injection of DiR-encapsulated control particles. This indicated that kinetics in ours and other studies may be more so mediated by the chemical nature of the dye itself rather than actual uptake by particles into tissue. Nanoparticle-mediated drug delivery studies often use spectroscopic measurements of dye in tissue to claim that dye-encapsulated nanoparticles have entered tissue, however, we argue that payload transfer from particles to tissue may be a confounding factor for data reported using these methods.

Comparing treatment of orthotopic GBM with camptothecin-loaded nanoparticles, we found no significant differences in survival or tumor growth in mice treated with targeted vs untargeted formulations. This was likely due to the loss of targeting affect observed 2-hours post-injection in biodistribution studies combined with the need for constant exposure of chemotherapeutics to malignant cells for a significant affect to be seen. Altogether, these data indicate that the stability of the targeting moiety used and the surrogate payload chosen for measuring nanoparticle distribution are essential factors to consider when designing a new treatment platform in the field of particle-based drug delivery.

5.2. Summary of Chapter 3

Given the recent success of immunotherapies for improving outcomes for many cancer patients but the relative lack of success for GBM patients, we sought to design an immunotherapy capable of having a widespread effect on the tumor as a whole, rather than on a subset of targetable cells. To this end, we designed the fusion protein ACDClx, short for anti-CD3/chlorotoxin. This molecule was modeled based on a bispecific protein fusion of opposing antibody variable fragments designed to simultaneously engage a T cell via a constant protein in the TCR complex, CD3, and a tumor cell via a surface-expressed tumor-specific or tumor-associated antigen. In the case of ACDClx, the tumor-specific antibody variable fragments are replaced with a 36-amino acid peptide, chlorotoxin. Chlorotoxin is naturally found in the venom of the dealthstalker scorpion; though it is a potent component of venom, its natural purpose is to paralyze insect prey and has since been shown to have no harmful effects to humans or other vertebrate animals. In the lab, chlorotoxin has been shown to selectively bind GBM and other

malignant cells of neuroectodermal origin relative to healthy tissue, thus it serves as an ideal targeting moiety for drug delivery or GBM targeting of imaging molecules. In a select number of studies, chlorotoxin has also been observed to penetrate the BBB when conjugated to therapeutic and imaging agents of various molecular weights. This has been observed in one *in vivo* model and several *in vitro* models, thus it may be possible for chlorotoxin to enhance entry of ACDClx into healthy brain tissue to target invasive cells in addition to the bulk tumor where a large proportion would be accessible via the EPR effect.

Chapter 3 focuses heavily on the attempt to produce ACDClx as a soluble protein in *N. benthamiana.* Protein production in plants is gaining popularity in response to the development of optimized viral vectors for enhancing yield, and was chosen for initial production of ACDClx due to the capacity for forming disulfide bonds, 6 of which are present in ACDClx, and for the economic viability of large scale protein production in comparison to other platforms capable of disulfide formation (reviewed in *Chapter 1)* which often require expensive media additives. Contrary to expectation, ACDClx containing a C-terminal histidine tag (ACDClx-His) produced in *N. benthamiana* was completely insoluble and required harsh conditions – denaturant and reducing agent - for solubilization. Even though this construct was completely insoluble, we demonstrated that following solubilization, purification, and oxidative refolding, ACDClx was capable of selectively activating T cells when GBM cells were also present.

To address the insolubility and relatively low yield of ACDClx, we then designed three new constructs, His-ACDClx, N-glycosylated His- ACDClx (Ngly-His-ACDClx), and CTB-ACDClx, and expressed them in *N. benthamiana*. We found that all three constructs expressed at higher levels compared to the original ACDClx-His construct, and that the Ngly-His-ACDClx expressed at significantly higher levels than all constructs, though purification was hindered by the plant protein, RuBisCo. Unfortunately, none of the constructs were able to produce soluble protein. Though we initially attributed the insolubility of ACDClx to the compactly-folded chlorotoxin domain, which contains 4/6 disulfide bonds, we observed that expression of the anti-CD3 domain alone was also largely insoluble. Due to the inherent insolubility of ACDClx in a system expected

to produce soluble protein, we opted to shift expression to a host expected to produce larger quantities of ACDClx in an insoluble form, discussed below.

5.3. Summary of Chapter 4

E. coli has long been co-opted as a host for expression of heterologous proteins and is often the expression host of choice due to its economic viability, ease of manipulation, and rapid growth characteristics. We thus chose *E. coli* BL21(DE3) to express His-ACDClx with the hypothesis that although insolubility was expected, an increase in yield at a faster rate compared to expression in plants was also anticipated. Consistent with this hypothesis, more ACDClx was expressed as an insoluble protein in 4 hours compared to the yield obtained from *N. benthamiana* in 4 days. However, because of the difference in protein yield, it also become more difficult to purify and refold ACDClx produced from *E. coli*, a process that was optimized to span 4-5 days before a final product was obtained. Studies during this optimization process concluded that denaturing purification via metal affinity chromatography was required to obtain high concentration elutions of ACDClx, and that the addition of 0.5 M L-arginine to the refolding buffer was essential to the successful production of refolded protein. Though testing for functionality revealed that T cell activation was measurable following treatment with His-ACDClx in the presence of GBM cells, the extent of activation was much lower, likely due the excessive processing the protein has to undergo before testing.

Based on previous studies of soluble production of short peptides containing numerous disulfide bonds in *E. coli,* we also attempted to produce ACDClx as a periplasm-targeted C-terminal fusion to the *E. coli* protein, DsbC, which enabled production of properly folded peptides by others when targeted to the oxidative environment of the periplasm [194]. Contrary to expectation, DsbC-His-ACDClx was neither insoluble nor found to be located within the periplasm following expression in *E. coli*. Attempts to remove DsbC-His from ACDClx via TEV protease-mediated scission, while partially successful in the scission process, was not successful in separating the three components (TEV, DsbC-His, and ACDClx) following scission. Thus,

During these studies we also designed ACDClxΔ15, a truncated form of ACDClx that resulted in the deletion of the last 22 amino acids of chlorotoxin and exposed an internal C-terminal arginine, which has been hypothesized by others to improve the affinity for GBM cells compared to full-length chlorotoxin. We hypothesized that this 22 amino acid deletion would also facilitate the production of the fusion protein as a result of 3 disulfide bonds being removed. Although production of ACDClxΔ15 was equally difficult as full-length ACDClx, binding of ACDClxΔ15 to GBM cells was measured via flow cytometry, indicating that ACDClxΔ15 may be a viable option for use as an immunotherapy moving forward, However, more testing is necessary to determine if truncated chlorotoxin retains the same excellent selectivity for GBM cells as full-length chlorotoxin.

Lastly, we were able to show that due to the inherent insolubility of ACDClx and ACDClxΔ15, it is possible to purify these protein fusions without the need for a histidine tag. This was accomplished by removing contaminating host proteins from the insoluble fraction by the addition of denaturant, which leaves most ACDClx and ACDClxΔ15 insoluble, but solubilizes the majority of contaminating proteins, which can be subsequently removed following centrifugation. The remaining insoluble fraction, composed primarily of ACDClx, can then be solubilized with denaturant plus reducing agent and processed as necessary. Though successful, a fraction of ACDClx can be inconsistently soluble in denaturant alone, which results in a lower overall yield. We conclude that this method of purification would be a viable method if the production of untagged protein is necessary for downstream use.

5.4. Outlook and future directions

Though small and often easy to produce, the use of peptides in the context of therapeutic development present unique challenges. For RVG-29, stability in an aqueous environment was an issue that is likely not observed for the full length RVG protein given its natural capacity to maintain neurotropism following display on a viral particle, excretion in saliva, and transfer to the brain of an unwilling host via skin puncture. For chlorotoxin, the unique arrangement of four

disulfide bonds within a 36-amino acid sequence presents a significant obstacle to the recombinant expression and proper assembly of the knotted structure in the context of a fusion protein such as ACDClx. Advances in peptide stabilization and disulfide formation are thus necessary for the success of the two therapeutics described in this dissertation. For RVG-29, substitution of amino acids especially sensitive to hydrolysis or deamidation, such as serine or Asn-Gly pairs, with more stable amino acids may be useful in promoting peptide stability. For chlorotoxin, native disulfide formation has been successful in mammalian expression systems as a secreted fusion with siderocalin [199], which may also be effective for production and purification of ACDClx. Synthetic production of chlorotoxin with correctly-arranged disulfides is also possible and opens opportunities for covalently linking anti-CD3 Fv to chlorotoxin following separate expression or synthesis.

In the absence of a new expression system for producing soluble, properly folded ACDClx, continued optimization of refolding and downstream characterization of the resultant isoforms for ACDClx is necessary. The production of multiple isoforms without individual biochemical characterization of structure or function presents potential issues in calculating effective dose. One might imagine a scenario of two isoforms present in equal quantities: one of which is fully functional and thus capable of binding both intended cell targets, and one which only binds a single cell target. In this case, the effective concentration of protein is reduced by half, given that the intended effect of ACDClx is to engage two cell types simultaneously. The second isoform, binding only one cell type, may also serve to further inhibit the effectiveness of the fully functional isoform by serving as a blocking agent for available binding sites of functional protein. Determination of which isoform is most likely to be correctly folded might first be investigated by reverse-phase HPLC, which has been used for chlorotoxin [190] and other proteins under the assumption that correctly folded water soluble proteins have fewer exposed hydrophobic residues and would thus have lower retention times Following analysis, refolding optimization towards a single isoform can be more confidently performed.

Functional ACDClx produced in high yield should then be analyzed for functionality in various *in vitro* and *in vivo* assays for to obtain pre-clinical data. More specific assays of T cell

activation are warranted, such as measuring inflammatory cytokine production and proliferation in T cells and measuring GBM cell death following incubation of T cells, ACDClx, and GBM cells. Inflammatory cytokine production in treated T cells would indicate that these cells are not only activated, but capable of potentiating an anti-tumor response by secreting cytokines to alert nearby cells of a problem. Similarly, T cell proliferation in this context would indicate that the T cells are reacting in such a way that an overwhelming response can be produced. Most importantly, T cell-mediated killing of GBM cells when co-incubated with ACDClx would be an excellent indicator of the fusion protein's promise for treatment of GBM *in vivo*.

ACDClx as described in chapters 3 and 4 is designed to bind CD3 present on mouse T cells. Thus, the first iteration of ACDClx was originally intended to be tested in an immunocompetent mouse model of GBM in order to appropriately study the immune cell dynamics that might occur in a host harboring an orthotopic GBM tumor. Measuring the characteristics of overall short and long term immune response following treatment various doses and dosing regiments of ACDClx will be important for determining whether ACDClx has the capacity to induce a pro-tumor response with a low number of doses, indicating that ACDClx capable of reversing immunosuppression with the tumor microenvironment, or requires constant, long term exposure to maintain tumor reduction over time. It will also be important to test various methods of delivering ACDClx, such as intravenous, intratumoral, and intrathecal injection, to determine which method produces the greatest benefit for tumor reduction and overall survival. Lastly, given the strong role of immune checkpoint proteins to prevent immune-mediated tumor destruction, it will be critical to test ACDClx as a co-therapy with immune checkpoint blockade if strong survival trends are not observed with ACDClx alone.

In the new era of emerging nanotechnologies and immunotherapies, the reduction of mortality in cancer patients has finally begun to progress faster than ever before and is expected to continue as new therapies are developed and become more affordable and more widely available. At the same time, technologies for early detection of various malignancies are being developed that will no doubt enable better prognosis if treatment is also started early. For GBM, even more obstacles need to be overcome before mortality rates decrease to the level of most

peripheral tumors. Methods for studying glioma stem cells that promote tumor cell repopulation are in development and are desperately needed to evaluate methods for their destruction [200,201]. Methods for tracking therapeutics to enable better methods for improving delivery to tumor cells are also needed and underway [202]. Overall, the successful treatment of GBM will likely be a unique combination of therapies capable of enabling tumor cell destruction and maintaining immune memory for destruction of new malignant cells. To combat GBM, an ongoing anti-tumor front will be absolutely necessary for preventing the tumor recurrence and is likely to partially take the form of a living, replicating system, such as the immune system or tightly regulated virotherapies.

REFERENCES

[1] Q.T. Ostrom, H. Gittleman, G. Truitt, A. Boscia, C. Kruchko, J.S. Barnholtz-Sloan, CBTRUS Statistical Report: Primary Brain and Other Central Nervous System Tumors Diagnosed in the United States in 2011-2015, Neuro-Oncol. 20 (2018) iv1–iv86. doi:10.1093/neuonc/noy131.

[2] E.M. Sizoo, L. Braam, T.J. Postma, H.R.W. Pasman, J.J. Heimans, M. Klein, J.C. Reijneveld, M.J.B. Taphoorn, Symptoms and problems in the end-of-life phase of high-grade glioma patients, Neuro-Oncol. 12 (2010) 1162–1166. doi:10.1093/neuonc/nop045.

[3] L. DN, O. H, W. OD, C. WK, WHO Classification of Tumours of the Central Nervous System, n.d. http://publications.iarc.fr/Book-And-Report-Series/Who-Iarc-Classification-Of-Tumours/Who-Classification-Of-Tumours-Of-The-Central-Nervous-System-2016 (accessed February 4, 2019).

[4] D.N. Louis, A. Perry, G. Reifenberger, A. von Deimling, D. Figarella-Branger, W.K. Cavenee, H. Ohgaki, O.D. Wiestler, P. Kleihues, D.W. Ellison, The 2016 World Health Organization Classification of Tumors of the Central Nervous System: a summary, Acta Neuropathol. (Berl.). 131 (2016) 803–820. doi:10.1007/s00401-016-1545-1.

[5] H. Yan, D.W. Parsons, G. Jin, R. McLendon, B.A. Rasheed, W. Yuan, I. Kos, I. Batinic-Haberle, S. Jones, G.J. Riggins, H. Friedman, A. Friedman, D. Reardon, J. Herndon, K.W. Kinzler, V.E. Velculescu, B. Vogelstein, D.D. Bigner, IDH1 and IDH2 mutations in gliomas, N. Engl. J. Med. 360 (2009) 765–773. doi:10.1056/NEJMoa0808710.

[6] M. Ceccarelli, F.P. Barthel, T.M. Malta, T.S. Sabedot, S.R. Salama, B.A. Murray, O. Morozova, Y. Newton, A. Radenbaugh, S.M. Pagnotta, S. Anjum, J. Wang, G. Manyam, P. Zoppoli, S. Ling, A.A. Rao, M. Grifford, A.D. Cherniack, H. Zhang, L. Poisson, C.G. Carlotti, D.P. da C. Tirapelli, A. Rao, T. Mikkelsen, C.C. Lau, W.K.A. Yung, R. Rabadan, J. Huse, D.J. Brat, N.L. Lehman, J.S. Barnholtz-Sloan, S. Zheng, K. Hess, G. Rao, M. Meyerson, R. Beroukhim, L. Cooper, R. Akbani, M. Wrensch, D. Haussler, K.D. Aldape, P.W. Laird, D.H. Gutmann, S. Anjum, H. Arachchi, J.T. Auman, M. Balasundaram, S. Balu, G. Barnett, S. Baylin, S. Bell, C. Benz, N. Bir, K.L. Black, T. Bodenheimer, L. Boice, M.S. Bootwalla, J. Bowen, C.A. Bristow, Y.S.N. Butterfield, Q.-R. Chen, L. Chin, J. Cho, E. Chuah, S. Chudamani, S.G. Coetzee, M.L. Cohen, H. Colman, M. Couce, F. D'Angelo, T. Davidsen, A. Davis, J.A. Demchok, K. Devine, L. Ding, R. Duell, J.B. Elder, J.M. Eschbacher, A. Fehrenbach, M. Ferguson, S. Frazer, G. Fuller, J. Fulop, S.B. Gabriel, L. Garofano, J.M. Gastier-Foster, N. Gehlenborg, M. Gerken, G. Getz, C. Giannini, W.J. Gibson, A. Hadjipanayis, D.N. Hayes, D.I. Heiman, B. Hermes, J. Hilty, K.A. Hoadley, A.P. Hoyle, M. Huang, S.R. Jefferys, C.D. Jones, S.J.M. Jones, Z. Ju, A. Kastl, A. Kendler, J. Kim, R. Kucherlapati, P.H. Lai, M.S. Lawrence, S. Lee, K.M. Leraas, T.M. Lichtenberg, P. Lin, Y. Liu, J. Liu, J.Y. Ljubimova, Y. Lu, Y. Ma, D.T. Maglinte, H.S. Mahadeshwar, M.A. Marra, M. McGraw, C. McPherson, S. Meng, P.A. Mieczkowski, C.R. Miller, G.B. Mills, R.A. Moore, L.E. Mose, A.J. Mungall, R. Naresh, T. Naska, L. Neder, M.S. Noble, A. Noss, B.P. O'Neill, Q.T. Ostrom, C. Palmer, A. Pantazi, M. Parfenov, P.J. Park, J.S. Parker, C.M. Perou, C.R. Pierson, T. Pihl, A. Protopopov, A. Radenbaugh, N.C. Ramirez, W.K. Rathmell, X. Ren, J. Roach, A.G. Robertson, G. Saksena, J.E. Schein, S.E. Schumacher, J. Seidman, K. Senecal, S. Seth, H. Shen, Y. Shi, J. Shih, K. Shimmel, H. Sicotte, S. Sifri, T. Silva, J.V. Simons, R. Singh, T. Skelly, A.E. Sloan, H.J. Sofia, M.G. Soloway, X. Song, C. Sougnez, C. Souza, S.M. Staugaitis, H. Sun, C. Sun, D. Tan, J. Tang, Y. Tang, L. Thorne, F.A. Trevisan, T. Triche, D.J. Van Den Berg, U. Veluvolu, D. Voet, Y. Wan, Z. Wang, R. Warnick, J.N. Weinstein, D.J. Weisenberger, M.D. Wilkerson, F. Williams, L. Wise, Y. Wolinsky, J. Wu, A.W. Xu, L. Yang, L. Yang, T.I. Zack, J.C. Zenklusen, J. Zhang, W. Zhang, J. Zhang, E. Zmuda, H. Noushmehr, A. Iavarone, R.G.W. Verhaak, Molecular Profiling Reveals

Biologically Discrete Subsets and Pathways of Progression in Diffuse Glioma, Cell. 164 (2016) 550–563. doi:10.1016/j.cell.2015.12.028.

[7] Cancer Genome Atlas Research Network, D.J. Brat, R.G.W. Verhaak, K.D. Aldape, W.K.A. Yung, S.R. Salama, L.A.D. Cooper, E. Rheinbay, C.R. Miller, M. Vitucci, O. Morozova, A.G. Robertson, H. Noushmehr, P.W. Laird, A.D. Cherniack, R. Akbani, J.T. Huse, G. Ciriello, L.M. Poisson, J.S. Barnholtz-Sloan, M.S. Berger, C. Brennan, R.R. Colen, H. Colman, A.E. Flanders, C. Giannini, M. Grifford, A. Iavarone, R. Jain, I. Joseph, J. Kim, K. Kasaian, T. Mikkelsen, B.A. Murray, B.P. O'Neill, L. Pachter, D.W. Parsons, C. Sougnez, E.P. Sulman, S.R. Vandenberg, E.G. Van Meir, A. von Deimling, H. Zhang, D. Crain, K. Lau, D. Mallery, S. Morris, J. Paulauskis, R. Penny, T. Shelton, M. Sherman, P. Yena, A. Black, J. Bowen, K. Dicostanzo, J. Gastier-Foster, K.M. Leraas, T.M. Lichtenberg, C.R. Pierson, N.C. Ramirez, C. Taylor, S. Weaver, L. Wise, E. Zmuda, T. Davidsen, J.A. Demchok, G. Eley, M.L. Ferguson, C.M. Hutter, K.R. Mills Shaw, B.A. Ozenberger, M. Sheth, H.J. Sofia, R. Tarnuzzer, Z. Wang, L. Yang, J.C. Zenklusen, B. Ayala, J. Baboud, S. Chudamani, M.A. Jensen, J. Liu, T. Pihl, R. Raman, Y. Wan, Y. Wu, A. Ally, J.T. Auman, M. Balasundaram, S. Balu, S.B. Baylin, R. Beroukhim, M.S. Bootwalla, R. Bowlby, C.A. Bristow, D. Brooks, Y. Butterfield, R. Carlsen, S. Carter, L. Chin, A. Chu, E. Chuah, K. Cibulskis, A. Clarke, S.G. Coetzee, N. Dhalla, T. Fennell, S. Fisher, S. Gabriel, G. Getz, R. Gibbs, R. Guin, A. Hadjipanayis, D.N. Hayes, T. Hinoue, K. Hoadley, R.A. Holt, A.P. Hoyle, S.R. Jefferys, S. Jones, C.D. Jones, R. Kucherlapati, P.H. Lai, E. Lander, S. Lee, L. Lichtenstein, Y. Ma, D.T. Maglinte, H.S. Mahadeshwar, M.A. Marra, M. Mayo, S. Meng, M.L. Meyerson, P.A. Mieczkowski, R.A. Moore, L.E. Mose, A.J. Mungall, A. Pantazi, M. Parfenov, P.J. Park, J.S. Parker, C.M. Perou, A. Protopopov, X. Ren, J. Roach, T.S. Sabedot, J. Schein, S.E. Schumacher, J.G. Seidman, S. Seth, H. Shen, J.V. Simons, P. Sipahimalani, M.G. Soloway, X. Song, H. Sun, B. Tabak, A. Tam, D. Tan, J. Tang, N. Thiessen, T. Triche, D.J. Van Den Berg, U. Veluvolu, S. Waring, D.J. Weisenberger, M.D. Wilkerson, T. Wong, J. Wu, L. Xi, A.W. Xu, L. Yang, T.I. Zack, J. Zhang, B.A. Aksoy, H. Arachchi, C. Benz, B. Bernard, D. Carlin, J. Cho, D. DiCara, S. Frazer, G.N. Fuller, J. Gao, N. Gehlenborg, D. Haussler, D.I. Heiman, L. Iype, A. Jacobsen, Z. Ju, S. Katzman, H. Kim, T. Knijnenburg, R.B. Kreisberg, M.S. Lawrence, W. Lee, K. Leinonen, P. Lin, S. Ling, W. Liu, Y. Liu, Y. Liu, Y. Lu, G. Mills, S. Ng, M.S. Noble, E. Paull, A. Rao, S. Reynolds, G. Saksena, Z. Sanborn, C. Sander, N. Schultz, Y. Senbabaoglu, R. Shen, I. Shmulevich, R. Sinha, J. Stuart, S.O. Sumer, Y. Sun, N. Tasman, B.S. Taylor, D. Voet, N. Weinhold, J.N. Weinstein, D. Yang, K. Yoshihara, S. Zheng, W. Zhang, L. Zou, T. Abel, S. Sadeghi, M.L. Cohen, J. Eschbacher, E.M. Hattab, A. Raghunathan, M.J. Schniederjan, D. Aziz, G. Barnett, W. Barrett, D.D. Bigner, L. Boice, C. Brewer, C. Calatozzolo, B. Campos, C.G. Carlotti, T.A. Chan, L. Cuppini, E. Curley, S. Cuzzubbo, K. Devine, F. DiMeco, R. Duell, J.B. Elder, A. Fehrenbach, G. Finocchiaro, W. Friedman, J. Fulop, J. Gardner, B. Hermes, C. Herold-Mende, C. Jungk, A. Kendler, N.L. Lehman, E. Lipp, O. Liu, R. Mandt, M. McGraw, R. Mclendon, C. McPherson, L. Neder, P. Nguyen, A. Noss, R. Nunziata, Q.T. Ostrom, C. Palmer, A. Perin, B. Pollo, A. Potapov, O. Potapova, W.K. Rathmell, D. Rotin, L. Scarpace, C. Schilero, K. Senecal, K. Shimmel, V. Shurkhay, S. Sifri, R. Singh, A.E. Sloan, K. Smolenski, S.M. Staugaitis, R. Steele, L. Thorne, D.P.C. Tirapelli, A. Unterberg, M. Vallurupalli, Y. Wang, R. Warnick, F. Williams, Y. Wolinsky, S. Bell, M. Rosenberg, C. Stewart, F. Huang, J.L. Grimsby, A.J. Radenbaugh, J. Zhang, Comprehensive, Integrative Genomic Analysis of Diffuse Lower-Grade Gliomas, N. Engl. J. Med. 372 (2015) 2481–2498. doi:10.1056/NEJMoa1402121.

[8] R. Stupp, W.P. Mason, M.J. van den Bent, M. Weller, B. Fisher, M.J.B. Taphoorn, K. Belanger, A.A. Brandes, C. Marosi, U. Bogdahn, J. Curschmann, R.C. Janzer, S.K. Ludwin, T. Gorlia, A. Allgeier, D. Lacombe, J.G. Cairncross, E. Eisenhauer, R.O. Mirimanoff, European Organisation for Research and Treatment of Cancer Brain Tumor and Radiotherapy Groups, National Cancer Institute of Canada Clinical Trials Group, Radiotherapy plus concomitant and adjuvant temozolomide for glioblastoma, N. Engl. J. Med. 352 (2005) 987–996. doi:10.1056/NEJMoa043330.

[9] W.M. Pardridge, The blood-brain barrier: bottleneck in brain drug development, NeuroRx J. Am. Soc. Exp. Neurother. 2 (2005) 3–14. doi:10.1602/neurorx.2.1.3.

[10] M. Meyer, J. Reimand, X. Lan, R. Head, X. Zhu, M. Kushida, J. Bayani, J.C. Pressey, A.C. Lionel, I.D. Clarke, M. Cusimano, J.A. Squire, S.W. Scherer, M. Bernstein, M.A. Woodin, G.D. Bader, P.B. Dirks, Single cell-derived clonal analysis of human glioblastoma links functional and genomic heterogeneity, Proc. Natl. Acad. Sci. U. S. A. 112 (2015) 851–856. doi:10.1073/pnas.1320611111.

[11] P. Perng, M. Lim, Immunosuppressive Mechanisms of Malignant Gliomas: Parallels at Non-CNS Sites, Front. Oncol. 5 (2015). doi:10.3389/fonc.2015.00153.

[12] W. Dang, T. Daviau, H. Brem, Morphological characterization of polyanhydride biodegradable implant gliadel during in vitro and in vivo erosion using scanning electron microscopy, Pharm. Res. 13 (1996) 683–691.

[13] J. Murphy, M.E. Bowers, L. Barron, Optune®: Practical Nursing Applications, Clin. J. Oncol. Nurs. 20 (2016) S14-19. doi:10.1188/16.CJON.S1.14-19.

[14] R. Stupp, S. Taillibert, A. Kanner, W. Read, D. Steinberg, B. Lhermitte, S. Toms, A. Idbaih, M.S. Ahluwalia, K. Fink, F. Di Meco, F. Lieberman, J.-J. Zhu, G. Stragliotto, D. Tran, S. Brem, A. Hottinger, E.D. Kirson, G. Lavy-Shahaf, U. Weinberg, C.-Y. Kim, S.-H. Paek, G. Nicholas, J. Bruna, H. Hirte, M. Weller, Y. Palti, M.E. Hegi, Z. Ram, Effect of Tumor-Treating Fields Plus Maintenance Temozolomide vs Maintenance Temozolomide Alone on Survival in Patients With Glioblastoma: A Randomized Clinical Trial, JAMA. 318 (2017) 2306–2316. doi:10.1001/jama.2017.18718.

[15] M.J.B. Taphoorn, L. Dirven, A.A. Kanner, G. Lavy-Shahaf, U. Weinberg, S. Taillibert, S.A. Toms, J. Honnorat, T.C. Chen, J. Sroubek, C. David, A. Idbaih, J.C. Easaw, C.-Y. Kim, J. Bruna, A.F. Hottinger, Y. Kew, P. Roth, R. Desai, J.L. Villano, E.D. Kirson, Z. Ram, R. Stupp, Influence of Treatment With Tumor-Treating Fields on Health-Related Quality of Life of Patients With Newly Diagnosed Glioblastoma: A Secondary Analysis of a Randomized Clinical Trial, JAMA Oncol. 4 (2018) 495–504. doi:10.1001/jamaoncol.2017.5082.

[16] D.A. Reardon, J. Schuster, D.D. Tran, K.L. Fink, L.B. Nabors, G. Li, D.A. Bota, R.V. Lukas, A. Desjardins, L.S. Ashby, J.P. Duic, M.M. Mrugala, A. Werner, T. Hawthorne, Y. He, J.A. Green, M.J. Yellin, C.D. Turner, T.A. Davis, J.H. Sampson, ReACT: Overall survival from a randomized phase II study of rindopepimut (CDX-110) plus bevacizumab in relapsed glioblastoma., J. Clin. Oncol. 33 (2015) 2009–2009. doi:10.1200/jco.2015.33.15_suppl.2009.

[17] M. Weller, N. Butowski, D.D. Tran, L.D. Recht, M. Lim, H. Hirte, L. Ashby, L. Mechtler, S.A. Goldlust, F. Iwamoto, J. Drappatz, D.M. O'Rourke, M. Wong, M.G. Hamilton, G. Finocchiaro, J. Perry, W. Wick, J. Green, Y. He, C.D. Turner, M.J. Yellin, T. Keler, T.A. Davis, R. Stupp, J.H. Sampson, N. Butowski, J. Campian, L. Recht, M. Lim, L. Ashby, J. Drappatz, H. Hirte, F. Iwamoto, L. Mechtler, S. Goldlust, K. Becker, G. Barnett, G. Nicholas, A. Desjardins, T. Benkers, N. Wagle, M. Groves, S. Kesari, Z. Horvath, R. Merrell, R. Curry, J. O'Rourke, D. Schuster, M. Wong, M. Mrugala, R. Jensen, J. Trusheim, G. Lesser, K. Belanger, A. Sloan, B. Purow, K. Fink, J. Raizer, M. Schulder, S. Nair, S. Peak, J. Perry, A. Brandes, M. Weller, N. Mohile, J. Landolfi, J. Olson, G. Finocchiaro, R. Jennens, P. DeSouza, B. Robinson, M. Crittenden, K. Shih, A. Flowers, S. Ong, J. Connelly, C. Hadjipanayis, P. Giglio, F. Mott, D. Mathieu, N. Lessard, S.J. Sepulveda, J. Lövey, H. Wheeler, P.-L. Inglis, C. Hardie, D. Bota, M. Lesniak, J. Portnow, B. Frankel, L. Junck, R. Thompson, L. Berk, J. McGhie, D. Macdonald, F. Saran, R. Soffietti, D. Blumenthal, S.B.C.M. André de, A. Nowak, N. Singhal, A. Hottinger, A. Schmid, G. Srkalovic, D. Baskin, C. Fadul, L. Nabors, R. LaRocca, J. Villano, N. Paleologos, P. Kavan, M. Pitz, B. Thiessen, A. Idbaih, J.S. Frenel, J. Domont, O. Grauer,

P. Hau, C. Marosi, J. Sroubek, E. Hovey, P.S. Sridhar, L. Cher, E. Dunbar, T. Coyle, J. Raymond, K. Barton, M. Guarino, S. Raval, B. Stea, J. Dietrich, K. Hopkins, S. Erridge, J.-P. Steinbach, L.E. Pineda, Q.C. Balana, B.B. Sonia del, M. Wenczl, K. Molnár, K. Hideghéty, A. Lossos, L. Myra van, A. Levy, R. Harrup, W. Patterson, Z. Lwin, S. Sathornsumetee, E.-J. Lee, J.-T. Ho, S. Emmons, J.P. Duic, S. Shao, H. Ashamalla, M. Weaver, J. Lutzky, N. Avgeropoulos, W. Hanna, M. Nadipuram, G. Cecchi, R. O'Donnell, S. Pannullo, J. Carney, M. Hamilton, M. MacNeil, R. Beaney, M. Fabbro, O. Schnell, R. Fietkau, G. Stockhammer, B. Malinova, K. Odrazka, M. Sames, G. Miguel Gil, E. Razis, K. Lavrenkov, G. Castro, F. Ramirez, C. Baldotto, F. Viola, S. Malheiros, J. Lickliter, S. Gauden, A. Dechaphunkul, I. Thaipisuttikul, Z. Thotathil, H.-I. Ma, W.-Y. Cheng, C.-H. Chang, F. Salas, P.-Y. Dietrich, C. Mamot, L. Nayak, S. Nag, Rindopepimut with temozolomide for patients with newly diagnosed, EGFRvIII-expressing glioblastoma (ACT IV): a randomised, double-blind, international phase 3 trial, Lancet Oncol. 18 (2017) 1373–1385. doi:10.1016/S1470-2045(17)30517-X.

[18] S. Saikali, T. Avril, B. Collet, A. Hamlat, J.-Y. Bansard, B. Drenou, Y. Guegan, V. Quillien, Expression of nine tumour antigens in a series of human glioblastoma multiforme: interest of EGFRvIII, IL-13Rα2, gp100 and TRP-2 for immunotherapy, J. Neurooncol. 81 (2006) 139–148. doi:10.1007/s11060-006-9220-3.

[19] D.M. O'Rourke, M.P. Nasrallah, A. Desai, J.J. Melenhorst, K. Mansfield, J.J.D. Morrissette, M. Martinez-Lage, S. Brem, E. Maloney, A. Shen, R. Isaacs, S. Mohan, G. Plesa, S.F. Lacey, J.-M. Navenot, Z. Zheng, B.L. Levine, H. Okada, C.H. June, J.L. Brogdon, M.V. Maus, A single dose of peripherally infused EGFRvIII-directed CAR T cells mediates antigen loss and induces adaptive resistance in patients with recurrent glioblastoma, Sci. Transl. Med. 9 (2017) eaaa0984. doi:10.1126/scitranslmed.aaa0984.

[20] D.A. Reardon, A. Omuro, A.A. Brandes, J. Rieger, A. Wick, J. Sepulveda, S. Phuphanich, P. de Souza, M.S. Ahluwalia, M. Lim, G. Vlahovic, J. Sampson, OS10.3 Randomized Phase 3 Study Evaluating the Efficacy and Safety of Nivolumab vs Bevacizumab in Patients With Recurrent Glioblastoma: CheckMate 143, Neuro-Oncol. 19 (2017) iii21–iii21. doi:10.1093/neuonc/nox036.071.

[21] T.F. Cloughesy, A.Y. Mochizuki, J.R. Orpilla, W. Hugo, A.H. Lee, T.B. Davidson, A.C. Wang, B.M. Ellingson, J.A. Rytlewski, C.M. Sanders, E.S. Kawaguchi, L. Du, G. Li, W.H. Yong, S.C. Gaffey, A.L. Cohen, I.K. Mellinghoff, E.Q. Lee, D.A. Reardon, B.J. O'Brien, N.A. Butowski, P.L. Nghiemphu, J.L. Clarke, I.C. Arrillaga-Romany, H. Colman, T.J. Kaley, J.F. de Groot, L.M. Liau, P.Y. Wen, R.M. Prins, Neoadjuvant anti-PD-1 immunotherapy promotes a survival benefit with intratumoral and systemic immune responses in recurrent glioblastoma, Nat. Med. (2019) 1. doi:10.1038/s41591-018-0337-7.

[22] K.A. Schalper, M.E. Rodriguez-Ruiz, R. Diez-Valle, A. López-Janeiro, A. Porciuncula, M.A. Idoate, S. Inogés, C. de Andrea, A.L.-D. de Cerio, S. Tejada, P. Berraondo, F. Villarroel-Espindola, J. Choi, A. Gúrpide, M. Giraldez, I. Goicoechea, J.G. Perez-Larraya, M.F. Sanmamed, J.L. Perez-Gracia, I. Melero, Neoadjuvant nivolumab modifies the tumor immune microenvironment in resectable glioblastoma, Nat. Med. 25 (2019) 470. doi:10.1038/s41591-018-0339-5.

[23] J. Zhao, A.X. Chen, R.D. Gartrell, A.M. Silverman, L. Aparicio, T. Chu, D. Bordbar, D. Shan, J. Samanamud, A. Mahajan, I. Filip, R. Orenbuch, M. Goetz, J.T. Yamaguchi, M. Cloney, C. Horbinski, R.V. Lukas, J. Raizer, A.I. Rae, J. Yuan, P. Canoll, J.N. Bruce, Y.M. Saenger, P. Sims, F.M. Iwamoto, A.M. Sonabend, R. Rabadan, Immune and genomic correlates of response to anti-PD-1 immunotherapy in glioblastoma, Nat. Med. 25 (2019) 462–469. doi:10.1038/s41591-019-0349-y.

[24] S.C. Thust, M.J. van den Bent, M. Smits, Pseudoprogression of brain tumors, J. Magn. Reson. Imaging. 48 (2018) 571–589. doi:10.1002/jmri.26171.

[25] M.K. Merrill, G. Bernhardt, J.H. Sampson, C.J. Wikstrand, D.D. Bigner, M. Gromeier, Poliovirus receptor CD155-targeted oncolysis of glioma, Neuro-Oncol. 6 (2004) 208–217. doi:10.1215/S1152851703000577.

[26] A. Desjardins, M. Gromeier, J.E. Herndon, N. Beaubier, D.P. Bolognesi, A.H. Friedman, H.S. Friedman, F. McSherry, A.M. Muscat, S. Nair, K.B. Peters, D. Randazzo, J.H. Sampson, G. Vlahovic, W.T. Harrison, R.E. McLendon, D. Ashley, D.D. Bigner, Recurrent Glioblastoma Treated with Recombinant Poliovirus, N. Engl. J. Med. 379 (2018) 150–161. doi:10.1056/NEJMoa1716435.

[27] F.F. Lang, C. Conrad, C. Gomez-Manzano, W.K.A. Yung, R. Sawaya, J.S. Weinberg, S.S. Prabhu, G. Rao, G.N. Fuller, K.D. Aldape, J. Gumin, L.M. Vence, I. Wistuba, J. Rodriguez-Canales, P.A. Villalobos, C.M.F. Dirven, S. Tejada, R.D. Valle, M.M. Alonso, B. Ewald, J.J. Peterkin, F. Tufaro, J. Fueyo, Phase I Study of DNX-2401 (Delta-24-RGD) Oncolytic Adenovirus: Replication and Immunotherapeutic Effects in Recurrent Malignant Glioma, J. Clin. Oncol. 36 (2018) 1419–1427. doi:10.1200/JCO.2017.75.8219.

[28] K. Geletneky, J. Hajda, A.L. Angelova, B. Leuchs, D. Capper, A.J. Bartsch, J.-O. Neumann, T. Schöning, J. Hüsing, B. Beelte, I. Kiprianova, M. Roscher, R. Bhat, A. von Deimling, W. Brück, A. Just, V. Frehtman, S. Löbhard, E. Terletskaia-Ladwig, J. Fry, K. Jochims, V. Daniel, O. Krebs, M. Dahm, B. Huber, A. Unterberg, J. Rommelaere, Oncolytic H-1 Parvovirus Shows Safety and Signs of Immunogenic Activity in a First Phase I/IIa Glioblastoma Trial, Mol. Ther. 25 (2017) 2620–2634. doi:10.1016/j.ymthe.2017.08.016.

[29] D. Ostertag, K.K. Amundson, F. Lopez Espinoza, B. Martin, T. Buckley, A.P.G. da Silva, A.H. Lin, D.T. Valenta, O.D. Perez, C.E. Ibañez, C.-I. Chen, P.L. Pettersson, R. Burnett, V. Daublebsky, J. Hlavaty, W. Gunzburg, N. Kasahara, H.E. Gruber, D.J. Jolly, J.M. Robbins, Brain tumor eradication and prolonged survival from intratumoral conversion of 5-fluorocytosine to 5-fluorouracil using a nonlytic retroviral replicating vector, Neuro-Oncol. 14 (2012) 145–159. doi:10.1093/neuonc/nor199.

[30] T.F. Cloughesy, J. Landolfi, M.A. Vogelbaum, D. Ostertag, J.B. Elder, S. Bloomfield, B. Carter, C.C. Chen, S.N. Kalkanis, S. Kesari, A. Lai, I.Y. Lee, L.M. Liau, T. Mikkelsen, P. Nghiemphu, D. Piccioni, W. Accomando, O.R. Diago, D.J. Hogan, D. Gammon, N. Kasahara, T. Kheoh, D.J. Jolly, H.E. Gruber, A. Das, T. Walbert, Durable complete responses in some recurrent high-grade glioma patients treated with Toca 511 + Toca FC, Neuro-Oncol. 20 (2018) 1383–1392. doi:10.1093/neuonc/noy075.

[31] N. McDannold, N. Vykhodtseva, S. Raymond, F.A. Jolesz, K. Hynynen, MRI-guided targeted blood-brain barrier disruption with focused ultrasound: histological findings in rabbits, Ultrasound Med. Biol. 31 (2005) 1527–1537. doi:10.1016/j.ultrasmedbio.2005.07.010.

[32] S.A. Quadri, M. Waqas, I. Khan, M.A. Khan, S.S. Suriya, M. Farooqui, B. Fiani, High-intensity focused ultrasound: past, present, and future in neurosurgery, Neurosurg. Focus. 44 (2018) E16. doi:10.3171/2017.11.FOCUS17610.

[33] K.T. Householder, D.M. DiPerna, E.P. Chung, G.M. Wohlleb, H.D. Dhruv, M.E. Berens, R.W. Sirianni, Intravenous delivery of camptothecin-loaded PLGA nanoparticles for the treatment of intracranial glioma, Int. J. Pharm. 479 (2015) 374–380. doi:10.1016/j.ijpharm.2015.01.002.

[34] K.T. Householder, D.M. DiPerna, E.P. Chung, A.R. Luning, D.T. Nguyen, S.E. Stabenfeldt, S. Mehta, R.W. Sirianni, pH driven precipitation of quisinostat onto PLA-PEG nanoparticles

enables treatment of intracranial glioblastoma, Colloids Surf. B Biointerfaces. 166 (2018) 37–44. doi:10.1016/j.colsurfb.2018.02.048.

[35] J. Zhou, T.R. Patel, R.W. Sirianni, G. Strohbehn, M.-Q. Zheng, N. Duong, T. Schafbauer, A.J. Huttner, Y. Huang, R.E. Carson, Y. Zhang, D.J. Sullivan, J.M. Piepmeier, W.M. Saltzman, Highly penetrative, drug-loaded nanocarriers improve treatment of glioblastoma, Proc. Natl. Acad. Sci. U. S. A. 110 (2013) 11751–11756. doi:10.1073/pnas.1304504110.

[36] K.T. Householder, Nanoparticle Drug Delivery to Brain Tumors: From Intravenous to Intrathecal, (2018). https://search.proquest.com/openview/2d76e0ff1f4fadb59001a8f76aa622d9/1?pq-origsite=gscholar&cbl=18750&diss=y.

[37] O. Grauer, M. Jaber, K. Hess, M. Weckesser, W. Schwindt, S. Maring, J. Wölfer, W. Stummer, Combined intracavitary thermotherapy with iron oxide nanoparticles and radiotherapy as local treatment modality in recurrent glioblastoma patients, J. Neurooncol. 141 (2019) 83–94. doi:10.1007/s11060-018-03005-x.

[38] S. Pinel, N. Thomas, C. Boura, M. Barberi-Heyob, Approaches to physical stimulation of metallic nanoparticles for glioblastoma treatment, Adv. Drug Deliv. Rev. 138 (2019) 344–357. doi:10.1016/j.addr.2018.10.013.

[39] S.M. Carvalho, A.G. Leonel, A.A.P. Mansur, I.C. Carvalho, K. Krambrock, H.S. Mansur, Bifunctional magnetopolymersomes of iron oxide nanoparticles and carboxymethylcellulose conjugated with doxorubicin for hyperthermo-chemotherapy of brain cancer cells, Biomater. Sci. 7 (2019) 2102–2122. doi:10.1039/c8bm01528g.

[40] H. Kafa, J.T.-W. Wang, K.T. Al-Jamal, Current Perspective of Carbon Nanotubes Application in Neurology, Int. Rev. Neurobiol. 130 (2016) 229–263. doi:10.1016/bs.irn.2016.07.001.

[41] M. Ouyang, E.E. White, H. Ren, Q. Guo, I. Zhang, H. Gao, S. Yanyan, X. Chen, Y. Weng, A. Da Fonseca, S. Shah, E.R. Manuel, L. Zhang, S.L. Vonderfecht, D. Alizadeh, J.M. Berlin, B. Badie, Metronomic Doses of Temozolomide Enhance the Efficacy of Carbon Nanotube CpG Immunotherapy in an Invasive Glioma Model, PloS One. 11 (2016) e0148139. doi:10.1371/journal.pone.0148139.

[42] S. Romano-Feinholz, A. Salazar-Ramiro, E. Muñoz-Sandoval, R. Magaña-Maldonado, N. Hernández Pedro, E. Rangel López, A. González Aguilar, A. Sánchez García, J. Sotelo, V. Pérez de la Cruz, B. Pineda, Cytotoxicity induced by carbon nanotubes in experimental malignant glioma, Int. J. Nanomedicine. 12 (2017) 6005–6026. doi:10.2147/IJN.S139004.

[43] Y. Wang, W. Qu, S.H. Choi, FDA's Regulatory Science Program for Generic PLA/ PLGA-Based Drug Products, Am. Pharm. Rev. (2016). http://www.americanpharmaceuticalreview.com/Featured-Articles/188841-FDA-s-Regulatory-Science-Program-for-Generic-PLA-PLGA-Based-Drug-Products/ (accessed April 25, 2019).

[44] R.L. McCall, J. Cacaccio, E. Wrabel, M.E. Schwartz, T.P. Coleman, R.W. Sirianni, Pathogen-inspired drug delivery to the central nervous system, Tissue Barriers. 2 (2014) e944449. doi:10.4161/21688362.2014.944449.

[45] W. Tomaszewski, L. Sanchez-Perez, T.F. Gajewski, J.H. Sampson, Brain Tumor Microenvironment and Host State: Implications for Immunotherapy, Clin. Cancer Res. Off. J. Am. Assoc. Cancer Res. (2019). doi:10.1158/1078-0432.CCR-18-1627.

[46] A. Wu, J. Wei, L.-Y. Kong, Y. Wang, W. Priebe, W. Qiao, R. Sawaya, A.B. Heimberger, Glioma cancer stem cells induce immunosuppressive macrophages/microglia, Neuro-Oncol. 12 (2010) 1113–1125. doi:10.1093/neuonc/noq082.

[47] J. Wei, J. Barr, L.-Y. Kong, Y. Wang, A. Wu, A.K. Sharma, J. Gumin, V. Henry, H. Colman, W. Priebe, R. Sawaya, F.F. Lang, A.B. Heimberger, Glioblastoma cancer-initiating cells inhibit T-cell proliferation and effector responses by the signal transducers and activators of transcription 3 pathway, Mol. Cancer Ther. 9 (2010) 67–78. doi:10.1158/1535-7163.MCT-09-0734.

[48] S. Roesch, C. Rapp, S. Dettling, C. Herold-Mende, When Immune Cells Turn Bad-Tumor-Associated Microglia/Macrophages in Glioma, Int. J. Mol. Sci. 19 (2018). doi:10.3390/ijms19020436.

[49] G.T. Norris, J. Kipnis, Immune cells and CNS physiology: Microglia and beyond, J. Exp. Med. 216 (2019) 60–70. doi:10.1084/jem.20180199.

[50] R.M. Ransohoff, B. Engelhardt, The anatomical and cellular basis of immune surveillance in the central nervous system, Nat. Rev. Immunol. 12 (2012) 623–635. doi:10.1038/nri3265.

[51] A. Louveau, I. Smirnov, T.J. Keyes, J.D. Eccles, S.J. Rouhani, J.D. Peske, N.C. Derecki, D. Castle, J.W. Mandell, K.S. Lee, T.H. Harris, J. Kipnis, Structural and functional features of central nervous system lymphatic vessels, Nature. 523 (2015) 337–341. doi:10.1038/nature14432.

[52] E.T. Ha, J.P. Antonios, H. Soto, R.M. Prins, I. Yang, N. Kasahara, L.M. Liau, C.A. Kruse, Chronic inflammation drives glioma growth: cellular and molecular factors responsible for an immunosuppressive microenvironment, Neuroimmunol. Neuroinflammation. 2014 (2014) 66–76. doi:10.4103/2347-8659.139717.

[53] R.A. Morantz, G.W. Wood, M. Foster, M. Clark, K. Gollahon, Macrophages in experimental and human brain tumors. Part 2: studies of the macrophage content of human brain tumors, J. Neurosurg. 50 (1979) 305–311. doi:10.3171/jns.1979.50.3.0305.

[54] I.F. Parney, J.S. Waldron, A.T. Parsa, Flow cytometry and in vitro analysis of human glioma-associated macrophages. Laboratory investigation, J. Neurosurg. 110 (2009) 572–582. doi:10.3171/2008.7.JNS08475.

[55] D.F. Quail, J.A. Joyce, The microenvironmental landscape of brain tumors, Cancer Cell. 31 (2017) 326–341. doi:10.1016/j.ccell.2017.02.009.

[56] V.F. Zhu, J. Yang, D.G. Lebrun, M. Li, Understanding the role of cytokines in Glioblastoma Multiforme pathogenesis, Cancer Lett. 316 (2012) 139–150. doi:10.1016/j.canlet.2011.11.001.

[57] D.A. Thomas, J. Massagué, TGF-beta directly targets cytotoxic T cell functions during tumor evasion of immune surveillance, Cancer Cell. 8 (2005) 369–380. doi:10.1016/j.ccr.2005.10.012.

[58] H. Maeda, H. Kuwahara, Y. Ichimura, M. Ohtsuki, S. Kurakata, A. Shiraishi, TGF-beta enhances macrophage ability to produce IL-10 in normal and tumor-bearing mice, J. Immunol. Baltim. Md 1950. 155 (1995) 4926–4932.

[59] M. Matsuda, F. Salazar, M. Petersson, G. Masucci, J. Hansson, P. Pisa, Q.J. Zhang, M.G. Masucci, R. Kiessling, Interleukin 10 pretreatment protects target cells from tumor- and allo-specific cytotoxic T cells and downregulates HLA class I expression, J. Exp. Med. 180 (1994) 2371–2376.

[60] M.-L. Chen, M.J. Pittet, L. Gorelik, R.A. Flavell, R. Weissleder, H. von Boehmer, K. Khazaie, Regulatory T cells suppress tumor-specific CD8 T cell cytotoxicity through TGF-beta signals in vivo, Proc. Natl. Acad. Sci. U. S. A. 102 (2005) 419–424. doi:10.1073/pnas.0408197102.

[61] Z. Li, X. Liu, R. Guo, P. Wang, CD4+Foxp3- type 1 regulatory T cells in glioblastoma multiforme suppress T cell responses through multiple pathways and are regulated by tumor-associated macrophages, Int. J. Biochem. Cell Biol. 81 (2016) 1–9. doi:10.1016/j.biocel.2016.09.013.

[62] B.E. Hoffman, A.T. Martino, B.K. Sack, O. Cao, G. Liao, C. Terhorst, R.W. Herzog, Nonredundant Roles of IL-10 and TGF-β in Suppression of Immune Responses to Hepatic AAV-Factor IX Gene Transfer, Mol. Ther. 19 (2011) 1263–1272. doi:10.1038/mt.2011.33.

[63] J.D. Fontenot, M.A. Gavin, A.Y. Rudensky, Foxp3 programs the development and function of CD4+CD25+ regulatory T cells, Nat. Immunol. 4 (2003) 330–336. doi:10.1038/ni904.

[64] R. Bacchetta, L. Passerini, E. Gambineri, M. Dai, S.E. Allan, L. Perroni, F. Dagna-Bricarelli, C. Sartirana, S. Matthes-Martin, A. Lawitschka, C. Azzari, S.F. Ziegler, M.K. Levings, M.G. Roncarolo, Defective regulatory and effector T cell functions in patients with FOXP3 mutations, J. Clin. Invest. 116 (2006) 1713–1722. doi:10.1172/JCI25112.

[65] Y.C. Ooi, P. Tran, N. Ung, K. Thill, A. Trang, B.M. Fong, D.T. Nagasawa, M. Lim, I. Yang, The role of regulatory T-cells in glioma immunology, Clin. Neurol. Neurosurg. 119 (2014) 125–132. doi:10.1016/j.clineuro.2013.12.004.

[66] P.E. Fecci, D.A. Mitchell, J.F. Whitesides, W. Xie, A.H. Friedman, G.E. Archer, J.E. Herndon, D.D. Bigner, G. Dranoff, J.H. Sampson, Increased regulatory T-cell fraction amidst a diminished CD4 compartment explains cellular immune defects in patients with malignant glioma, Cancer Res. 66 (2006) 3294–3302. doi:10.1158/0008-5472.CAN-05-3773.

[67] K. Akane, S. Kojima, T.W. Mak, H. Shiku, H. Suzuki, CD8+CD122+CD49dlow regulatory T cells maintain T-cell homeostasis by killing activated T cells via Fas/FasL-mediated cytotoxicity, Proc. Natl. Acad. Sci. U. S. A. 113 (2016) 2460–2465. doi:10.1073/pnas.1525098113.

[68] W.J. Grossman, J.W. Verbsky, W. Barchet, M. Colonna, J.P. Atkinson, T.J. Ley, Human T regulatory cells can use the perforin pathway to cause autologous target cell death, Immunity. 21 (2004) 589–601. doi:10.1016/j.immuni.2004.09.002.

[69] D.C. Gondek, L.-F. Lu, S.A. Quezada, S. Sakaguchi, R.J. Noelle, Cutting edge: contact-mediated suppression by CD4+CD25+ regulatory cells involves a granzyme B-dependent, perforin-independent mechanism, J. Immunol. Baltim. Md 1950. 174 (2005) 1783–1786.

[70] A.M. Thornton, E.M. Shevach, CD4+CD25+ immunoregulatory T cells suppress polyclonal T cell activation in vitro by inhibiting interleukin 2 production, J. Exp. Med. 188 (1998) 287–296.

[71] D. Zagzag, K. Salnikow, L. Chiriboga, H. Yee, L. Lan, M.A. Ali, R. Garcia, S. Demaria, E.W. Newcomb, Downregulation of major histocompatibility complex antigens in invading glioma cells: stealth invasion of the brain, Lab. Investig. J. Tech. Methods Pathol. 85 (2005) 328–341. doi:10.1038/labinvest.3700233.

[72] J.M. Schartner, A.R. Hagar, M. Van Handel, L. Zhang, N. Nadkarni, B. Badie, Impaired capacity for upregulation of MHC class II in tumor-associated microglia, Glia. 51 (2005) 279–285. doi:10.1002/glia.20201.

[73] B. Akkaya, Y. Oya, M. Akkaya, J.A. Souz, A.H. Holstein, O. Kamenyeva, J. Kabat, R. Matsumura, D.W. Dorward, D.D. Glass, E.M. Shevach, Regulatory T cells mediate specific suppression by depleting peptide–MHC class II from dendritic cells, Nat. Immunol. 20 (2019) 218. doi:10.1038/s41590-018-0280-2.

[74] A. Ribas, J.D. Wolchok, Cancer immunotherapy using checkpoint blockade, Science. 359 (2018) 1350–1355. doi:10.1126/science.aar4060.

[75] K. Woroniecka, P. Chongsathidkiet, K. Rhodin, H. Kemeny, C. Dechant, S.H. Farber, A.A. Elsamadicy, X. Cui, S. Koyama, C. Jackson, L.J. Hansen, T.M. Johanns, L. Sanchez-Perez, V. Chandramohan, Y.-R.A. Yu, D.D. Bigner, A. Giles, P. Healy, G. Dranoff, K.J. Weinhold, G.P. Dunn, P.E. Fecci, T-Cell Exhaustion Signatures Vary with Tumor Type and Are Severe in Glioblastoma, Clin. Cancer Res. Off. J. Am. Assoc. Cancer Res. 24 (2018) 4175–4186. doi:10.1158/1078-0432.CCR-17-1846.

[76] U.D. Staerz, O. Kanagawa, M.J. Bevan, Hybrid antibodies can target sites for attack by T cells, Nature. 314 (1985) 628–631.

[77] M. Mack, G. Riethmüller, P. Kufer, A small bispecific antibody construct expressed as a functional single-chain molecule with high tumor cell cytotoxicity., Proc. Natl. Acad. Sci. U. S. A. 92 (1995) 7021–7025.

[78] J. De Jonge, J. Brissinck, C. Heirman, C. Demanet, O. Leo, M. Moser, K. Thielemans, Production and characterization of bispecific single-chain antibody fragments, Mol. Immunol. 32 (1995) 1405–1412.

[79] J. Kriangkum, B. Xu, C. Gervais, D. Paquette, F.A. Jacobs, L. Martin, M.R. Suresh, Development and characterization of a bispecific single-chain antibody directed against T cells and ovarian carcinoma, Hybridoma. 19 (2000) 33–41. doi:10.1089/027245700315770.

[80] S.R. Frankel, P.A. Baeuerle, Targeting T cells to tumor cells using bispecific antibodies, Curr. Opin. Chem. Biol. 17 (2013) 385–392. doi:10.1016/j.cbpa.2013.03.029.

[81] D. Przepiorka, C.-W. Ko, A. Deisseroth, C.L. Yancey, R. Candau-Chacon, H.-J. Chiu, B.J. Gehrke, C. Gomez-Broughton, R.C. Kane, S. Kirshner, N. Mehrotra, T.K. Ricks, D. Schmiel, P. Song, P. Zhao, Q. Zhou, A.T. Farrell, R. Pazdur, FDA Approval: Blinatumomab, Clin. Cancer Res. 21 (2015) 4035–4039. doi:10.1158/1078-0432.CCR-15-0612.

[82] FDA Approves BLINCYTO blinatumomab To Treat Minimal Residual DiseasePositive BCell Precursor Acute Lymphoblastic Leukemia In Adults And Children, (n.d.). https://www.amgen.com/media/news-releases/2018/03/fda-approves-blincyto-blinatumomab-to-treat-minimal-residual-diseasepositive-bcell-precursor-acute-lymphoblastic-leukemia-in-adults-and-children/ (accessed May 8, 2019).

[83] J.D. Stone, D.H. Aggen, A. Schietinger, H. Schreiber, D.M. Kranz, A sensitivity scale for targeting T cells with chimeric antigen receptors (CARs) and bispecific T-cell Engagers (BiTEs), Oncoimmunology. 1 (2012) 863–873. doi:10.4161/onci.20592.

[84] C.Y. Slaney, P. Wang, P.K. Darcy, M.H. Kershaw, CARs versus BiTEs: A Comparison between T Cell–Redirection Strategies for Cancer Treatment, Cancer Discov. 8 (2018) 1–11. doi:10.1158/2159-8290.CD-18-0297.

[85] J.H. Sampson, A.B. Heimberger, G.E. Archer, K.D. Aldape, A.H. Friedman, H.S. Friedman, M.R. Gilbert, J.E. Herndon, R.E. McLendon, D.A. Mitchell, D.A. Reardon, R. Sawaya, R.J. Schmittling, W. Shi, J.J. Vredenburgh, D.D. Bigner, Immunologic Escape After Prolonged

Progression-Free Survival With Epidermal Growth Factor Receptor Variant III Peptide Vaccination in Patients With Newly Diagnosed Glioblastoma, J. Clin. Oncol. 28 (2010) 4722–4729. doi:10.1200/JCO.2010.28.6963.

[86] W.M. Pardridge, Drug transport across the blood–brain barrier, J. Cereb. Blood Flow Metab. 32 (2012) 1959–1972. doi:10.1038/jcbfm.2012.126.

[87] C.A. Lipinski, F. Lombardo, B.W. Dominy, P.J. Feeney, Experimental and computational approaches to estimate solubility and permeability in drug discovery and development settings, Adv. Drug Deliv. Rev. 46 (2001) 3–26.

[88] W. Pan, A.J. Kastin, Changing the chemokine gradient: CINC1 crosses the blood-brain barrier, J. Neuroimmunol. 115 (2001) 64–70.

[89] S.J. Madsen, H. Hirschberg, Site-specific opening of the blood-brain barrier, J. Biophotonics. 3 (2010) 356–367. doi:10.1002/jbio.200900095.

[90] J.A. DeBin, J.E. Maggio, G.R. Strichartz, Purification and characterization of chlorotoxin, a chloride channel ligand from the venom of the scorpion, Am. J. Physiol. - Cell Physiol. 264 (1993) C361–C369.

[91] N. Ullrich, H. Sontheimer, Biophysical and pharmacological characterization of chloride currents in human astrocytoma cells, Am. J. Physiol. - Cell Physiol. 270 (1996) C1511–C1521.

[92] S.A. Lyons, J. O'Neal, H. Sontheimer, Chlorotoxin, a scorpion-derived peptide, specifically binds to gliomas and tumors of neuroectodermal origin, Glia. 39 (2002) 162–173. doi:10.1002/glia.10083.

[93] O. Veiseh, C. Sun, C. Fang, N. Bhattarai, J. Gunn, F. Kievit, K. Du, B. Pullar, D. Lee, R.G. Ellenbogen, J. Olson, M. Zhang, Specific Targeting of Brain Tumors with an Optical/Magnetic Resonance Imaging Nanoprobe across the Blood-Brain Barrier, Cancer Res. 69 (2009) 6200–6207. doi:10.1158/0008-5472.CAN-09-1157.

[94] M. Veiseh, P. Gabikian, S.-B. Bahrami, O. Veiseh, M. Zhang, R.C. Hackman, A.C. Ravanpay, M.R. Stroud, Y. Kusuma, S.J. Hansen, D. Kwok, N.M. Munoz, R.W. Sze, W.M. Grady, N.M. Greenberg, R.G. Ellenbogen, J.M. Olson, Tumor Paint: A Chlorotoxin:Cy5.5 Bioconjugate for Intraoperative Visualization of Cancer Foci, Cancer Res. 67 (2007) 6882–6888. doi:10.1158/0008-5472.CAN-06-3948.

[95] M. Akcan, M.R. Stroud, S.J. Hansen, R.J. Clark, N.L. Daly, D.J. Craik, J.M. Olson, Chemical Re-engineering of Chlorotoxin Improves Bioconjugation Properties for Tumor Imaging and Targeted Therapy, J. Med. Chem. 54 (2011) 782–787. doi:10.1021/jm101018r.

[96] P.V. Butte, A. Mamelak, J. Parrish-Novak, D. Drazin, F. Shweikeh, P.R. Gangalum, A. Chesnokova, J.Y. Ljubimova, K. Black, Near-infrared imaging of brain tumors using the Tumor Paint BLZ-100 to achieve near-complete resection of brain tumors, Neurosurg. Focus. 36 (2014) E1. doi:10.3171/2013.11.FOCUS13497.

[97] Study of Tozuleristide and the Canvas Imaging System in Pediatric Subjects With CNS Tumors Undergoing Surgery - Full Text View - ClinicalTrials.gov, (n.d.). https://clinicaltrials.gov/ct2/show/NCT03579602 (accessed May 1, 2019).

[98] Study of BLZ-100 in Pediatric Subjects With CNS Tumors - Full Text View - ClinicalTrials.gov, (n.d.). https://clinicaltrials.gov/ct2/show/NCT02462629?term=blz-100&rank=3 (accessed April 5, 2017).

[99] Safety Study of BLZ-100 in Adult Subjects With Glioma Undergoing Surgery - Full Text View - ClinicalTrials.gov, (n.d.). https://clinicaltrials.gov/ct2/show/NCT02234297 (accessed May 1, 2019).

[100] Exploratory Study of Safety and ex Vivo Fluorescence of BLZ-100 in Adult Subjects With Solid Tumors Undergoing Surgery - Full Text View - ClinicalTrials.gov, (n.d.). https://clinicaltrials.gov/ct2/show/NCT02496065 (accessed May 1, 2019).

[101] D. Miller, C. Patil, D. Walker, D. Kittle, K. Nufer, M. Yamada, P. Butte, T. Prow, J. Novak, K. Black, A. Mamelak, ACTR-49. PHASE 1 SAFETY STUDY OF BLZ-100 FOR FLUORESCENCE-GUIDED RESECTION OF GLIOMA IN ADULT SUBJECTS, Neuro-Oncol. 18 (2016) vi12–vi13. doi:10.1093/neuonc/now212.047.

[102] X.-C. Zeng, W.-X. Li, S.-Y. Zhu, F. Peng, Z.-H. Zhu, K.-L. Wu, F.-H. Yiang, Cloning and characterization of a cDNA sequence encoding the precursor of a chlorotoxin-like peptide from the Chinese scorpion Buthus martensii Karsch, Toxicon. 38 (2000) 1009–1014. doi:10.1016/S0041-0101(99)00212-3.

[103] I. Rjeibi, K. Mabrouk, H. Mosrati, C. Berenguer, H. Mejdoub, C. Villard, D. Laffitte, D. Bertin, L. Ouafik, J. Luis, M. ElAyeb, N. Srairi-Abid, Purification, synthesis and characterization of AaCtx, the first chlorotoxin-like peptide from Androctonus australis scorpion venom, Peptides. 32 (2011) 656–663. doi:10.1016/j.peptides.2011.01.015.

[104] J.M. Toivonen, S. Oliván, R. Osta, Tetanus toxin C-fragment: the courier and the cure?, Toxins. 2 (2010) 2622–2644. doi:10.3390/toxins2112622.

[105] M.J. Schnell, J.P. McGettigan, C. Wirblich, A. Papaneri, The cell biology of rabies virus: using stealth to reach the brain, Nat. Rev. Microbiol. 8 (2010) 51–61. doi:10.1038/nrmicro2260.

[106] R.L. Cook, K.T. Householder, E.P. Chung, A.V. Prakapenka, D.M. DiPerna, R.W. Sirianni, A critical evaluation of drug delivery from ligand modified nanoparticles: Confounding small molecule distribution and efficacy in the central nervous system, J. Controlled Release. 220, Part A (2015) 89–97. doi:10.1016/j.jconrel.2015.10.013.

[107] J. Dumont, D. Euwart, B. Mei, S. Estes, R. Kshirsagar, Human cell lines for biopharmaceutical manufacturing: history, status, and future perspectives, Crit. Rev. Biotechnol. 36 (2016) 1110–1122. doi:10.3109/07388551.2015.1084266.

[108] P.O. Magalhães, A.M. Lopes, P.G. Mazzola, C. Rangel-Yagui, T.C.V. Penna, A. Pessoa, Methods of endotoxin removal from biological preparations: a review, J. Pharm. Pharm. Sci. Publ. Can. Soc. Pharm. Sci. Soc. Can. Sci. Pharm. 10 (2007) 388–404.

[109] A.M. Vieira Gomes, T. Souza Carmo, L. Silva Carvalho, F. Mendonça Bahia, N.S. Parachin, Comparison of Yeasts as Hosts for Recombinant Protein Production, Microorganisms. 6 (2018). doi:10.3390/microorganisms6020038.

[110] S.R. Hamilton, T.U. Gerngross, Glycosylation engineering in yeast: the advent of fully humanized yeast, Curr. Opin. Biotechnol. 18 (2007) 387–392. doi:10.1016/j.copbio.2007.09.001.

[111] T.S. Mor, Molecular pharming's foot in the FDA's door: Protalix's trailblazing story, Biotechnol. Lett. 37 (2015) 2147–2150. doi:10.1007/s10529-015-1908-z.

[112] X. Qiu, G. Wong, J. Audet, A. Bello, L. Fernando, J.B. Alimonti, H. Fausther-Bovendo, H. Wei, J. Aviles, E. Hiatt, A. Johnson, J. Morton, K. Swope, O. Bohorov, N. Bohorova, C. Goodman, D. Kim, M.H. Pauly, J. Velasco, J. Pettitt, G.G. Olinger, K. Whaley, B. Xu, J.E. Strong, L. Zeitlin, G.P. Kobinger, Reversion of advanced Ebola virus disease in nonhuman primates with ZMapp, Nature. 514 (2014) 47–53. doi:10.1038/nature13777.

[113] PREVAIL II Writing Group, Multi-National PREVAIL II Study Team, R.T. Davey, L. Dodd, M.A. Proschan, J. Neaton, J. Neuhaus Nordwall, J.S. Koopmeiners, J. Beigel, J. Tierney, H.C. Lane, A.S. Fauci, M.B.F. Massaquoi, F. Sahr, D. Malvy, A Randomized, Controlled Trial of ZMapp for Ebola Virus Infection, N. Engl. J. Med. 375 (2016) 1448–1456. doi:10.1056/NEJMoa1604330.

[114] Y. Zhang, D. Li, X. Jin, Z. Huang, Fighting Ebola with ZMapp: spotlight on plant-made antibody, Sci. China Life Sci. 57 (2014) 987–988. doi:10.1007/s11427-014-4746-7.

[115] K.J. Whaley, A. Hiatt, L. Zeitlin, Emerging antibody products and Nicotiana manufacturing, Hum. Vaccin. 7 (2011) 349–356. doi:10.4161/hv.7.3.14266.

[116] R. Strasser, J. Stadlmann, M. Schähs, G. Stiegler, H. Quendler, L. Mach, J. Glössl, K. Weterings, M. Pabst, H. Steinkellner, Generation of glyco-engineered Nicotiana benthamiana for the production of monoclonal antibodies with a homogeneous human-like N-glycan structure, Plant Biotechnol. J. 6 (2008) 392–402. doi:10.1111/j.1467-7652.2008.00330.x.

[117] A. Castilho, H. Steinkellner, Glyco-engineering in plants to produce human-like N-glycan structures, Biotechnol. J. 7 (2012) 1088–1098. doi:10.1002/biot.201200032.

[118] F. Altmann, The role of protein glycosylation in allergy, Int. Arch. Allergy Immunol. 142 (2007) 99–115. doi:10.1159/000096114.

[119] A.G. Diamos, S.H. Rosenthal, H.S. Mason, 5′ and 3′ Untranslated Regions Strongly Enhance Performance of Geminiviral Replicons in Nicotiana benthamiana Leaves, Plant Biotechnol. (2016) 200. doi:10.3389/fpls.2016.00200.

[120] S.B. Gelvin, AGROBACTERIUM AND PLANT GENES INVOLVED IN T-DNA TRANSFER AND INTEGRATION, Annu. Rev. Plant Physiol. Plant Mol. Biol. 51 (2000) 223–256. doi:10.1146/annurev.arplant.51.1.223.

[121] Y.Y. Gleba, D. Tusé, A. Giritch, Plant viral vectors for delivery by Agrobacterium, Curr. Top. Microbiol. Immunol. 375 (2014) 155–192. doi:10.1007/82_2013_352.

[122] Kentucky BioProcessing, Inc., (n.d.). https://www.kentuckybioprocessing.com/ (accessed May 7, 2019).

[123] J.W. Wang, R.B.S. Roden, Virus-like particles for the prevention of human papillomavirus-associated malignancies, Expert Rev. Vaccines. 12 (2013) 129–141. doi:10.1586/erv.12.151.

[124] D.L. Jarvis, Baculovirus-insect cell expression systems, Methods Enzymol. 463 (2009) 191–222. doi:10.1016/S0076-6879(09)63014-7.

[125] A. Croset, L. Delafosse, J.-P. Gaudry, C. Arod, L. Glez, C. Losberger, D. Begue, A. Krstanovic, F. Robert, F. Vilbois, L. Chevalet, B. Antonsson, Differences in the glycosylation

of recombinant proteins expressed in HEK and CHO cells, J. Biotechnol. 161 (2012) 336–348. doi:10.1016/j.jbiotec.2012.06.038.

[126] D. Gagoski, M.E. Polinkovsky, S. Mureev, A. Kunert, W. Johnston, Y. Gambin, K. Alexandrov, Performance benchmarking of four cell-free protein expression systems, Biotechnol. Bioeng. 113 (2016) 292–300. doi:10.1002/bit.25814.

[127] T.R. Patel, Nanocarrier-based therapies for CNS tumors, CNS Oncol. 3 (2014) 115–122. doi:10.2217/cns.14.2.

[128] M. Li, H. Deng, H. Peng, Q. Wang, Functional nanoparticles in targeting glioma diagnosis and therapies, J. Nanosci. Nanotechnol. 14 (2014) 415–432.

[129] S. Tortorella, T.C. Karagiannis, The significance of transferrin receptors in oncology: the development of functional nano-based drug delivery systems, Curr. Drug Deliv. 11 (2014) 427–443.

[130] R. van der Meel, L.J.C. Vehmeijer, R.J. Kok, G. Storm, E.V.B. van Gaal, Ligand-targeted particulate nanomedicines undergoing clinical evaluation: current status, Adv. Drug Deliv. Rev. 65 (2013) 1284–1298. doi:10.1016/j.addr.2013.08.012.

[131] J. Kreuter, Drug delivery to the central nervous system by polymeric nanoparticles: what do we know?, Adv. Drug Deliv. Rev. 71 (2014) 2–14. doi:10.1016/j.addr.2013.08.008.

[132] M.I. Alam, S. Beg, A. Samad, S. Baboota, K. Kohli, J. Ali, A. Ahuja, M. Akbar, Strategy for effective brain drug delivery, Eur. J. Pharm. Sci. Off. J. Eur. Fed. Pharm. Sci. 40 (2010) 385–403. doi:10.1016/j.ejps.2010.05.003.

[133] U. Prabhakar, H. Maeda, R.K. Jain, E.M. Sevick-Muraca, W. Zamboni, O.C. Farokhzad, S.T. Barry, A. Gabizon, P. Grodzinski, D.C. Blakey, Challenges and key considerations of the enhanced permeability and retention effect for nanomedicine drug delivery in oncology, Cancer Res. 73 (2013) 2412–2417. doi:10.1158/0008-5472.CAN-12-4561.

[134] C. Langevin, H. Jaaro, S. Bressanelli, M. Fainzilber, C. Tuffereau, Rabies virus glycoprotein (RVG) is a trimeric ligand for the N-terminal cysteine-rich domain of the mammalian p75 neurotrophin receptor, J. Biol. Chem. 277 (2002) 37655–37662. doi:10.1074/jbc.M201374200.

[135] M. Lafon, Rabies virus receptors, J. Neurovirol. 11 (2005) 82–87. doi:10.1080/13550280590900427.

[136] P. Kumar, H. Wu, J.L. McBride, K.-E. Jung, M. Hee Kim, B.L. Davidson, S. Kyung Lee, P. Shankar, N. Manjunath, Transvascular delivery of small interfering RNA to the central nervous system, Nature. 448 (2007) 39–43. doi:10.1038/nature05901.

[137] Y. Liu, R. Huang, L. Han, W. Ke, K. Shao, L. Ye, J. Lou, C. Jiang, Brain-targeting gene delivery and cellular internalization mechanisms for modified rabies virus glycoprotein RVG29 nanoparticles, Biomaterials. 30 (2009) 4195–4202. doi:10.1016/j.biomaterials.2009.02.051.

[138] S. Son, D.W. Hwang, K. Singha, J.H. Jeong, T.G. Park, D.S. Lee, W.J. Kim, RVG peptide tethered bioreducible polyethylenimine for gene delivery to brain, J. Control. Release Off. J. Control. Release Soc. 155 (2011) 18–25. doi:10.1016/j.jconrel.2010.08.011.

[139] D.W. Hwang, S. Son, J. Jang, H. Youn, S. Lee, D. Lee, Y.-S. Lee, J.M. Jeong, W.J. Kim, D.S. Lee, A brain-targeted rabies virus glycoprotein-disulfide linked PEI nanocarrier for delivery of neurogenic microRNA, Biomaterials. 32 (2011) 4968–4975. doi:10.1016/j.biomaterials.2011.03.047.

[140] Y. Liu, Y. Guo, S. An, Y. Kuang, X. He, H. Ma, J. Li, J. Lv, N. Zhang, C. Jiang, Targeting Caspase-3 as Dual Therapeutic Benefits by RNAi Facilitating Brain-Targeted Nanoparticles in a Rat Model of Parkinson's Disease, PLoS ONE. 8 (2013) e62905. doi:10.1371/journal.pone.0062905.

[141] S. Zadran, G. Akopian, H. Zadran, J. Walsh, M. Baudry, RVG-Mediated Calpain2 Gene Silencing in the Brain Impairs Learning and Memory, NeuroMolecular Med. 15 (2012) 74–81. doi:10.1007/s12017-012-8196-8.

[142] J.-Y. Kim, W.I. Choi, Y.H. Kim, G. Tae, Brain-targeted delivery of protein using chitosan- and RVG peptide-conjugated, pluronic-based nano-carrier, Biomaterials. 34 (2013) 1170–1178. doi:10.1016/j.biomaterials.2012.09.047.

[143] Y. Liu, Y. Hu, Y. Guo, H. Ma, J. Li, C. Jiang, Targeted imaging of activated caspase-3 in the central nervous system by a dual functional nano-device, J. Control. Release Off. J. Control. Release Soc. 163 (2012) 203–210. doi:10.1016/j.jconrel.2012.09.001.

[144] Y. Tao, J. Han, H. Dou, Brain-targeting gene delivery using a rabies virus glycoprotein peptide modulated hollow liposome: bio-behavioral study, J. Mater. Chem. 22 (2012) 11808–11815. doi:10.1039/C2JM31675G.

[145] L. Alvarez-Erviti, Y. Seow, H. Yin, C. Betts, S. Lakhal, M.J.A. Wood, Delivery of siRNA to the mouse brain by systemic injection of targeted exosomes, Nat. Biotechnol. 29 (2011) 341–345. doi:10.1038/nbt.1807.

[146] L. Xiang, R. Zhou, A. Fu, X. Xu, Y. Huang, C. Hu, Targeted delivery of large fusion protein into hippocampal neurons by systemic administration, J. Drug Target. 19 (2011) 632–636. doi:10.3109/1061186X.2010.523788.

[147] A. Fu, Y. Wang, L. Zhan, R. Zhou, Targeted Delivery of Proteins into the Central Nervous System Mediated by Rabies Virus Glycoprotein-Derived Peptide, Pharm. Res. 29 (2012) 1562–1569. doi:10.1007/s11095-012-0667-y.

[148] W. Chen, C. Zhan, B. Gu, Q. Meng, H. Wang, W. Lu, H. Hou, Targeted brain delivery of itraconazole via RVG29 anchored nanoparticles, J. Drug Target. 19 (2010) 228–234. doi:10.3109/1061186X.2010.492523.

[149] R.L. McCall, R.W. Sirianni, PLGA nanoparticles formed by single- or double-emulsion with vitamin E-TPGS, J. Vis. Exp. JoVE. (2013) 51015. doi:10.3791/51015.

[150] T.M. Fahmy, R.M. Samstein, C.C. Harness, W. Mark Saltzman, Surface modification of biodegradable polyesters with fatty acid conjugates for improved drug targeting, Biomaterials. 26 (2005) 5727–5736. doi:10.1016/j.biomaterials.2005.02.025.

[151] P.A. McCarron, W.M. Marouf, D.J. Quinn, F. Fay, R.E. Burden, S.A. Olwill, C.J. Scott, Antibody targeting of camptothecin-loaded PLGA nanoparticles to tumor cells, Bioconjug. Chem. 19 (2008) 1561–1569. doi:10.1021/bc800057g.

[152] C.L. Dora, M. Alvarez-Silva, A.G. Trentin, T.J. de Faria, D. Fernandes, R. da Costa, M. Stimamiglio, E. Lemos-Senna, Evaluation of antimetastatic activity and systemic toxicity of

camptothecin-loaded microspheres in mice injected with B16-F10 melanoma cells, J. Pharm. Pharm. Sci. Publ. Can. Soc. Pharm. Sci. Société Can. Sci. Pharm. 9 (2006) 22–31.

[153] A.D. Meikle, A.H. Martin, A rapid method for removal of the spinal cord, Stain Technol. 56 (1981) 235–237.

[154] B.P. Chugh, J.P. Lerch, L.X. Yu, M. Pienkowski, R.V. Harrison, R.M. Henkelman, J.G. Sled, Measurement of cerebral blood volume in mouse brain regions using micro-computed tomography, NeuroImage. 47 (2009) 1312–1318. doi:10.1016/j.neuroimage.2009.03.083.

[155] V.L. Jacobs, P.A. Valdes, W.F. Hickey, J.A. De Leo, Current review of in vivo GBM rodent models: emphasis on the CNS-1 tumour model, ASN Neuro. 3 (2011) e00063. doi:10.1042/AN20110014.

[156] M.G. Abdelwahab, T. Sankar, M.C. Preul, A.C. Scheck, Intracranial Implantation with Subsequent 3D In Vivo Bioluminescent Imaging of Murine Gliomas, J. Vis. Exp. (2011). doi:10.3791/3403.

[157] K. Sempf, T. Arrey, S. Gelperina, T. Schorge, B. Meyer, M. Karas, J. Kreuter, Adsorption of plasma proteins on uncoated PLGA nanoparticles, Eur. J. Pharm. Biopharm. Off. J. Arbeitsgemeinschaft Für Pharm. Verfahrenstechnik EV. 85 (2013) 53–60. doi:10.1016/j.ejpb.2012.11.030.

[158] P. Calvo, B. Gouritin, H. Villarroya, F. Eclancher, C. Giannavola, C. Klein, J.P. Andreux, P. Couvreur, Quantification and localization of PEGylated polycyanoacrylate nanoparticles in brain and spinal cord during experimental allergic encephalomyelitis in the rat, Eur. J. Neurosci. 15 (2002) 1317–1326.

[159] T. Saxena, K.H. Loomis, S.B. Pai, L. Karumbaiah, E. Gaupp, K. Patil, R. Patkar, R.V. Bellamkonda, Nanocarrier-mediated inhibition of macrophage migration inhibitory factor attenuates secondary injury after spinal cord injury, ACS Nano. 9 (2015) 1492–1505. doi:10.1021/nn505980z.

[160] Y.-C. Wang, Y.-T. Wu, H.-Y. Huang, H.-I. Lin, L.-W. Lo, S.-F. Tzeng, C.-S. Yang, Sustained intraspinal delivery of neurotrophic factor encapsulated in biodegradable nanoparticles following contusive spinal cord injury, Biomaterials. 29 (2008) 4546–4553. doi:10.1016/j.biomaterials.2008.07.050.

[161] S.A. Chvatal, Y.-T. Kim, A.M. Bratt-Leal, H. Lee, R.V. Bellamkonda, Spatial distribution and acute anti-inflammatory effects of Methylprednisolone after sustained local delivery to the contused spinal cord, Biomaterials. 29 (2008) 1967–1975. doi:10.1016/j.biomaterials.2008.01.002.

[162] A. Gaudin, M. Yemisci, H. Eroglu, S. Lepetre-Mouelhi, O.F. Turkoglu, B. Dönmez-Demir, S. Caban, M.F. Sargon, S. Garcia-Argote, G. Pieters, O. Loreau, B. Rousseau, O. Tagit, N. Hildebrandt, Y. Le Dantec, J. Mougin, S. Valetti, H. Chacun, V. Nicolas, D. Desmaële, K. Andrieux, Y. Capan, T. Dalkara, P. Couvreur, Squalenoyl adenosine nanoparticles provide neuroprotection after stroke and spinal cord injury, Nat. Nanotechnol. 9 (2014) 1054–1062. doi:10.1038/nnano.2014.274.

[163] V. Bartanusz, D. Jezova, B. Alajajian, M. Digicaylioglu, The blood-spinal cord barrier: morphology and clinical implications, Ann. Neurol. 70 (2011) 194–206. doi:10.1002/ana.22421.

[164] N.G. Bowery, A.L. Hudson, G.W. Price, GABAA and GABAB receptor site distribution in the rat central nervous system, Neuroscience. 20 (1987) 365–383.

[165] H. Ulukan, P.W. Swaan, Camptothecins: a review of their chemotherapeutic potential, Drugs. 62 (2002) 2039–2057.

[166] R.W. Sirianni, M.-Q. Zheng, T.R. Patel, T. Shafbauer, J. Zhou, W.M. Saltzman, R.E. Carson, Y. Huang, Radiolabeling of poly(lactic-co-glycolic acid) (PLGA) nanoparticles with biotinylated F-18 prosthetic groups and imaging of their delivery to the brain with positron emission tomography, Bioconjug. Chem. 25 (2014) 2157–2165. doi:10.1021/bc500315j.

[167] P. Xu, E. Gullotti, L. Tong, C.B. Highley, D.R. Errabelli, T. Hasan, J.-X. Cheng, D.S. Kohane, Y. Yeo, Intracellular drug delivery by poly(lactic-co-glycolic acid) nanoparticles, revisited, Mol. Pharm. 6 (2009) 190–201. doi:10.1021/mp800137z.

[168] G. Bastiat, C.O. Pritz, C. Roider, F. Fouchet, E. Lignières, A. Jesacher, R. Glueckert, M. Ritsch-Marte, A. Schrott-Fischer, P. Saulnier, J.-P. Benoit, A new tool to ensure the fluorescent dye labeling stability of nanocarriers: a real challenge for fluorescence imaging, J. Control. Release Off. J. Control. Release Soc. 170 (2013) 334–342. doi:10.1016/j.jconrel.2013.06.014.

[169] H. Chen, S. Kim, L. Li, S. Wang, K. Park, J.-X. Cheng, Release of hydrophobic molecules from polymer micelles into cell membranes revealed by Forster resonance energy transfer imaging, Proc. Natl. Acad. Sci. U. S. A. 105 (2008) 6596–6601. doi:10.1073/pnas.0707046105.

[170] E. Gullotti, Y. Yeo, Beyond the imaging: limitations of cellular uptake study in the evaluation of nanoparticles, J. Control. Release Off. J. Control. Release Soc. 164 (2012) 170–176. doi:10.1016/j.jconrel.2012.04.042.

[171] P.A. Baeuerle, C. Reinhardt, Bispecific T-Cell Engaging Antibodies for Cancer Therapy, Cancer Res. 69 (2009) 4941–4944. doi:10.1158/0008-5472.CAN-09-0547.

[172] B.D. Choi, C.-T. Kuan, M. Cai, G.E. Archer, D.A. Mitchell, P.C. Gedeon, L. Sanchez-Perez, I. Pastan, D.D. Bigner, J.H. Sampson, Systemic administration of a bispecific antibody targeting EGFRvIII successfully treats intracerebral glioma, Proc. Natl. Acad. Sci. 110 (2013) 270–275. doi:10.1073/pnas.1219817110.

[173] B.D. Choi, P.C. Gedeon, J.E. Herndon, G.E. Archer, E.A. Reap, L. Sanchez-Perez, D.A. Mitchell, D.D. Bigner, J.H. Sampson, Human Regulatory T Cells Kill Tumor Cells through Granzyme-Dependent Cytotoxicity upon Retargeting with a Bispecific Antibody, Cancer Immunol. Res. 1 (2013) 163–167. doi:10.1158/2326-6066.CIR-13-0049.

[174] N. Ullrich, A. Bordey, G.Y. Gillespie, H. Sontheimer, Expression of voltage-activated chloride currents in acute slices of human gliomas, Neuroscience. 83 (1998) 1161–1173. doi:10.1016/S0306-4522(97)00456-9.

[175] J. Deshane, C.C. Garner, H. Sontheimer, Chlorotoxin Inhibits Glioma Cell Invasion via Matrix Metalloproteinase-2, J. Biol. Chem. 278 (2003) 4135–4144. doi:10.1074/jbc.M205662200.

[176] K. Kesavan, J. Ratliff, E.W. Johnson, W. Dahlberg, J.M. Asara, P. Misra, J.V. Frangioni, D.B. Jacoby, Annexin A2 Is a Molecular Target for TM601, a Peptide with Tumor-targeting

and Anti-angiogenic Effects, J. Biol. Chem. 285 (2010) 4366–4374. doi:10.1074/jbc.M109.066092.

[177] D. Kolber-Simonds, J. Wu, U. Majumder, D. Custar, D. Li, H. Du, M.H. Postema, T. Noland, A. Hart, G. Lai, S. Eckley, V. Dixit, K. Tendyke, K. Nomoto, M. Woodall-Jappe, S. McGonigle, Abstract 3961: Role for neuropilin1 in mode of action of chlorotoxin, Cancer Res. 78 (2018) 3961–3961. doi:10.1158/1538-7445.AM2018-3961.

[178] RCSB PDB - Protein Feature View - Chlorotoxin - P45639 (CTXL_LEIQU), (n.d.). http://www.rcsb.org/pdb/protein/P45639 (accessed May 9, 2019).

[179] Q. Chen, J. He, W. Phoolcharoen, H.S. Mason, Geminiviral vectors based on bean yellow dwarf virus for production of vaccine antigens and monoclonal antibodies in plants, Hum. Vaccin. 7 (2011) 331–338.

[180] N. Matoba, H. Kajiura, I. Cherni, J.D. Doran, M. Bomsel, K. Fujiyama, T.S. Mor, Biochemical and immunological characterization of the plant-derived candidate human immunodeficiency virus type 1 mucosal vaccine CTB–MPR649–684, Plant Biotechnol. J. 7 (2009) 129–145. doi:10.1111/j.1467-7652.2008.00381.x.

[181] B.C. Geyer, L. Kannan, I. Cherni, R.R. Woods, H. Soreq, T.S. Mor, Transgenic plants as a source for the bioscavenging enzyme, human butyrylcholinesterase, Plant Biotechnol. J. 8 (2010) 873–886. doi:10.1111/j.1467-7652.2010.00515.x.

[182] L. Kollipara, R.P. Zahedi, Protein carbamylation: in vivo modification or in vitro artefact?, Proteomics. 13 (2013) 941–944. doi:10.1002/pmic.201200452.

[183] L. Zhai, L. Wu, F. Li, R.S. Burnham, J.C. Pizarro, B. Xu, A Rapid Method for Refolding Cell Surface Receptors and Ligands, Sci. Rep. 6 (2016). doi:10.1038/srep26482.

[184] B.C. Geyer, S.P. Fletcher, T.A. Griffin, M.J. Lopker, H. Soreq, T.S. Mor, Translational control of recombinant human acetylcholinesterase accumulation in plants, BMC Biotechnol. 7 (2007) 27. doi:10.1186/1472-6750-7-27.

[185] S.A. Kessans, M.D. Linhart, N. Matoba, T. Mor, Biological and biochemical characterization of HIV-1 Gag/dgp41 virus-like particles expressed in Nicotiana benthamiana, Plant Biotechnol. J. 11 (2013) 681–690. doi:10.1111/pbi.12058.

[186] M. Malhotra, D. Sahal, Anomalous mobility of sulfitolysed proteins in SDS-PAGE. Analysis and applications, Int. J. Pept. Protein Res. 48 (1996) 240–248.

[187] K.T. Hamorsky, J.C. Kouokam, J.M. Jurkiewicz, B. Nelson, L.J. Moore, A.S. Husk, H. Kajiura, K. Fujiyama, N. Matoba, N-Glycosylation of cholera toxin B subunit in Nicotiana benthamiana: impacts on host stress response, production yield and vaccine potential, Sci. Rep. 5 (2015). doi:10.1038/srep08003.

[188] M.T. Dertzbaugh, L.M. Cox, The affinity of cholera toxin for Ni2+ ion., Protein Eng. Des. Sel. 11 (1998) 577–581. doi:10.1093/protein/11.7.577.

[189] P.C. Gedeon, T.H. Schaller, S.K. Chitneni, B.D. Choi, C.-T. Kuan, C.M. Suryadevara, D.J. Snyder, R.J. Schmittling, S.E. Szafranski, X. Cui, P. Healy, J.E. Herndon, R.E. McLendon, S.T. Keir, G.E. Archer, E. Reap, L. Sanchez-Perez, D.D. Bigner, J.H. Sampson, A rationally designed fully human EGFRvIII:CD3-targeted bispecific antibody redirects human T cells to treat patient-derived intracerebral malignant glioma, Clin. Cancer Res. (2018) clincanres.0126.2017. doi:10.1158/1078-0432.CCR-17-0126.

[190] X.-M. Wang, X. Luo, Z.-Y. Guo, Recombinant expression and downstream processing of the disulfide-rich tumor-targeting peptide chlorotoxin, Exp. Ther. Med. 6 (2013) 1049. doi:10.3892/etm.2013.1234.

[191] T. Kasai, K. Nakamura, A. Vaidyanath, L. Chen, S. Sekhar, S. El-Ghlban, M. Okada, A. Mizutani, T. Kudoh, H. Murakami, M. Seno, T. Kasai, K. Nakamura, A. Vaidyanath, L. Chen, S. Sekhar, S. El-Ghlban, M. Okada, A. Mizutani, T. Kudoh, H. Murakami, M. Seno, Chlorotoxin Fused to IgG-Fc Inhibits Glioblastoma Cell Motility via Receptor-Mediated Endocytosis, Chlorotoxin Fused to IgG-Fc Inhibits Glioblastoma Cell Motility via Receptor-Mediated Endocytosis, J. Drug Deliv. J. Drug Deliv. 2012, 2012 (2012) e975763. doi:10.1155/2012/975763, 10.1155/2012/975763.

[192] M.-E. Goebeler, S. Knop, A. Viardot, P. Kufer, M.S. Topp, H. Einsele, R. Noppeney, G. Hess, S. Kallert, A. Mackensen, K. Rupertus, L. Kanz, M. Libicher, D. Nagorsen, G. Zugmaier, M. Klinger, A. Wolf, B. Dorsch, B.D. Quednau, M. Schmidt, J. Scheele, P.A. Baeuerle, E. Leo, R.C. Bargou, Bispecific T-Cell Engager (BiTE) Antibody Construct Blinatumomab for the Treatment of Patients With Relapsed/Refractory Non-Hodgkin Lymphoma: Final Results From a Phase I Study, J. Clin. Oncol. (2016) JCO591586. doi:10.1200/JCO.2014.59.1586.

[193] B. Jürgen, A. Breitenstein, V. Urlacher, K. Büttner, H. Lin, M. Hecker, T. Schweder, P. Neubauer, Quality control of inclusion bodies in Escherichia coli, Microb. Cell Factories. 9 (2010) 41. doi:10.1186/1475-2859-9-41.

[194] A.F. Sequeira, J. Turchetto, N.J. Saez, F. Peysson, L. Ramond, Y. Duhoo, M. Blémont, V.O. Fernandes, L.T. Gama, L.M.A. Ferreira, C.I.P.I. Guerreiro, N. Gilles, H. Darbon, C.M.G.A. Fontes, R. Vincentelli, Gene design, fusion technology and TEV cleavage conditions influence the purification of oxidized disulphide-rich venom peptides in Escherichia coli, Microb. Cell Factories. 16 (2017). doi:10.1186/s12934-016-0618-0.

[195] C. Bae, J. Kalia, I. Song, J. Yu, H.H. Kim, K.J. Swartz, J.I. Kim, High Yield Production and Refolding of the Double-Knot Toxin, an Activator of TRPV1 Channels, PLOS ONE. 7 (2012) e51516. doi:10.1371/journal.pone.0051516.

[196] Y. Aida, M.J. Pabst, Removal of endotoxin from protein solutions by phase separation using triton X-114, J. Immunol. Methods. 132 (1990) 191–195. doi:10.1016/0022-1759(90)90029-U.

[197] H. Lai, J. He, J. Hurtado, J. Stahnke, A. Fuchs, E. Mehlhop, S. Gorlatov, A. Loos, M.S. Diamond, Q. Chen, Structural and functional characterization of an anti-West Nile virus monoclonal antibody and its single-chain variant produced in glycoengineered plants, Plant Biotechnol. J. 12 (2014) 1098–1107. doi:10.1111/pbi.12217.

[198] K. Tsumoto, M. Umetsu, I. Kumagai, D. Ejima, J.S. Philo, T. Arakawa, Role of Arginine in Protein Refolding, Solubilization, and Purification, Biotechnol. Prog. 20 (2004) 1301–1308. doi:10.1021/bp0498793.

[199] C.E. Correnti, M.M. Gewe, C. Mehlin, A.D. Bandaranayake, W.A. Johnsen, P.B. Rupert, M.-Y. Brusniak, M. Clarke, S.E. Burke, W. De Van Der Schueren, K. Pilat, S.M. Turnbaugh, D. May, A. Watson, M.K. Chan, C.D. Bahl, J.M. Olson, R.K. Strong, Screening, large-scale production and structure-based classification of cystine-dense peptides, Nat. Struct. Mol. Biol. (2018) 1. doi:10.1038/s41594-018-0033-9.

[200] J.M. Heffernan, D.J. Overstreet, S. Srinivasan, L.D. Le, B.L. Vernon, R.W. Sirianni, Temperature responsive hydrogels enable transient three-dimensional tumor cultures via rapid cell recovery, J. Biomed. Mater. Res. A. 104 (2016) 17–25. doi:10.1002/jbm.a.35534.

[201] J.M. Heffernan, J.B. McNamara, S. Borwege, B.L. Vernon, N. Sanai, S. Mehta, R.W. Sirianni, PNIPAAm-co-Jeffamine® (PNJ) scaffolds as in vitro models for niche enrichment of glioblastoma stem-like cells, Biomaterials. 143 (2017) 149–158. doi:10.1016/j.biomaterials.2017.05.007.

[202] D.X. Medina, K.T. Householder, R. Ceton, T. Kovalik, J.M. Heffernan, R.V. Shankar, R.P. Bowser, R.J. Wechsler-Reya, R.W. Sirianni, Optical barcoding of PLGA for multispectral analysis of nanoparticle fate in vivo, J. Controlled Release. (n.d.). doi:10.1016/j.jconrel.2017.02.033.

APPENDIX A

SUPPLEMENTARY FIGURES

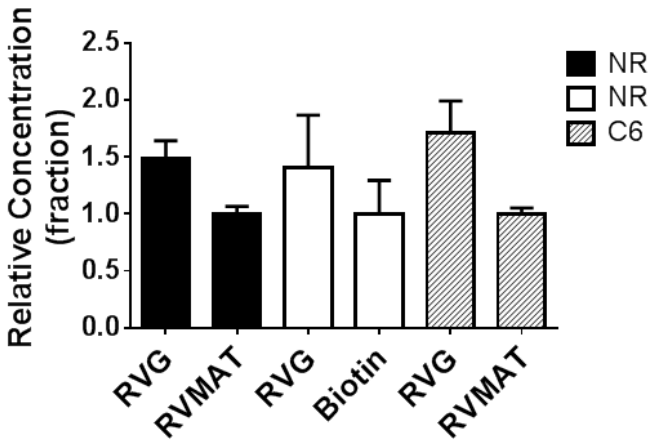

Supplementary Figure 1*: Improved targeting of payload to the brain after two hours using RVG29-modified PLGA nanoparticles is consistent across different fluorescent encapsulated molecules. RV-MAT is a control peptide derived from the matrix protein of rabies virus, which has no known role in rabies virus neurotropism (sequence: N term-MNLLRKIVKNRRDEDTQKSSPASAPLDDG-C2-Biotin). These data demonstrate consistency of apparent targeting in experimental repeats, and also across both a biotin and an RV-MAT control. Each set of data represents an independent experiment, with n=3-5 mice per treatment group and delivered dose of 4-6mg PLGA per mouse. Ratios are normalized to RV-MAT or biotin control, as labeled for each data set. NR = Nile red. C6 = Coumarin 6*

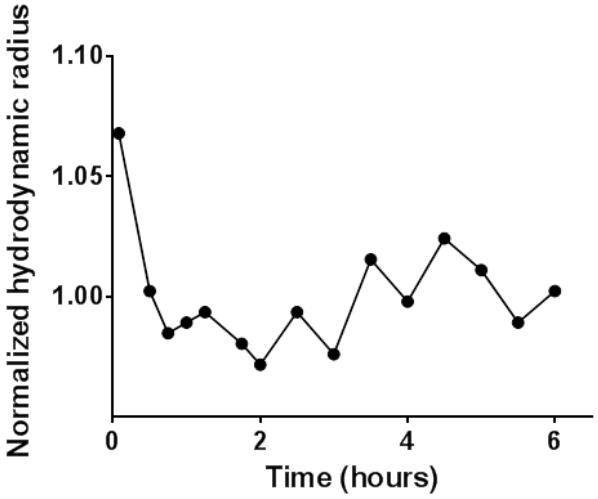

Supplementary Figure 2: *The hydrodynamic radius of RVG-PLGA-DiR does not change over a period of six hours for nanoparticles maintained in aqueous conditions at 37°C.*

APPENDIX B

AMINO ACID SEQUENCES OF CONSTRUCTS USED IN CHAPTER 3

1. ACDClx-His

(Barly alpha amylase signal peptide-anti-CD3 V_H-$Linker_3$-anti-CD3 V_L-Linker-Chlorotoxin-PreScission Protease Recognition Site-His tag)

MANKHLSLSLFLVLLGLSASLASGMEVQLVESGGGLVQPGKSLKLSCEASGFTFSGYGMHWVRQAPGRGLESVAYITSSSINIKYADAVKGRFTVSRDNAKNLLFLQMNILKSEDTAMYYCARFDWDKNYWGQGTMVTVSSGGGGSGGGGSGGGGSQMTQSPSSLPASLGDRVTINCQASQDISNYLNWYQQKPGKAPKLLIYYTNKLADGVPSRFSGSGSGRDSSFTISSLESEDIGSYYCQQYYNYPWTFGPGTKLEIKRGGGGSMCMPCFTTDHQMARKCDDCCGGKGRGKCYGPQCLCRLEVLFQGPHHHHHH

2. ACDClx_**K270R**-His

(Barly alpha amylase signal peptide-anti-CD3 V_H-$Linker_3$-anti-CD3 V_L-Linker-Chlorotoxin-PreScission Protease Recognition Site-His tag)

MANKHLSLSLFLVLLGLSASLASGMEVQLVESGGGLVQPGKSLKLSCEASGFTFSGYGMHWVRQAPGRGLESVAYITSSSINIKYADAVKGRFTVSRDNAKNLLFLQMNILKSEDTAMYYCARFDWDKNYWGQGTMVTVSSGGGGSGGGGSGGGGSQMTQSPSSLPASLGDRVTINCQASQDISNYLNWYQQKPGKAPKLLIYYTNKLADGVPSRFSGSGSGRDSSFTISSLESEDIGSYYCQQYYNYPWTFGPGTKLEIKRGGGGSMCMPCFTTDHQMARKCDDCCGGKGRG**R**CYGPQCLCRLEVLFQGPHHHHHH

3. His-ACDClx

(Barly alpha amylase signal peptide-His tag-TEV protease recognition site-anti-CD3 V_H-Linker$_3$-anti-CD3 V_L-Linker-Chlorotoxin)

MANKHLSLSLFLVLLGLSASLASGHHHHHHHHENLYFQGEVQLVESGGGLVQPGKSLKLSCEASGFTFSGYGMHWVRQAPGRGLESVAYITSSSINIKYADAVKGRFTVSRDNAKNLLFLQMNILKSEDTAMYYCARFDWDKNYWGQGTMVTVSSGGGGSGGGGSGGGGSQMTQSPSSLPASLGDRVTINCQASQDISNYLNWYQQKPGKAPKLLIYYTNKLADGVPSRFSGSGSGRDSSFTISSLESEDIGSYYCQQYYNYPWTFGPGTKLEIKRGGGGSMCMPCFTTDHQMARKCDDCCGGKGRGKCYGPQCLCR

4. Ngly-His-ACDClx

(Barly alpha amylase signal peptide-Nglycosylation site-His tag-TEV protease recognition site-anti-CD3 V_H-Linker$_3$-anti-CD3 V_L-Linker-Chlorotoxin)

MANKHLSLSLFLVLLGLSASLASGNITHHHHHHHHENLYFQGEVQLVESGGGLVQPGKSLKLSCEASGFTFSGYGMHWVRQAPGRGLESVAYITSSSINIKYADAVKGRFTVSRDNAKNLLFLQMNILKSEDTAMYYCARFDWDKNYWGQGTMVTVSSGGGGSGGGGSGGGGSQMTQSPSSLPASLGDRVTINCQASQDISNYLNWYQQKPGKAPKLLIYYTNKLADGVPSRFSGSGSGRDSSFTISSLESEDIGSYYCQQYYNYPWTFGPGTKLEIKRGGGGSMCMPCFTTDHQMARKCDDCCGGKGRGKCYGPQCLCR

5. CTB-ACDClx

(Barly alpha amylase signal peptide-Cholera toxin subunit B-Linker- TEV protease recognition site-anti-CD3 V_H-Linker$_3$-anti-CD3 V_L-Linker-Chlorotoxin)

MANKHLSLSLFLVLLGLSASLASGTPQNITDLCAEYHNTQIHTLNDKIFSYTESLAGKREMAIITFK
NGATFQVEVPGSQHIDSQKKAIERMKDTLRIAYLTEAKVEKLCVWNNKTPHAIAAISMANGGGGS
ENLYFQGEVQLVESGGGLVQPGKSLKLSCEASGFTFSGYGMHWVRQAPGRGLESVAYITSSSI
NIKYADAVKGRFTVSRDNAKNLLFLQMNILKSEDTAMYYCARFDWDKNYWGQGTMVTVSSGGG
GSGGGGSGGGGSQMTQSPSSLPASLGDRVTINCQASQDISNYLNWYQQKPGKAPKLLIYYTNK
LADGVPSRFSGSGSGRDSSFTISSLESEDIGSYYCQQYYNYPWTFGPGTKLEIKRGGGGSMCM
PCFTTDHQMARKCDDCCGGKGRGKCYGPQCLCR

6. Anti-CD3 scFv

(Barly alpha amylase signal peptide-Nglycosylation site-His tag-TEV protease recognition site-anti-CD3 V_H-Linker$_3$-anti-CD3 V_L-Linker)

MANKHLSLSLFLVLLGLSASLASGNITHHHHHHHHENLYFQGEVQLVESGGGLVQPGKSLKLSC
EASGFTFSGYGMHWVRQAPGRGLESVAYITSSSINIKYADAVKGRFTVSRDNAKNLLFLQMNILK
SEDTAMYYCARFDWDKNYWGQGTMVTVSSGGGGSGGGGSGGGGSQMTQSPSSLPASLGDR
VTINCQASQDISNYLNWYQQKPGKAPKLLIYYTNKLADGVPSRFSGSGSGRDSSFTISSLESEDI
GSYYCQQYYNYPWTFGPGTKLEIKRGGGGS

APPENDIX C

AMINO ACID SEQUENCES OF CONSTRUCTS USED IN CHAPTER 4

1. DsbC-ACDClx

(DsbC signal peptide-DsbC (Disulfide bond isomerase C)-His tag- TEV protease recognition site-anti-CD3 V_H-Linker$_3$-anti-CD3 V_L-Linker-Chlorotoxin)

MKKGFMLFTLLAAFSGFAQADDAAIQQTLAKMGIKSSDIQPAPVAGMKTVLTNSGVLYITDDGKHI
IQGPMYDVSGTAPVNVTNKMLLKQLNALEKEMIVYKAPQEKHVITVFTDITCGYCHKLHEQMADY
NALGITVRYLAFPRQGLDSDAEKEMKAIWCAKDKNKAFDDVMAGKSVAPASCDVDIADHYALGV
QLGVSGTPAVVLSNGTLVPGYQPPKEMKEFLDEHQKMTSGKHHHHHHHHENLYFQGEVQLVE
SGGGLVQPGKSLKLSCEASGFTFSGYGMHWVRQAPGRGLESVAYITSSSINIKYADAVKGRFTV
SRDNAKNLLFLQMNILKSEDTAMYYCARFDWDKNYWGQGTMVTVSSGGGGSGGGGSGGGGS
QMTQSPSSLPASLGDRVTINCQASQDISNYLNWYQQKPGKAPKLLIYYTNKLADGVPSRFSGSG
SGRDSSFTISSLESEDIGSYYCQQYYNYPWTFGPGTKLEIKRGGGGSMCMPCFTTDHQMARKC
DDCCGGKGRGKCYGPQCLCR

2. His-ACDClx

(His tag-TEV protease recognition site-anti-CD3 V_H-Linker$_3$-anti-CD3 V_L-Linker-Chlorotoxin)

MHHHHHHHHENLYFQGEVQLVESGGGLVQPGKSLKLSCEASGFTFSGYGMHWVRQAPGRGL
ESVAYITSSSINIKYADAVKGRFTVSRDNAKNLLFLQMNILKSEDTAMYYCARFDWDKNYWGQGT
MVTVSSGGGGSGGGGSGGGGSQMTQSPSSLPASLGDRVTINCQASQDISNYLNWYQQKPGK
APKLLIYYTNKLADGVPSRFSGSGSGRDSSFTISSLESEDIGSYYCQQYYNYPWTFGPGTKLEIK
RGGGGSMCMPCFTTDHQMARKCDDCCGGKGRGKCYGPQCLCR

3. ACDClx

(anti-CD3 V_H-Linker$_3$-anti-CD3 V_L-Linker-Chlorotoxin)

MEVQLVESGGGLVQPGKSLKLSCEASGFTFSGYGMHWVRQAPGRGLESVAYITSSSINIKYADA
VKGRFTVSRDNAKNLLFLQMNILKSEDTAMYYCARFDWDKNYWGQGTMVTVSSGGGGSGGG
GSGGGGSQMTQSPSSLPASLGDRVTINCQASQDISNYLNWYQQKPGKAPKLLIYYTNKLADGVP
SRFSGSGSGRDSSFTISSLESEDIGSYYCQQYYNYPWTFGPGTKLEIKRGGGGSMCMPCFTTD
HQMARKCDDCCGGKGRGKCYGPQCLCR

4. His-ACDClxΔ15

(His tag-TEV protease recognition site-anti-CD3 V_H-Linker$_3$-anti-CD3 V_L-Linker-ChlorotoxinΔ15)

MHHHHHHHHENLYFQGEVQLVESGGGLVQPGKSLKLSCEASGFTFSGYGMHWVRQAPGRGL
ESVAYITSSSINIKYADAVKGRFTVSRDNAKNLLFLQMNILKSEDTAMYYCARFDWDKNYWGQGT
MVTVSSGGGGSGGGGSGGGGSQMTQSPSSLPASLGDRVTINCQASQDISNYLNWYQQKPGK
APKLLIYYTNKLADGVPSRFSGSGSGRDSSFTISSLESEDIGSYYCQQYYNYPWTFGPGTKLEIK
RGGGGSMCMPCFTTDHQMAR

5. ACDClxΔ15

(anti-CD3 V_H-Linker$_3$-anti-CD3 V_L-Linker-ChlorotoxinΔ15)

MEVQLVESGGGLVQPGKSLKLSCEASGFTFSGYGMHWVRQAPGRGLESVAYITSSSINIKYADA
VKGRFTVSRDNAKNLLFLQMNILKSEDTAMYYCARFDWDKNYWGQGTMVTVSSGGGGSGGG
GSGGGGSQMTQSPSSLPASLGDRVTINCQASQDISNYLNWYQQKPGKAPKLLIYYTNKLADGVP
SRFSGSGSGRDSSFTISSLESEDIGSYYCQQYYNYPWTFGPGTKLEIKRGGGGSMCMPCFTTD
HQMAR

APPENDIX D

CO-AUTHOR APPROVAL OF PUBLICATION USAGE

All co-authors of previously published works have given their permission for the reproduction of this material in this document.